

Molecular Mechanisms of Protein Degradation Studied at the Single Molecule Level

By

Juan Carlos Cordova

Dissertation

Submitted to the Faculty of the  
Graduate School of Vanderbilt University  
in partial fulfillment of the requirements  
for the degree of

DOCTOR OF PHILOSOPHY

in

Chemical Engineering

August, 2016


Nashville, Tennessee

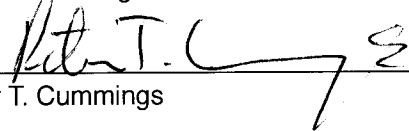
Approved:

Date:

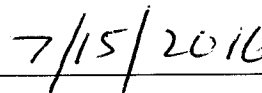
  
\_\_\_\_\_


Matthew J. Lang

  
\_\_\_\_\_

  
\_\_\_\_\_

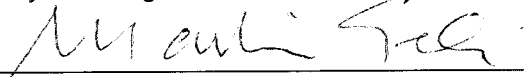
Peter T. Cummings

  
\_\_\_\_\_

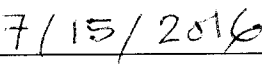
  
\_\_\_\_\_

Jamey D. Young

  
\_\_\_\_\_

  
\_\_\_\_\_

Martin Egli

  
\_\_\_\_\_

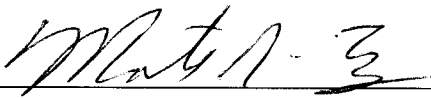
# Molecular mechanisms of protein degradation studied at the single molecule level

Juan Carlos Cordova

Department of Chemical and Biomolecular Engineering

Enzymatic proteins catalyze biochemical reactions central to many cellular processes. Across all kingdoms of life, members of the AAA+ (ATPases associated with diverse cellular activities plus) superfamily of enzymes convert chemical energy to mechanical work through hydrolysis of the molecule adenosine triphosphate (ATP). One of the best characterized AAA+ systems is the ClpXP protease, which degrades cellular proteins targeted for disposal. As an oligomeric stacked ring structure comprised of the AAA+ ClpX unfoldase and the ClpP peptidase, ClpXP repeatedly pulls against a targeted protein until it ultimately mechanically unfolds the substrate. Upon unfolding, ClpX translocates the polypeptide into the ClpP peptidase for degradation. Although structural and ensemble biochemical studies have established many of the operating principles of ClpXP, a detailed mechanochemical model for protein degradation remains largely unknown.

Here we employ and engineer novel singlemolecule approaches to elucidate the underlying physical mechanisms of protein unfolding and polypeptide translocation by ClpXP at the single molecule level. Using a highresolution optical trapping assay, we directly monitor degradation of homopolymer substrates to establish the kinetics of protein unfolding which are tightly linked to substrate stability near the site of ClpX pulling. During translocation, ClpXP spools polypeptides in ~14nm steps, even when only two of six subunits are active in ClpX mutants, suggesting a large amount of subunit cooperativity within the ClpX ring. Using these findings, we present a mechanochemical model for protein degradation by the ClpXP protease. Furthermore, we develop singlemolecule fluorescence assays to report on nucleotide binding to single ClpX subunits, as well as vital structural rearrangements in the ClpX ring. These fluorescence approaches are then combined with optical trapping to simultaneously visualize ClpX conformation, nucleotide binding, and mechanical activity. Lastly, a synthetic technique for functionalizing highly stable optical trapping handles with proteins and nucleic acids is presented.

  
\_\_\_\_\_  
Advisor: Matthew J. Lang

  
\_\_\_\_\_  
Date

To my beloved parents, Emilia and Ricardo Cordova

## ACKNOWLEDGMENTS

First and foremost, I would like to thank my advisor Matt Lang, who is not only an outstanding scientist, but an even better person. I am extremely lucky to have had the chance to join Matt's group as he started a lab at Vanderbilt. Matt gave me the opportunity to work on cutting edge science while allowing me to grow into a well-rounded and independent researcher. There will never be a bigger influence than his in my scientific career. I would also like to thank the members of my thesis committee Peter Cummings, Martin Egli, David Piston, and Jamey Young for their advice and helpful discussions about research and life throughout my graduate career.

Of course, I would like to thank past and present members of the Lang Lab. I continually felt lucky to work in such a supportive and friendly environment. I will always consider Sonia Brady, Dev Das, Harris Manning, and Yongdae Shin as some of my closest friends. Furthermore, I am thankful to all of my friends and classmates from the chemical engineering department who made my time in and out of the lab an enjoyable one. I am also thankful to the undergraduate students I had the pleasure of working with including Kelsea Best, Alyssa Jaffe, Dan Laky, and Charles Wang for their commitment and research assistance.

This thesis is dedicated to my family. Whatever success I have achieved is only because I have you as my foundation. I am extremely grateful for your endless support through the good and bad times.

Finally, I would like to thank my beautiful fiancée and best friend Kristen Kingry. None of this would have been possible without your unwavering love, support, and encouragement. You are my biggest blessing.

# TABLE OF CONTENTS

	Page
Abstract.....	ii
Dedication .....	iii
Acknowledgments.....	iv
List of Figures.....	vii
Chapter	
I. Introduction .....	1
Molecular machines .....	1
Intracellular protein degradation by AAA+ proteases.....	6
The ClpXP protease.....	10
Single molecule techniques .....	15
II. Stochastic but highly coordinated protein unfolding and polypeptide translocation by the ClpXP proteolytic machine .....	29
Introduction .....	30
Results .....	33
Discussion.....	46
Experimental procedures .....	60
Supplemental results .....	65
Supplemental discussion .....	67
Supplemental experimental procedures.....	68
III. Direct visualization of nucleotide turnover during protein degradation by a AAA+ molecular machine .....	81
Introduction .....	82
Results .....	83
Discussion.....	94
Methods .....	97
IV. Real-time visualization of subunit conformational switching during protein degradation by a AAA+ machine .....	104

Introduction .....	105
Results .....	107
Discussion.....	120
Methods .....	124
V. Bio-functionalization of core-shell particles with enhanced trapping stability .....	130
Introduction .....	131
Materials and Methods.....	133
Results and Discussion.....	139
Conclusions .....	145
VI. Conclusions and future directions .....	148
Appendix	
A. Protocols .....	155
PCR amplification of dsDNA for ClpXP assays .....	156
DNA-Amine to thiol-HaloTag ligand conjugation.....	158
Making ATP regeneration solution for ClpXP experiments.....	160
ClpXP dumbbell assay.....	161
Anti-Digoxigenin coated beads .....	164
TiO <sub>2</sub> core-shell microsphere synthesis .....	165

## LIST OF FIGURES

Figure	Page
1.1. The crowded intracellular environment .....	2
1.2. Macroscopic and molecular motors .....	4
1.3. Minimal model for protein degradation by AAA+ proteases .....	9
1.4. The ClpXP protease .....	13
1.5. Simplified ray optic description of optical trapping .....	17
1.6. Sample optical layout of a combined force-fluorescence instrument .....	20
2.1. Single-molecule unfolding and translocation of substrates .....	32
2.2. ClpXP unfolding of domains in multi-domain substrates .....	35
2.3. Translocation and pausing .....	39
2.4. Physical steps during titin translocation .....	41
2.5. Unfolding and translocation by RWERWE ClpX .....	45
2.6. Solution degradation times are poorly predicted by single-molecule unfolding and translocation times .....	48
2.7. Mechanochemical models for ClpXP function.....	56
2.S1. Randomness simulations.....	72
2.S2. Single and double exponential fits of preunfolding dwell times .....	73
2.S3. Experimental and simulated prestep dwell distributions .....	74
2.S4. Distributions of ClpXP translocation step sizes and dwell durations .....	75
2.S5. ClpXP unfolding of the C-Terminal elements of secondary structure in the Titin <sup>127</sup> or Halo domains .....	76

2.S6. Experimental and simulated distributions of translocation step sizes.....	77
2.S7. Observed and simulated memory in translocation stepping.....	78
2.S8. Controls for accuracy of translocation-step detection.....	79
3.1. Protein degradation in using the ATPQ nucleotide.....	85
3.2. Single molecule degradation using ATP and ATPQ.....	88
3.3. Binding of ATPQ to ClpX results in fluorescence quenching.....	92
3.4. Combined force-fluorescence measurements.....	95
3.5. Residence times for ATPQ in a ClpX subunit.....	96
4.1. Engineering of ClpX variant to report on subunit conformation.....	110
4.2. Observation of dynamic switching in single ClpX subunits.....	112
4.3. Kinetics of L-U switching.....	114
4.4. Monitoring degradation using a surface-tethered assay.....	117
4.5. Combined force-fluorescence experiments.....	119
4.6. Monitoring subunit conformation during protein unfolding.....	121
5.1. Synthetic strategy for the production of anatase-titania core-shell particles.....	135
5.2. Synthesis and characterization of core-shell particles.....	138
5.3. Effect of heating time on core-shell properties.....	141
5.4. Stretching DNA using core-shell particles.....	143
5.5. Protein coated core-shell particles.....	144
6.1. ClpXP degradation under an assisting load.....	151



# CHAPTER 1

## Introduction

### MOLECULAR MACHINES

Biological cells are the fundamental building blocks of life. Together, groups of cells differentiate to form tissues and organs that comprise metazoan bodies, including *homo sapiens* ourselves. Even simple single-cell organisms, like the bacteria *E. coli*, have genomes containing thousands of genes, which encode the ~3 million proteins that make up a cell. With an approximate cellular volume  $\sim 0.7\mu\text{m}^3$  for *E. Coli*, the most studied model cell system, this results in a cellular environment that is extremely crowded (Figure 1A). For visualization purposes, a recent study used computational modeling to provide a realistic view of the proteome (Figure 1B) and the close proximity between proteins in the cytosol of the cell, as well as the high amount of kinetic energy in the cellular environment that leads to intimate interactions between different proteins (McGuffee, et al. 2010). All of these proteins are employed by the cell to perform highly specific and vital tasks.

For instance, one can focus on the central dogma of biology. Albeit incomplete on its own, the central dogma of biology states that DNA makes RNA, which in turn makes protein. To fulfill this dogma, the cell employs a type of proteins known as enzymes to catalyze biochemical reactions like RNA and protein synthesis. For example, in the

central dogma of biology DNA is transcribed into RNA by the enzyme RNA polymerase. This messenger RNA is then translated into protein by the ribosome enzyme. Many of these enzymes function as molecular motors given that they catalyze biochemical reactions by converting the free energy derived from breaking chemical bonds into mechanical work or motion.

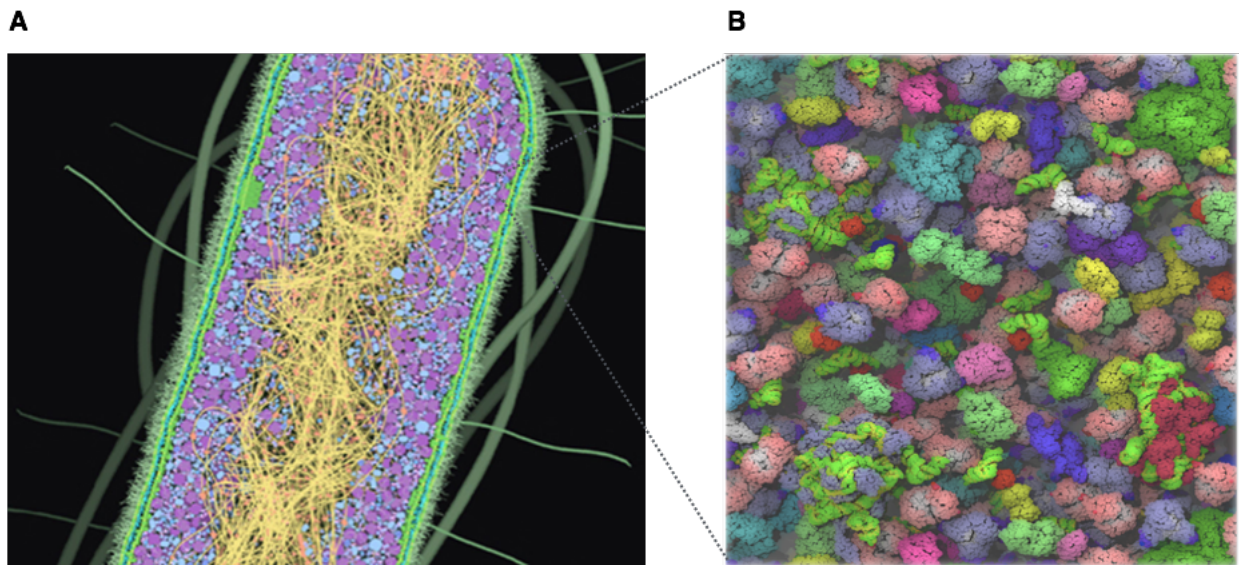


**Figure 1.** (A) Cartoon illustration for a cross-section of an *E. Coli* cell showing the flagella and cell wall (green), cytoplasmic proteins (purple and blue), and DNA (yellow) (image adapted from Goodsell et al. 2009). (B) Visualization of the extremely crowded cellular environment and the intimate contact between cytosolic proteins and nucleic acids (yellow/green) as estimated by a Brownian dynamics simulation (image adapted from McGuffee, et al. 2010).

Perhaps the most common example of this is in enzymes that are dependent on the molecule adenosine triphosphate (ATP) as fuel. ATP dependent molecular motors bind ATP and hydrolyze into adenosine diphosphate (ADP) and inorganic phosphate ( $P_i$ ). Hydrolysis of the phosphoanhydride bond in the ATP molecule releases  $\sim 7.3$  kcal/mol of energy. This chemical energy can be used to power conformational changes that

enzymes use to generate motion or mechanical work. Molecular motors are central players in the majority of cellular tasks across all lifeforms. Apart from their involvement in the central dogma of biology, molecular motors are also involved in proteome maintenance including protein folding (Hayer-Hartl, et al. 2016), transporting cellular cargo across cells (Cho, et al. 2014), unfolding of protein aggregates (DeSantis, et al. 2012), and protein degradation (Bar-Nun, et al. 2012).

From an engineering perspective, molecular motors are analogous to the macroscopic machines we employ in everyday life. While conventional engines, like the internal combustion engine, use fuel to power piston movement (Figure 2A) that can be translated into mechanical force, and ultimately movement, molecular motors use chemical energy to power conformational changes in protein structure that generate work on a substrate (*e.g.* strands of nucleic acids or polypeptides) (Figure 2B). In a motor where movement of a piston is translated into motion of a gear, fuel ignition leads to volume expansion that results in piston displacement. This process requires work. Similarly, molecular motors require work to generate protein movement going from state 0 to 1 in Figure 2B. In comparison to man-made engines, molecular motors are much more efficient. Kinesin, perhaps the best characterized molecular motor, is involved in transporting cellular cargo away from the nucleus of eukaryotic cells (Vale, et al. 2000). Kinesin hydrolyzes a single ATP molecule to generate a fundamental step  $\sim 8.2\text{nm}$  in size (Schnitzer, et al. 1997), and can generate loads up to  $\sim 6\text{pN}$  (Svoboda, et al. 1994), which yields an efficiency  $\sim 60\%$  for converting chemical energy to mechanical work

(Bustamante, et al. 2004). Meanwhile, the internal combustion engine achieves ~20% efficiency given the large amount of energy loss due to friction between surfaces, and heat dissipation (Hugel, et al. 2010). A big difference between man-made and biological machines of course lies in scale. On the microscopic scale that molecular motors function at, the thermal free energy is large and helps overcome the energetic barrier in enzymatic reactions. At the macroscopic scale, man-made engines function at what can be approximated as constant temperature making the free energy from the environment negligible.

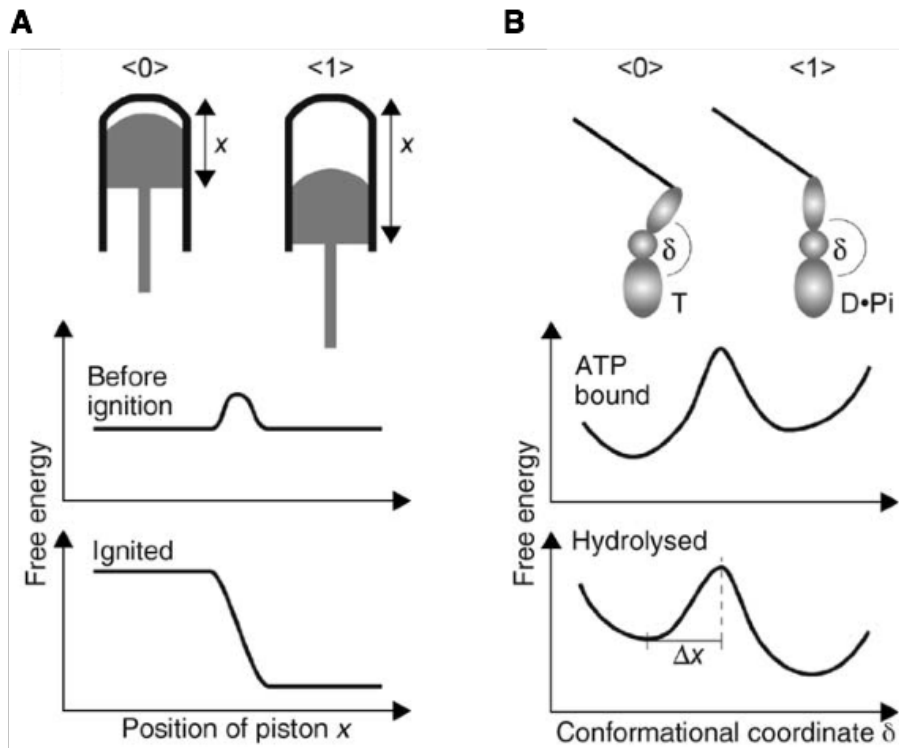


**Figure 2.** Macroscopic engines, such as a two cycle Otto motor, depend on fuel ignition to move a piston from position  $\langle 0 \rangle$  to  $\langle 1 \rangle$  (A). Analogously, microscopic engines, like molecular motors, switch conformations upon ATP hydrolysis (B). Cycles of conformational changes propagate through the protein and generate mechanical motion. Figure adapted from Hugel et al. 2010.

Cells from all lifeforms employ a superfamily of ATP dependent molecular motors referred to as ATPases associated with various cellular activities (AAA+). The majority of AAA+ motors are normally functional as ring-shaped hexamers (Ogura, et al. 2001), where conformational changes in a single subunit propagate around the ring (Hwang, et al. 2013). This biological equivalent of the six-cylinder engine couples nucleotide hydrolysis to conformational changes in the ring that ultimately produce mechanical work on a protein or nucleic acid substrate to accomplish functionally diverse cellular tasks. Some of these tasks include initiating DNA replication by clamp loaders (Davey, et al. 2002), transporting cargo along microtubules by dynein (Cho, et al. 2014), maintaining circadian rhythm by KaiC (Ooijen, et al. 2012), and resolubilizing protein stress-induced aggregates by Hsp104 (DeSantis, et al. 2012). Motors from the AAA+ family contain a conserved ~230 amino acid sequence that forms the ATP binding pocket. Within this sequence, Walker-A and -B, and Sensor-1 and -2 motifs are hallmark structural elements of AAA+ domains that directly interact with the ATP nucleotide (Wendler, et al. 2012). In fact, mutations in Walker-A and -B motifs uncouple a motor's ability to bind or hydrolyze nucleotide, respectively (Hanson, et al. 2005).

Mammalian cells encode ~50-80 different ATPases, and mutations or altered expression of AAA+ motors have been found to be directly and indirectly linked in numerous types of human disease (Ogura, et al. 2001). For example, mutations in dynein and paraplegin are associated with primary ciliary dyskinesia (Omran, et al. 200), and autosomal recessive spastic paraplegia (Casari, et al. 1998), respectively.

Furthermore, underexpression of N-ethylmaleimide-Sensitive Factor (NSF) is associated with schizophrenia and epilepsy (Guan, et al. 2001). Due to their involvement in fundamental cellular processes, AAA+ have become pharmaceutical drug targets (Tao, et al. 2015) (Brötz-Oesterhelt, et al. 2005), and their fundamentals continue to be the focus of basic research.

### **INTRACELLULAR PROTEIN DEGRADATION BY AAA+ PROTEASES**

The densely packed cellular environment (Figure 1A) and the thermal energy in the system result in constant collisions between proteins, unstructured polypeptides and nucleic acids. Proteome maintenance requires the disposal of unneeded or damaged cellular contents to prevent harmful aggregation, and remove functional proteins for regulatory purposes. Prokaryotic and eukaryotic cells both employ a well regulated cycle to control protein degradation, in which AAA+ molecular motors known as proteases catalyze protein destruction. While protein folding and unfolding are reversible reactions, the degradation reaction is an irreversible one by nature. Much like trying to piece together a shattered glass bottle, once a polypeptide chain has been cleaved into small fragments putting them back together is not possible. Remaking a protein or polypeptide that has been degraded requires it be re-expressed through the central dogma of biology, which results in high energetic costs for the cell. Furthermore, uncontrolled degradation of cellular contents and proteins can be catastrophic, and self-harmful, thus requiring the degradation process to be carefully regulated.

AAA+ proteases are multifaceted enzyme complexes characterized by the presence of a regulatory ATPase ring that partners with a compartmentalized peptidase (Sauer, et al. 2004). Known AAA+ proteases include ClpAP, ClpCP, ClpXP, ClpYQ, FtsH, Lon, PAN/20S, and 26S proteasome. Common to all of these proteases is a stacked ring geometry, with radial pore symmetry, between the unfoldase and barrel-like proteolytic chamber (Figure 4A). Peptidases, like ClpP and 20S, are made up of multiple face-to-face rings and are ATP-independent and thus not molecular motors. These peptidases house a high concentration (hundreds of millimolar) of active sites in the lumen of their barrel-like structure, which cleave peptide bonds when they come in contact with a polypeptide strand. Entrance into this highly destructive area of the peptidase can only be achieved through the central pore of each peptidase ring. These proteases self-compartmentalize since the radial channels are too narrow, normally less than 1 nm, to allow entry of any type of structured polypeptide and therefore only small unstructured sequences can access the active lumen of peptidases (Sauer, et al. 2004). To degrade long and structured polypeptides, the peptidase must partner with an ATP dependent regulatory motor which will not only specifically recognize proteins tagged for degradation, but also unfold the protein and spool the unstructured polypeptide into the peptidase for fragmentation (Figure 3). In this manner, the highly destructive active sites within the proteolytic barrel are only employed on substrates that have been selectively transferred to it.

The AAA+ regulatory enzymes, like ClpX and PAN, are ring structures formed by multiple ATPase modules. These motors recognize proteins tagged for degradation by binding specific peptide sequences, referred to as degrons, in unstructured portions of proteins like the N or C termini. Degrons can be naturally encoded as part of a protein, or appended postrationally. A well characterized degron motif is the eleven amino acid long SsrA tag, which is appended to the C-terminus of partially synthesized proteins during ribosome stalling (Keiler, et al. 1996). Engagement of degrons is carried out by pore-loops that extrude toward the radial pore of the AAA+ ring, and can be facilitated by adaptor proteins (Wah, et al. 2003).

Upon engaging a folded substrate, the AAA+ ring will undergo cycles of ATP binding and hydrolysis to mechanically pull the folded structure against that narrow pore of the ATPase ring (Figure 3). The majority of pulling events are normally unsuccessful in unfolding the protein, however a single pulling event can stochastically achieve unfolding of the substrate (Martin, et al. 2005). Once unfolded, the polypeptide is translocated through the central channel of the ATPase ring and into the lumen of the peptidase for degradation (Figure 3). A well characterized portion of this reaction includes substrate release after repeated cycles of unsuccessful unfolding. This is likely a mechanism by which AAA+ proteases can prevent mechanical clogging or trapping of the motor in a futile task that is energetically costly (Kenniston, et al. 2004).



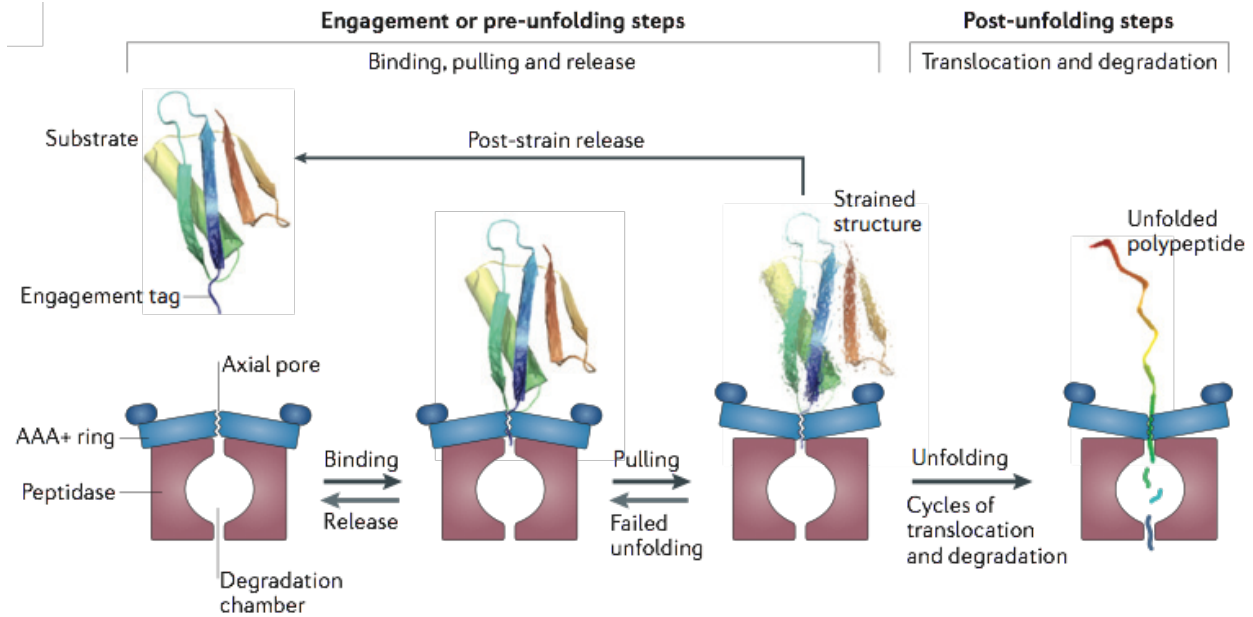


**Figure 3.** Minimal model for protein degradation by AAA+ proteases. A substrate tagged for degradation is first recognized by the axial pores of the AAA+ ring. In order to unfold the substrate, cycles of ATP dependent mechanical pulling are repeated until protein denaturation is achieved. If unfolding is unsuccessful, the substrate can be released to prevent motor stalling. Once unfolding occurs, the unstructured polypeptide is translocated into the peptidase where it is fragmented into short sequences. Figure adapted from (Olivares, et al. 2016).

A main difference between the various AAA+ proteases is that each of them will only recognize particular degradation tags, and in the case of the eukaryotic 26S proteasome the degradation tag is not a short peptide sequence, but rather the protein ubiquitin (Baker, et al. 2006). Thus, each AAA+ protease will only degrade specific proteins. Further differences between AAA+ proteases include the number of rings that make up the unfoldases. For example, ClpX, Pan and Lon form single hexameric rings while ClpA, FtsH and ClpC form two stacked rings (Olivares, et al. 2016). The mechanistic differences between single and double ring unfoldases have been well characterized for ClpX and ClpA. Olivares and coworkers observed ClpAP degrades protein substrates,

including titin<sup>127</sup> domains and GFP, ~3-fold faster than ClpXP although the velocity at which the unfolded polypeptide is translocated into ClpP is ~30% slower for ClpAP than ClpXP due to a smaller size of translocation steps (Olivares, et al. 2014). Thus, by encoding multiple AAA+ proteases, each with varying capabilities, the cell can employ specific proteases to ensure particular substrates are robustly removed. Investigating the mechanism of how this unfolding and translocation reactions are achieved by ClpXP protease is a major goal of the work presented in this thesis, and the ClpXP protease is introduced in the section below.

## **THE ClpXP PROTEASE**

One of the best characterized AAA+ motor systems is the ClpXP protease. ClpXP is largely involved in cytosolic protein degradation in bacteria, while in eukaryotes it is mostly active in mitochondria (Baker, et al. 2012). Recent studies suggest that apart from proteolysis, ClpXP is involved in mitochondrial energy metabolism (Fischer, et al. 2015). As a chaperone, ClpX was found to indirectly regulate heme biosynthesis in eukaryotes (Kardon, et al. 2015). In some bacteria ClpXP is an essential enzyme and therefore a pharmaceutical target for drug development. Acyldepsipeptides small molecule drugs have been used to target ClpP from *M. tuberculosis*, which cause entry pores of the peptidase to widen thereby allowing uncontrolled entry of any nascent and unfolded proteins it encounters into the proteolytic lumen (Brötz-Oesterhelt, et al. 2005). When these drugs are combined with antibiotics targeting RNA polymerase, even otherwise drug-resistant biofilms are destroyed (Conlon, et al. 2013).

Structurally, the ClpXP protease from *E. coli* is made up of the ClpX ATPase and the ClpP peptidase (Figure 4B). The ClpX ring consists of six identical subunits (Figure 4C-D), ~46 kDa in size, each of which contains an AAA+ conserved ATPase module and can therefore bind and hydrolyze ATP. The ATPase module, also referred to as the nucleotide binding pocket, can be thought of as a hinge connecting the large and small domain of a ClpX subunit. In the presence of nucleotide, ClpX subunits self-assemble into a ring structure where two main types of subunit orientations are observed. Crystal structures reveal the majority of subunits are in a loadable conformation (referred to as L subunits) where the nucleotide binding pocket is accessible and able to bind nucleotide. Interestingly, a minority of subunits are observed to be in an unloadable conformation (U subunit) in which the small domain is rotated ~80° about the hinge, which in turn makes the nucleotide binding pocket inaccessible to ATP (Glynn, et al. 2010). Thus, although identical in sequence, ClpX subunits switch between L and U conformations suggesting the ClpX ring is dynamic and flexible. Notably, experiments have shown ClpX can translocate multiple polypeptides that have been covalently crosslinked (Burton, et al. 2001).

Each ClpX subunit contains several different types of flexible loops that are used to recognize tagged substrates, grip the polypeptide track, and bind ClpP. Specifically, at the ClpX pore entrance RKH loops are positively charged and vital to degron recognition. Lining the ClpX pore are YVG loops that grip the substrate through non-specific van der Waals interactions and couple changes in subunit conformation to the

application of force on the polypeptide (Iosefson, et al. 2015). Another set of unstructured loops termed pore-2 loops and IGF loops are used to specifically stabilize the ClpX ring atop ClpP (Martin, et al. 2007).

The ClpP protease is formed by two stacked seven membered rings (Figure 4A & D). Each of the fourteen ClpP subunits, ~23 kDa in size, contain the catalytic triad Ser-His-Asp that cleave peptide bonds into fragments of ~10 residues. The stacked double rings form an active lumen ~5 nm in diameter, containing a local concentration of the active sites ~350mM, such that any polypeptide that is transferred into ClpP is quickly degraded (Baker, et al. 2012). Egress of degradation products from ClpP is thought to occur through transient openings between the two ClpP rings (Sprangers, et al. 2005). ClpX can bind either, or both, of the ClpP rings (Figure 4B) through the interaction of IGF loops of ClpX with a hydrophobic cleft at each ClpP subunit, and the interaction of ClpX pore-2 loops with the N-terminal loops of ClpP subunits (Martin, et al. 2007). The N-terminal loops in ClpP cap entry into the catalytic sites, except for small and unstructured peptides that diffuse through, in the absence of a regulatory partner like ClpX (Bewleya, et al. 2009). Binding of pore-2 and N-terminal loops not only co-aligns the radial pores of both rings, but also widens the ClpP pore size and creates a central channel for substrate processing (Baker, et al. 2012).

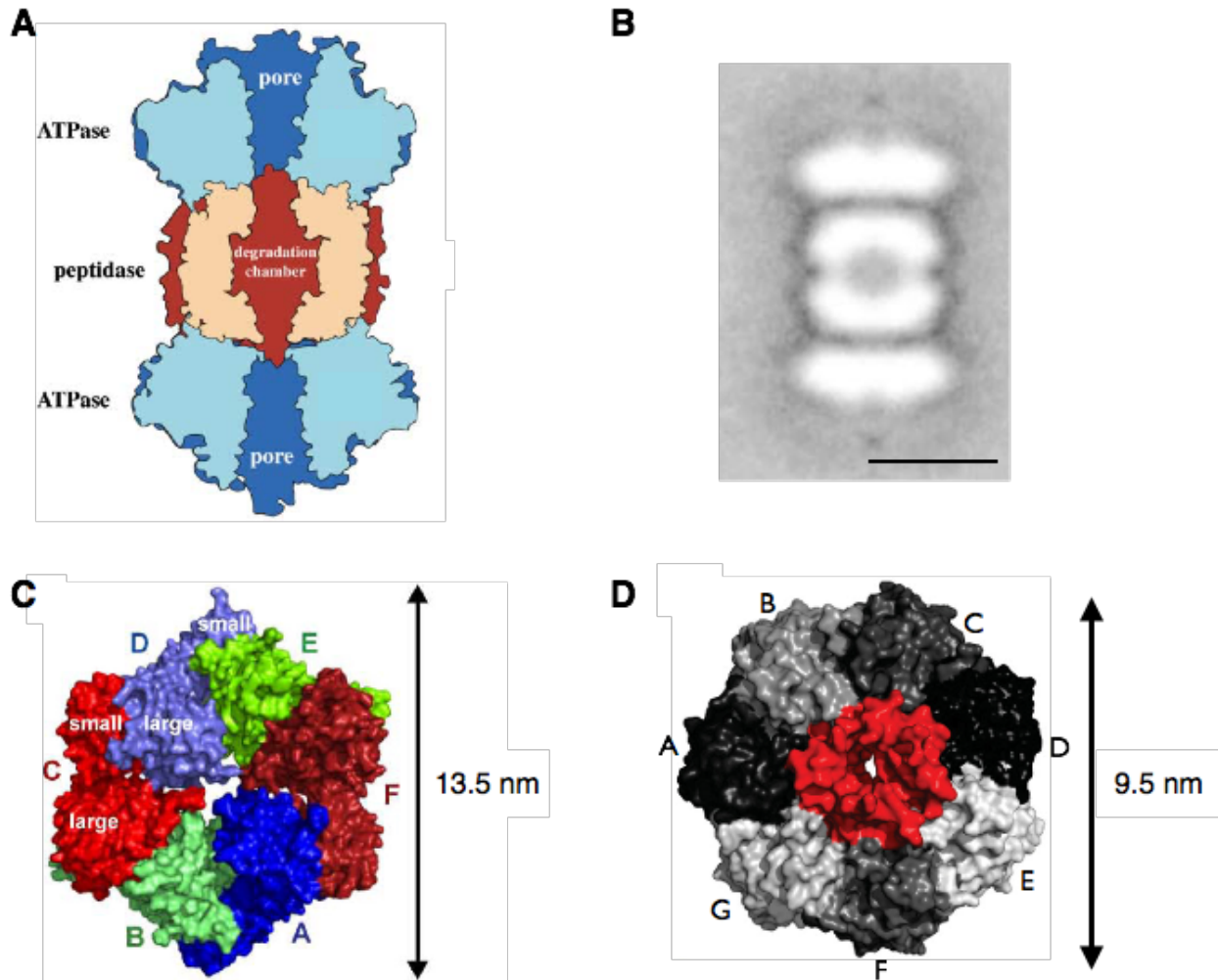


**Figure 4.** (A) Cartoon representation of the characteristic stacked ring assembly of AAA+ proteases. ATPase rings sit atop either interface of the peptidase, thereby controlling access into the degradation chamber (image adapted from Sauer, et al. 2004) (B) Electron micrograph of a pre-assembled ClpXP motor, where separate ClpX rings cap each side of the ClpP barrel. The size bar is 10nm (image adapted from Ortega et al. 2000). (C) Surface representation of the ClpX crystal structure (PDB entry 3HWS) color coded by subunit. Each ClpX subunit is formed by a large and small AAA+ domain, and at its widest the ClpX ring diameter is ~13.5nm (image adapted from Glynn et al. 2010). (D) Top down view of the ClpP heptameric ring (PDB entry 1YG6) color coded by subunit, with N-terminal pore-loops shown in red. The ClpP ring diameter is ~9.5nm (image adapted from Baker et al. 2012).

With more than 100 known substrates, ClpXP must be able to degrade proteins with varying stability. Previous biochemical experiments on ClpXP degradation of *ssrA*

tagged titin<sup>I27</sup> domains show a substrate stability dependence on the degradation kinetics and the ATP consumption. Kenniston and colleagues found unfolding of wild type titin<sup>I27</sup> domains by ClpXP requires hydrolysis of more than 500 ATPs, while translocation of the unfolded polypeptide requires about 100 ATPs. Contrastingly, as ClpXP encountered ssrA-titin<sup>V13P</sup> domains, a mechanically unstable substrate, an average of only 18 ATPs were used for unfolding (Kenniston, et al. 2003). Given the intimate contact between neighboring subunits, the unfolding and translocation mechanism may be a complex coordination of these six subunits.

Although single subunits self assemble into hexameric rings *in vivo*, Martin and coworkers developed a novel ClpX variant in which individual subunits were covalently linked by an unstructured loop (Martin, et al. 2005). This single chain ClpX ring was measured to hydrolyze ATP and degrading protein substrates at rates highly similar to those of wild type ClpX. A big advantage of a single chain ClpX variant is that it provides a chassis to investigate the effect of single subunits on the overall function of the ClpX ring. For example, biochemical studies have shown specific mutations can disturb functionality in a subunit, allowing investigation of ClpX hexamers with reduced number of wild-type subunits. ClpX mutants with as little as a single wild type subunit are capable of unfolding and translocating substrates in biochemical studies, suggesting a power stroke from a single ClpX subunit is sufficient for activity, albeit with slower kinetics (Martin, et al. 2005). Similarly, by covalently stapling individual subunits, Stinson

and coworkers showed U-L transitions are not required to power ATP hydrolysis, but they are vital for robust degradation (Stinson, et al. 2015).

Furthermore, a single chain ClpX variant allowed for protein engineering to introduce molecular and fluorescent tags, as well as for studying ClpXP function at the single molecule level (Shin, et al. 2009) where normally the concentrations (picoMolar) required for these experiments would have been too low to keep ClpX rings from disassembling. Recently, substrate degradation by single ClpXP motors was observed using optical tweezers to monitor unfolding and degradation of substrates including polyproteins of filamin and GFP (Aubin-Tam, et al. 2011) (Maillard, et al. 2011) (Sen, et al. 2013). These studies confirmed ClpXP uses a power stroke mechanism capable of generating more than 3 kcal/mol of work, and estimated a stall force for motor function near 30 pN. The translocation velocity of unfolded polypeptides into ClpP was found to decrease with load, with a calculated velocity under no load of 30 amino acids per second. In this thesis, we build on this work by using and developing single molecule techniques to probe the mechanochemical cycle of ClpXP activity, as well as monitor the conformational changes and nucleotide transactions during protein degradation.

## **SINGLE MOLECULE TECHNIQUES**

Ensemble biochemical experiments measure the behavior of millions of cells, and therefore provide highly averaged measurements that can obscure important molecular behavior. Advances in optics and photonics technology have paved the way for the

development of high-resolution techniques capable of tracking behavior from single molecules. Single molecule techniques are widely used in the field of biophysics, and normally belong to either force or fluorescence spectroscopy techniques. For example, atomic force microscopy (AFM), magnetic tweezers, and optical tweezers can impart forces across an object to probe force dependent bioreactions like protein folding/unfolding (Ritchie, et al. 2015), biopolymer stretching (Khalil, et al. 2007), and organelle transport (Schnitzer, et al. 1997).

The achievable force magnitudes, position resolution, rates of dynamic force control, and measurement throughput vary depending on the technique (Neuman, et al. 2008). For example, by imparting a magnetic field over a broad area ( $>100\mu\text{m}^2$ ), magnetic tweezers measurements can be multiplexed for high throughput data acquisition of single molecule interactions. Contrastingly, AFM and optical tweezers are usually limited to individual measurements, albeit with very high position resolution (Marszalek, et al. 1999). Thus, choosing a specific force spectroscopy technique over another largely depends on the question under investigation. For investigation of protein folding landscape, optical traps and AFM are widely used due to their well controlled force application and their high resolution (Stigler, et al. 2011). For experiments probing protein binding to DNA, RNA, or protein tethers often magnetic tweezers, or fluid flow, are sufficient to set tension across these biopolymers to investigate protein binding interactions (Collins, et al. 2014).



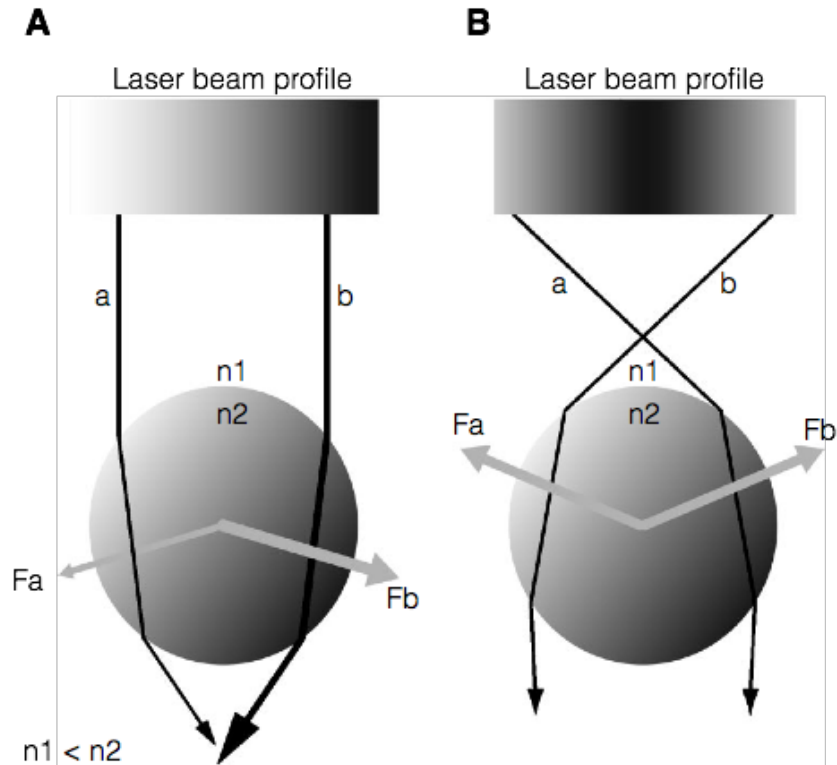


**Figure 5.** (A) Simplified ray optic description of the gradient force. For a beam of light with an intensity profile that increases from left to right, refraction of high intensity light will generate a larger gradient force ( $F_b$ ) than that of lower intensity light ( $F_a$ ) from the beam periphery. This force will push the bead down and to the right. (B) An optical trap is formed by a focusing a Gaussian beam to a diffraction limited spot. Here, a dielectric particle experiences gradient forces toward the high photon flux of the beam focus. Thus, the dielectric object is said to be trapped since repositioning of the beam focus results in concomitant bead movement. The bead is slightly above the focus due to scattering. Image based on (Neuman, et al. 2004).

In this thesis, we use optical trapping to probe protein degradation by the ClpXP molecular motor. Optical traps are some of the most widely used tools in single molecule biophysics due to the fact that they can generate piconewton forces, and track sub-nanometer displacements in real time. Given the fact that light has momentum, seminal work by Ashkin observed that when microscopic objects in solution come in contact with a beam of light they are pushed away in the same direction as the

propagation of the laser beam (A. Ashkin 1970). Interestingly, Ashkin and Chu later showed that when a laser beam is focused by a lens, dielectric particles are attracted towards the light focus due to a gradient force from photons that diffract through the transparent object (Ashkin, et al. 1986). This behavior can be understood using a simplified ray optics diagram for the interaction of a dielectric particle and a beam of light as described in Figure 5. When a biomolecule of interest is tethered between a trapping handle and a second surface, like a coverslip or another trapped object, optical force can be applied across the tether. By displacing the trapped bead from the focus, exquisite control of force magnitudes can be achieved given that the optical trap behaves as a Hookean spring at small displacements from the trap center (Neuman, et al. 2004).

Optical traps are by and large custom-built instruments employing somewhat complex optical arrangements. The layout of an optical trapping instrument is shown in Figure 6. While many designs have been developed, a few principles remain constant for optical trapping instruments. First, a high numerical aperture objective (normally  $NA > 1.2$ ) is used to focus a laser beam into a diffraction limited spot near the sample plane. In order to steer the position of the trap acousto-optic deflectors (AODs), picomirrors, or other steerable optics can be used. To detect movement of a trapped handle a video camera can be used, or scattered trapping photons can be imaged onto a photodetector. Another strategy images scattered photons from a separate laser used for detection in an interferometry approach.

High intensity lasers with low power fluctuations, and high pointing stabilities, must be used to achieve high resolution. Normally, laser power outputs are capable of reaching ~10W, although less than 1-2W actually reach the sample plane of the instrument. While any laser wavelength can be used to generate an optical trap, normally infrared lasers have been employed for biophysical measurements. This is due to the fact that biological buffers and systems are largely water based, and absorption of light by water and proteins is minimized at wavelength of ~750-1200nm (Svoboda, et al. 1994). Thus, a common wavelength for trapping lasers is 1062nm, and for instruments that employ low power detection beams normally 800-1000nm wavelengths are used. This not only minimizes phototoxicity and sample heating on biological systems, but it also leaves the visible spectrum ( $\lambda \sim 400-800\text{nm}$ ) open for fluorescence approaches.

While the majority of optical trapping experiments prove the mechanics of proteins and molecular motors in the order of picoNewtons (Fazal, et al. 2011), in some cases protein monomers self-assemble into aggregates that are able to withstand more than 200pN of force without disassembling (Dong, et al. 2010). For these systems, optical traps are hard pressed to generate high enough forces to fully characterize their dynamics. These mechanically stable protein aggregates have been identified as hallmarks of neurodegenerative disease making them high interest targets for study and pharmaceutical targeting (Narayan, et al. 2014). To study these, and other, stable structures recent development of trapping handles with enhanced trapping stability

provide a promising avenue to expand the force ranges that can be achieved using optical traps (Jannasch, et al. 2012).

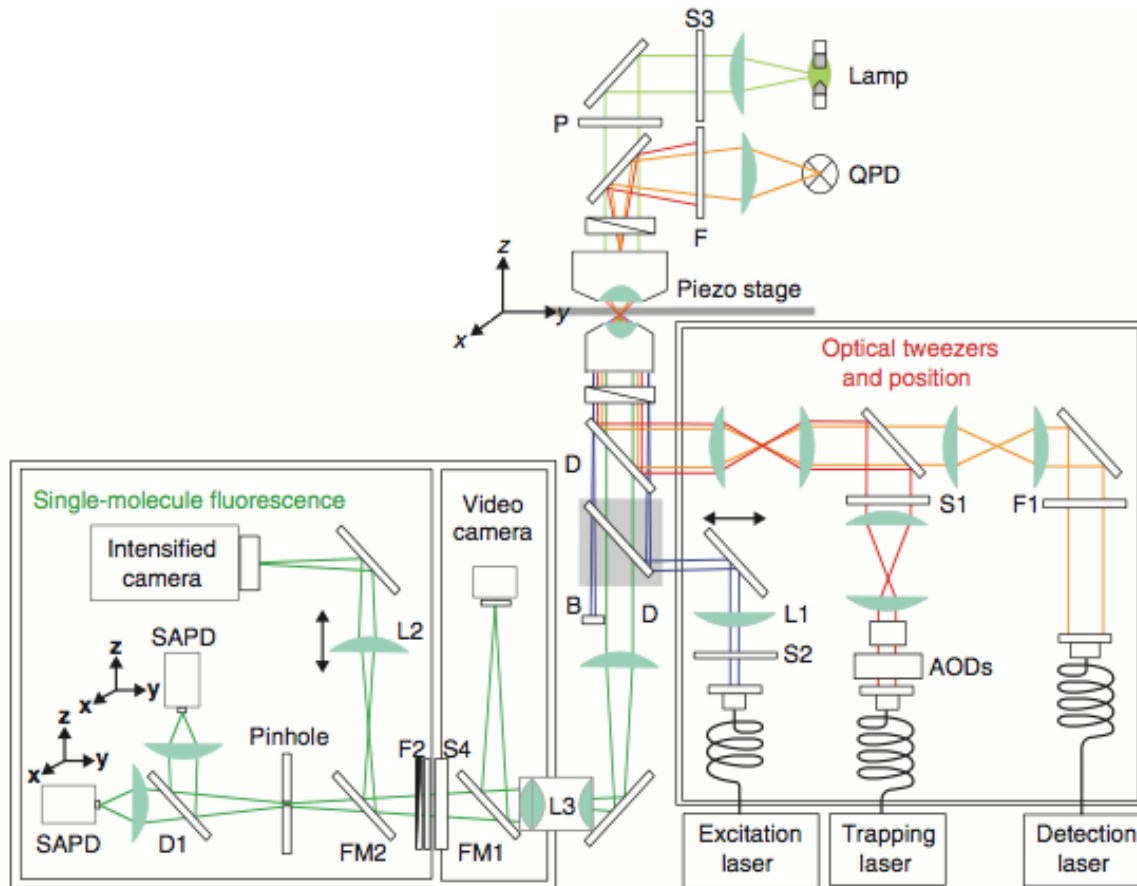


**Figure 6.** Sample optical layout of an optical tweezers instrument outfitted with a fluorescence branch. The trapping laser is expanded to overfill the back-aperture of a high numerical aperture objective. The trapping beam is focused at the sample stage, and can be steered using acousto-optic deflectors (AODs). A low power detection laser is used to monitor displacement of a trapped object by measuring scattered photons using a quadrant photodiode (QPD). A lamp provides brightfield illumination that is imaged by a video camera. Additionally, this instrument design incorporates objective-side TIRF illumination for fluorescence measurements. Fluorescence emission can be imaged by an intensified camera, or by separate silicon avalanche photodiodes (SAPD) with a confocal pinhole. The additional labels correspond to L-lens, S-shutter, F-filter, P-polarizer D-dichroic mirror, B-beam block, FM-flipper mirror. Figure adapted from Lang et al. 2003.

The next generation of biophysical assays employing optical traps will largely benefit from the addition of fluorescence capabilities. Single molecule fluorescence provides an avenue to measure nanoscale structural changes using fluorescence tools like fluorescence resonance energy transfer (FRET) (Tarsa, et al. 2007), and single molecule fluorescence quenching (Zhou, et al. 2011). Single molecule fluorescence experiments normally employ confocal or total internal reflection fluorescence (TIRF) illumination schemes to minimize background signal from dyes in solution. Seminal work combining optical trapping and fluorescence has shown the powerful tool it can become (Ishijima, et al. 1998) (Lang, et al. 2003), as well as some of the challenges involved. For example, the instruments can require many optics and components that are challenging to build but are necessary to control the assembly of the assay (a sample optical layout is shown in Figure 6). Additionally, fluorescence from a single fluorophore can be hard to measure since its intensity is more than ten orders of magnitude smaller than that of an optical trap (Lang, et al. 2003). Similarly, fluorophores are known to photobleach faster when in close proximity to an optical trap (Dijk, et al. 2004). For a thorough discussion of combined force-fluorescence approaches, the reader is referred to our review on the subject (Cordova, et al. 2014).

## REFERENCES

Ashkin, A., J. M. Dziedzic, J. E. Bjorkholm, and Steven Chu. "Observation of a single-beam gradient force optical trap for dielectric particles." *Optics Letters*, 1986: 288-290.

Ashkin, Arthur. "Acceleration and Trapping of Particles by Radiation Pressure." *Physical Review Letters*, 1970: 156-159.

Aubin-Tam, Marie-Eve, Adrian O. Olivares, Robert T. Sauer, Tania A. Baker, and Matthew J. Lang. "Single-Molecule Protein Unfolding and Translocation by an ATP-Fueled Proteolytic Machine." *Cell*, 2011: 257–267.

Baker, Tania A, and Robert T Sauer. "ATP-dependent proteases of bacteria: recognition logic and operating principles." *Trends in Biochemical Sciences*, 2006: 647–653.

Baker, Tania A, and Robert T Sauer. "ClpXP, an ATP-powered unfolding and protein-degradation machine." *Biochimica et Biophysica Acta (BBA) - Molecular Cell Research*, 2012: 15-28.

Bar-Nun, Shoshana, and Michael H. Glickman. "Proteasomal AAA-ATPases: Structure and function." *Biochimica et Biophysica Acta (BBA) - Molecular Cell Research*, 2012: 67-82.

Bewleya, Maria C., Vito Grazianob, Kathleen Griffina, and John M. Flanagan. "Turned on for degradation: ATPase-independent degradation by ClpP." *Journal of Structural Biology*, 2009: 118-125.

Conlon, et al. "Activated ClpP kills persisters and eradicates a chronic biofilm infection." *Nature*, 2013: 365-370.

Brötz-Oesterhelt, Heike, et al. "Dysregulation of bacterial proteolytic machinery by a new class of antibiotics." *Nature Medicine*, 2005: 1082-1087.

Brau, Ricardo R., Peter B. Tarsa, Jorge M. Ferrer, Peter Lee, and Matthew J. Lang. "Interlaced Optical Force-Fluorescence Measurements for Single Molecule Biophysics." *Biophysical Journal*, 2006: 1069-1077.

Burton, Randall E., Samia M. Siddiqui, Yong-In Kim, Tania A. Baker, and Robert T. Sauer. "Effects of protein stability and structure on substrate processing by the ClpXP unfolding and degradation machine." *The EMBO Journal*, 2001: 3092-3100.

Burton, Randall E., Tania A. Baker, and Robert T. Sauer. "Energy-dependent degradation: Linkage between ClpX-catalyzed nucleotide hydrolysis and protein-substrate processing." *Protein Science*, 2003: 893-902.

Bustamante, Carlos, Yann R. Chemla, Nancy R. Forde, and David Izhaky. "Mechanical Processes in Biochemistry." *Annual Reviews in Biochemistry*, 2004: 705-748.

Casari, Giorgio, et al. "Spastic Paraplegia and OXPHOS Impairment Caused by Mutations in Paraplegin, a Nuclear-Encoded Mitochondrial Metalloprotease." *Cell*, 1998: 973-983.

Castro, Carlos E., Jijun Dong, Mary C. Boyce, Susan Lindquist, and Matthew J. Lang. "Physical Properties of Polymorphic Yeast Prion Amyloid Fibers." *Biophysical Journal* 101, no. 2 (2011): 439-448.

Cho, Carol, and Ronald D. Vale. "The mechanism of dynein motility: Insight from crystal structures of the motor domain." *Biochimica et Biophysica Acta (BBA) - Molecular Cell Research*, 2014: 182-191.

Collins, Bridget E, Ling F Ye, Daniel Duzdevich, and Eric C Greene. "DNA curtains: Novel tools for imaging protein-nucleic acid interactions at the single-molecule level." *Methods in Cell Biology*, 2014: 217-234.

Cordova, Juan Carlos, Dibyendu Kumar Das, Harris W Manning, and Matthew J Lang. "Combining single-molecule manipulation and single-molecule detection." *Current Opinion in Structural Biology*, 2014: 142-148.

Cordova, Juan Carlos, et al. "Stochastic but highly coordinated protein unfolding and translocation by the ClpXP proteolytic machine." *Cell*, 2014: 647-658.

Crisalli, Pete, and Eric T. Kool. "Multi-Path Quenchers: Efficient Quenching of Common Fluorophores." *Bioconjugate Chemistry*, 2011: 2345-2354.

Davey, Megan J., David Jeruzalmi, John Kuriyan, and Mike O'Donnell. "Motors and switches: AAA+ machines within the replisome." *Nature Reviews Molecular Cell Biology*, 2002: 826-835.

DeSantis, Morgan E., and James Shorter. "The elusive middle domain of Hsp104 and ClpB: Location and function." *Biochimica et Biophysica Acta (BBA) - Molecular Cell Research*, 2012: 29-39.

Dijk, Meindert A. van, Lukas C. Kapitein, Joost van Mameren, Christoph F. Schmidt, and Erwin JG Peterman. "Combining Optical Trapping and Single-Molecule Fluorescence Spectroscopy: Enhanced Photobleaching of Fluorophores." *Journal of Physical Chemistry B*, 2004: 6479-6484.

Dong, Jijun, Carlos E Castro, Mary C Boyce, Matthew J Lang, and Susan Lindquist. "Optical trapping with high forces reveals unexpected behaviors of prion fibrils." *Nature Structural & Molecular Biology*, 2010: 1422-1430.

Fazal, Furqan M, and Steven M Block. "Optical tweezers study life under tension." *Nature Photonics* 5 (2011): 318-321.

Ferrer, Jorge M., D. Fangyuan, Ricardo R. Brau, Peter B. Tarsa, and Matthew J. Lang. "IOFF Generally Extends Fluorophore Longevity in the Presence of an Optical Trap." *Current Pharmaceutical Biotechnology*, 2009: 502-507.

Fischer, Fabian, Julian D. Langer, and Heinz D. Osiewacz. "Identification of potential mitochondrial CLPX protease interactors and substrates suggests its central role in energy metabolism." *Scientific Reports*, 2015: 18375.

Funatsu, Takashi, et al. "Imaging and nano-manipulation of single biomolecules." *Biophysical Chemistry*, 1997: 63-72.

Glynn, Steven E, Andrew R Nager, Tania A Baker, and Robert T Sauer. "Dynamic and static components power unfolding in topologically closed rings of a AAA plus proteolytic machine." *Nature Structural & Molecular Biology*, 2012: 616-622.

Glynn, Steven E., Andreas Martin, Andrew R. Nager, Tania A. Baker, and Robert T. Sauer. "Crystal structures of asymmetric ClpX hexamers reveal nucleotide-dependent motions in a AAA+ protein-unfolding machine." *Cell*, 2010: 744-756.

Goodsell, David S. "Miniseries: Illustrating the Machinery of Life ." *Biochemistry and Molecular Biology Education*, 2009: 325–332 .

Guan, Zhuo, et al. "A spontaneous recurrent seizure-related Rattus NSF gene identified by linker capture subtraction." *Molecular Brain Research*, 2001: 117-123.

Hanson, Phyllis I., and Sidney W. Whiteheart. "AAA+ proteins: have engine, will work." *Nature Reviews Molecular Cell Biology*, 2005: 519-529.

Hayer-Hartl, Manajit, Andreas Bracher, and F. Ulrich Hartl. "The GroEL–GroES Chaperonin Machine: A Nano-Cage for Protein Folding." *Trends in Biochemical Sciences*, 2016: 62-76.

Hugel, Thorsten, and Christina Lumme. "Bio-inspired novel design principles for artificial molecular motors." *Current Opinion in Biotechnology*, 2010: 683-689.

Hwang, Wonmuk, and Matthew J Lang. "Nucleotide-dependent control of internal strains in ring-shaped AAA+ motors." *Cellular and Molecular Bioengineering*, 2013: 65-73.

Iosefson, Ohad, Adrian O. Olivares, Tania A. Baker, and Robert T. Sauer. "Dissection of Axial-Pore Loop Function during Unfolding and Translocation by a AAA+ Proteolytic Machine." *Cell Reports*, 2015: 1032-1041.

Iosefson, Ohad, Andrew R Nager, Tania A Baker, and Robert T Sauer. "Coordinated gripping of substrate by subunits of a AAA+ proteolytic machine." *Nature Chemical Biology*, 2015: 201-206.

Ishijima, Akihiko, et al. "Simultaneous observation of individual ATPase and mechanical events by a single myosin molecule during interaction with actin." *Cell*, 1998: 161-171.



Jang, Kyung-Jin, and Jwa-Min Nam. "Direct-Write Nanoparticle Microarrays for Cell Assays." *Small*, 2008: 1930-1935.

Jannasch, Anita, Ahmet F. Demirörs, Peter D. J. van Oostrum, Alfons van Blaaderen, and Erik Schäffer. "Nanonewton optical force trap employing anti-reflection coated, high-refractive-index titania microspheres." *Nature Photonics*, 2012: 469-173.

Kakahara, Yoshito, and Walid A. Houry. "The R2TP complex: Discovery and functions." *Biochimica et Biophysica Acta (BBA) - Molecular Cell Research*, 2012: 101-107.

Kardon, Julia R., et al. "Mitochondrial ClpX activates a key enzyme for heme biosynthesis and erythropoiesis." *Cell*, 2015: 858–867.

Keiler, Kenneth C., Patrick R. H. Waller, and Robert T. Sauer. "Role of a peptide tagging system in degradation of proteins synthesized from damaged messenger RNA." *Science*, 1996: 990-993.

Kenniston, Jon A., Tania A. Baker, and Robert T. Sauer. "Partitioning between unfolding and release of native domains during ClpXP degradation determines substrate selectivity and partial processing." *Proceedings of the National Academy of Sciences*, 2004: 1390-1395.

Kenniston, Jon A., Tania A. Baker, Julio M. Fernandez, and Robert T. Sauer. "Linkage between ATP Consumption and Mechanical Unfolding during the Protein Processing Reactions of an AAA+ Degradation Machine." *Cell*, 2003: 511–520.

Khalil, Ahmad S., et al. "Single M13 bacteriophage tethering and stretching." *Proceedings of the National Academy of Sciences*, 2007: 4892-4897.

Kim, Young-Chan, Aaron Snoberger, Jane Schupp, and David M. Smith. "ATP binding to neighbouring subunits and intersubunit allosteric coupling underlie proteasomal ATPase function." *Nature Communications*, 2015: 1-13.

Lang, Matthew J, Polly M Fordyce, and Steven M Block. "Combined optical trapping and single-molecule fluorescence." *Journal of Biology*, 2003: 2-6.

Lang, Matthew J, Polly M Fordyce, Anita M Engh, Keir C Neuman, and Steven M Block. "Simultaneous, coincident optical trapping and single-molecule fluorescence." *Nature Methods*, 2004: 133-139.

Lang, Matthew J., Charles L. Asbury, Joshua W. Shaevitz, and Steven M. Block. "An Automated Two-Dimensional Optical Force Clamp for Single Molecule Studies." *Biophysical Journal*, 2002: 491-501.

Maillard, Rodrigo A., et al. "ClpX(P) generates mechanical force to unfold and translocate its protein substrates." *Cell*, 2011: 459-469.

- Marszalek, Piotr E., et al. "Mechanical unfolding intermediates in titin modules." *Nature*, 1999: 100-103.
- Martin, Andreas, Tania A. Baker, and Robert T. Sauer. "Distinct Static and Dynamic Interactions Control ATPase-Peptidase Communication in a AAA+ Protease." *Molecular Cell*, 2007: 41–52.
- Martin, Andreas, Tania A. Baker, and Robert T. Sauer. "Rebuilt AAA + motors reveal operating principles for ATP-fuelled machines." *Nature*, 2005: 1115-1120.
- McGuffee, Sean R., and Adrian H. Elcock. "Diffusion, Crowding & Protein Stability in a Dynamic Molecular Model of the Bacterial Cytoplasm." *PLOS Computational Biology*, 2010: e1000694.
- McKinney, Sean A., Chirlmin Joo, and Taekjip Ha. "Analysis of Single-Molecule FRET Trajectories Using Hidden Markov Modeling." *Biophysical Journal*, 2006: 1941-1951.
- Narayan, Priyanka, Sepehr Ehsani, and Susan Lindquist. "Combating neurodegenerative disease with chemical probes and model systems." *Nature Chemical Biology*, 2014: 911-920.
- Neuman, Keir C, and Attila Nagy. "Single-molecule force spectroscopy: optical tweezers, magnetic tweezers and atomic force microscopy." *Nature Methods*, 2008: 491-505.
- Neuman, Keir C, and Steven M Block. "Optical Trapping." *Review of Scientific Instruments*, 2004: 2787-2809.
- Ogura, Teru, and Anthony J Wilkinson. "AAA+ superfamily ATPases: common structure—diverse function." *Genes to Cells*, 2001: 575-597.
- Olivares, Adrian O, Andrew R Nager, Ohad Iosefson, Robert T Sauer, and Tania A Baker. "Mechanochemical basis of protein degradation by a double-ring AAA+ machine." *Nature Structural & Molecular Biology*, 2014: 871-875.
- Olivares, Adrian O., Tania A. Baker, and Robert T. Sauer. "Mechanistic insights into bacterial AAA+ proteases and protein-remodelling machines." *Nature Reviews Microbiology*, 2016: 33-44.
- Omran, Heymut, et al. "Homozygosity mapping of a gene locus for primary ciliary dyskinesia on chromosome 5p and identification of the heavy dynein chain DNAH5 as a candidate gene." *American Journal of Respiratory Cell and Molecular Biology*, 200: 696-702.
- Ooijen, Gerben van, and Andrew J. Millar. "Non-transcriptional oscillators in circadian timekeeping." *Trends in Biochemical Sciences*, 2012: 484–492.

Ortega, Joaquin, Satyendra K. Singh, Takashi Ishikawa, Michael R. Maurizi, and Alasdair C. Steven. "Visualization of Substrate Binding and Translocation by the ATP-Dependent Protease, ClpXP ." *Molecular Cell*, 2000: 1515-1521.

Ritchie, Dustin B, and Michael T Woodside. "Probing the structural dynamics of proteins and nucleic acids with optical tweezers." *Current Opinion in Structural Biology*, 2015: 43-51.

Sauer, Robert T., et al. "Sculpting the Proteome with AAA+ Proteases and Disassembly Machines." *Cell*, 2004: 9-18.

Schnitzer, Mark J., and Steven M. Block. "Kinesin hydrolyses one ATP per 8-nm step." *Nature*, 1997: 386-390.

Sen, Maya, et al. "The ClpXP Protease Unfolds Substrates Using a Constant Rate of Pulling but Different Gears." *Cell*, 2013: 636-646.

Shin, Yongdae, et al. "Single-molecule denaturation and degradation of proteins by the AAA+ ClpXP protease." *Proceedings of the National Academy of Sciences*, 2009: 19340-19345.

Sprangers, Remco, Anna Gribun, Peter M. Hwang, Walid A. Houry, and Lewis E. Kay. "Quantitative NMR spectroscopy of supramolecular complexes: Dynamic side pores in ClpP are important for product release." *Proceedings of the National Academy of Sciences*, 2005: 16678–16683.

Stigler, Johannes, Fabian Ziegler, Anja Gieseke, J. Christof M. Gebhardt, and Matthias Rief. "The complex folding network of single calmodulin molecules." *Science*, 2011: 512-516.

Stinson, Benjamin M, Vladimir Baytshtok, Karl R Schmitz, Tania A Baker, and Robert T Sauer. "Subunit asymmetry and roles of conformational switching in the hexameric AAA+ ring of ClpX." *Nature Structural & Molecular Biology*, 2015: 411-416.

Stinson, Benjamin M., Andrew R. Nager, Steven E. Glynn, Karl R. Schmitz, Tania A. Baker, and Robert T. Sauer. "Nucleotide binding and conformational switching in the hexameric ring of a AAA+ machine." *Cell*, 2013: 628-639.

Svoboda, Karel, and Steven M Block. "Biological Applications of Optical Forces." *Annual Review of Biophysics and Biomolecular Structure*, 1994: 247-285.

Svoboda, Karel, and Steven M. Block. "Force and velocity measured for single kinesin molecules." *Cell*, 1994: 773–784.

Tao, Shasha, et al. "Withaferin A Analogs That Target the AAA+ Chaperone p97." *ACS Chemical Biology*, 2015: 1916-1924.

Tarsa, Peter B., et al. "Detecting Force-Induced Molecular Transitions with Fluorescence Resonant Energy Transfer." *Angewandte Chemie International Edition* 46, no. 12 (2007): 1999-2001.

Vale, Ronald D., and Ronald A. Milligan. "The Way Things Move: Looking Under the Hood of Molecular Motor Proteins." *Science*, 2000: 88-95.

Wah, David A, Igor Levchenko, Gabrielle E Rieckhof, Daniel N Bolon, Tania A Baker, and Robert T Sauer. "Flexible linkers leash the substrate binding domain of SspB to a peptide module that stabilizes delivery complexes with the AAA+ ClpXP protease." *Molecular Cell*, 2003: 355–363,.

Wendler, Petra, Susanne Ciniawsky, Malte Kock, and Sebastian Kube. "Structure and function of the AAA+ nucleotide binding pocket." *Biochimica et Biophysica Acta (BBA) - Molecular Cell Research*, 2012: 2-14.

Zhou, Ruobo, Simone Kunzelmann, Martin R. Webb, and Taekjip Ha. "Detecting Intramolecular Conformational Dynamics of Single Molecules in Short Distance Range with Subnanometer Sensitivity." *Nano Letters*, 2011: 5482-5488.

## CHAPTER 2

### **Stochastic but highly coordinated protein unfolding and polypeptide translocation by the ClpXP proteolytic machine**

This chapter was published as referenced below:

Cordova, J. C. et al. Stochastic but highly coordinated protein unfolding and translocation by the ClpXP proteolytic machine. *Cell* 158, 647–658 (2014)

#### **ABSTRACT**

ClpXP and other AAA+ proteases recognize, mechanically unfold, and translocate target proteins into a chamber for proteolysis. It is not known if these remarkable molecular machines operate by a stochastic or sequential mechanism or how power strokes relate to the ATP-hydrolysis cycle. Single-molecule optical trapping allows ClpXP unfolding to be directly visualized and reveals translocation steps of ~1-4 nm in length, but how these activities relate to solution degradation and the physical properties of substrate proteins remains unclear. By studying single-molecule degradation using different multi-domain substrates and ClpXP variants, we answer many of these questions and provide evidence for stochastic unfolding and translocation. We also present a mechanochemical model that accounts for single-molecule, biochemical, and structural results, for our observation of enzymatic memory in translocation stepping, for the

kinetics of translocation steps of different sizes, and for probabilistic but highly coordinated subunit activity within the ClpX ring.

## **INTRODUCTION**

AAA+ proteases (ATPases associated with diverse cellular activities) maintain protein quality control in the cell by converting the energy derived from ATP binding and hydrolysis into work that powers mechanical protein unfolding, translocation, and ultimately degradation (Sauer and Baker, 2011). How these destructive enzymes degrade proteins with widely varying sequences, structures, and stabilities is only beginning to be understood. ClpXP, one of the best-characterized members of this family of degradation machines, consists of ClpX, a hexameric AAA+ ATPase, and ClpP, a barrel-shaped peptidase (Baker and Sauer, 2012). Degradation is initiated when the ClpX ring binds a substrate via an unstructured degron, such as the ssrA tag, and attempts to translocate this peptide through its narrow axial pore. For native substrates, degron translocation by ClpX pulls on the folded portion of the protein, driving mechanical denaturation that allows subsequent translocation steps to spool the unfolded polypeptide into ClpP for degradation.

Single-molecule studies, using optical tweezers to monitor ClpXP unfolding and translocation of multi-domain substrates, establish that ClpXP can work against forces of 20 pN or higher, demonstrate that the smallest translocation steps are ~1 nm (~4-8 amino acids), and reveal physical steps that are multiples of this value, resulting from

kinetic bursts of two, three, or four power strokes (Aubin-Tam et al. 2011; Maillard et al., 2011; Sen et al., 2013). Studies of variants containing inactive subunits support a probabilistic mechanism of ATP hydrolysis and mechanical function by ClpXP (Martin et al., 2005), but this model is not firmly established, and a related AAA+ protease has been proposed to operate by a sequential mechanism (Smith et al., 2011). At present, it is not known how the physical properties of native and unfolded substrates affect the kinetics of single-molecule ClpXP unfolding and translocation or if these reactions account for solution-degradation rates. Moreover, no current model satisfactorily explains how the ClpX ring generates translocation steps of different sizes, accounts for the kinetics of unfolding and translocation, or explains the linkage between ATP consumption and these mechanical reactions. Any deep understanding of AAA+ proteases and related remodeling machines requires answers to these questions.

Here, we use optical trapping to assay single-molecule ClpXP unfolding and translocation of substrates consisting of domains with varying stabilities and sequences. We find that ClpXP unfolds most domains by a single pathway, with kinetics that depend on the native fold and structural stability. Subsequent translocation or pausing occurs at rates that vary with the sequence of the unfolded substrate. During translocation, ClpXP does not exhibit a sequential pattern of step sizes, supporting a fundamentally stochastic reaction, but a mechanism of enzymatic memory results in short physical steps being more probable after short steps and longer physical steps being more likely after longer steps, allowing the enzyme to run at different speeds.

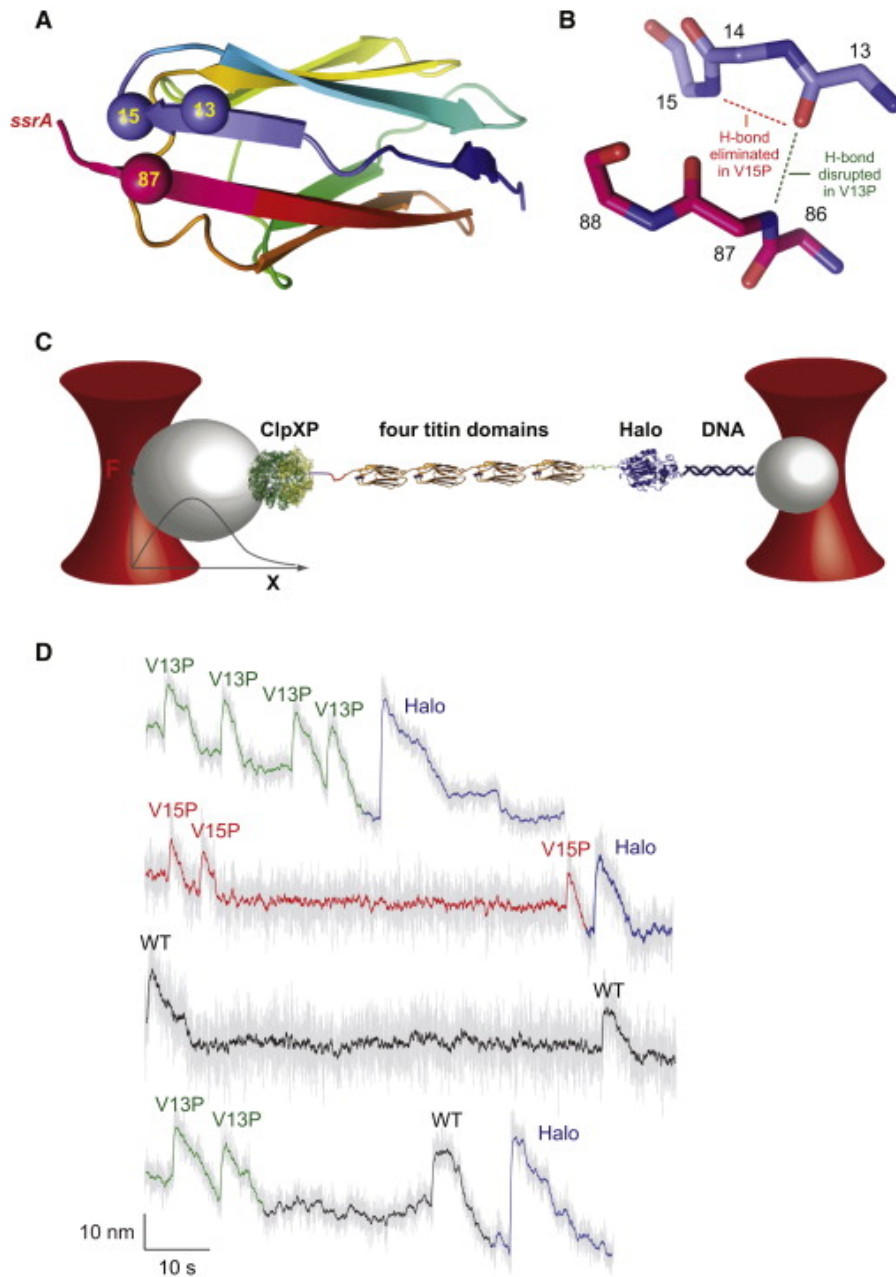


**Figure 1.** Single-molecule unfolding and translocation of substrates. (A) Cartoon structure of the titin<sup>I27</sup> domain (pdb code, 1tit), colored from the N terminus (blue) to the C terminus (red). Spheres show  $\alpha$  carbons for residues 13, 15, and 87. ClpXP pulling on an *ssrA* tag at the C terminus would be resisted by local titin structure, including  $\beta$ -sheet hydrogen bonding between the C-terminal  $\beta$  strand and the  $\beta$  strand with residues 13 and 15. (B) The V13P and V15P mutations disrupt hydrogen bonds that directly or indirectly stabilize the titin<sup>I27</sup> domain. (C) Experimental setup for single-molecule assays of ClpXP unfolding and translocation. ClpXP is attached to one laser-trapped bead and has engaged the *ssrA* tag of a multi-domain substrate consisting of four titin domains and a Halo domain, which is attached to a second laser-trapped bead via a DNA linker.



(D) Trajectories for ClpXP unfolding and translocation of multi-domain substrates. Unfolding of individual domains increases bead-bead distance (upward movement), whereas translocation decreases bead-bead distance (downward movement). After completed translocation of one domain, there is a variable dwell time before ClpXP unfolds the next domain. The dwell baselines between successive titin unfolding events are spaced as expected for the end-to-end distance of a native titin domain (4.4 nm) or native titin plus the linker to the Halo domain

Surprisingly, two ATP-hydrolysis events can drive more than two power strokes, as an engineered ClpX hexamer with just two active subunits also takes ~1-4 nm physical steps. Finally, we show that solution proteolysis is many times slower than predicted from single-molecule results. We discuss the implications of these results for understanding ClpXP structure and biological function and present a mechanochemical model in which initial stochastic ATP hydrolysis in the AAA+ ring can be followed by a cascade of coordinated power strokes. This model explains our single-molecule results and also accounts for a wide range of previous biochemical, genetic, and structural results.

## **RESULTS**

### **Substrate design and single-molecule degradation**

ClpXP degrades ssrA-tagged variants of the titin<sup>127</sup> domain at different rates (Kenniston et al., 2003). For example, the V13P and V15P mutations disrupt or eliminate hydrogen bonds close in space to the C-terminal ssrA tag (Figs. 1A, 1B), reduce thermodynamic, kinetic, and mechanical stability, and accelerate ClpXP degradation, with the wild-type (WT) domain being most stable and degradation resistant, V15P having intermediate stability and degradation rates, and V13P being least stable and most rapidly degraded

(Li et al., 2000; Kenniston et al., 2003). For single-molecule studies, we constructed Halo-WT-WT-WT-WT-ssrA, Halo-V13P-V13P-V13P-V13P-ssrA, Halo-V15P-V15P-V15P-V15P-ssrA, and Halo-WT-V13P-V13P-V13P-ssrA substrates, in which Halo is an N-terminal HaloTag domain that allows covalent attachment to a biotinylated DNA spacer. For optical-trapping (Fig. 1C), multi-domain substrates were attached via the Halo domain and DNA spacer to one streptavidin-coated bead, and a biotinylated variant of ClpXP was attached to a second streptavidin-coated bead (Aubin-Tam et al., 2011). In all substrates, the Halo domain was connected to the adjacent titin domain by a 22-residue linker, whereas the remaining titin domains were connected by 4-residue linkers.

Optical-trapping measurements under constant force (Aubin-Tam et al., 2011) were used to visualize single-molecule ClpXP unfolding and translocation. Individual traces displayed three signatures of ClpXP mechanical function as shown in Fig. 1D. First, abrupt increases in bead-to-bead distance occurred upon unfolding, with the size of the transition being smaller for titin domains than for the Halo domain. Second, bead-to-bead distance decreased following unfolding, as ClpXP translocated the unfolded polypeptide, with the total decrease depending upon the size of the denatured domain and the length of the linker to the next domain. Third, between completed translocation of one unfolded domain and denaturation of the next native domain, there was a pre-unfolding dwell with little change in bead-to-bead distance.

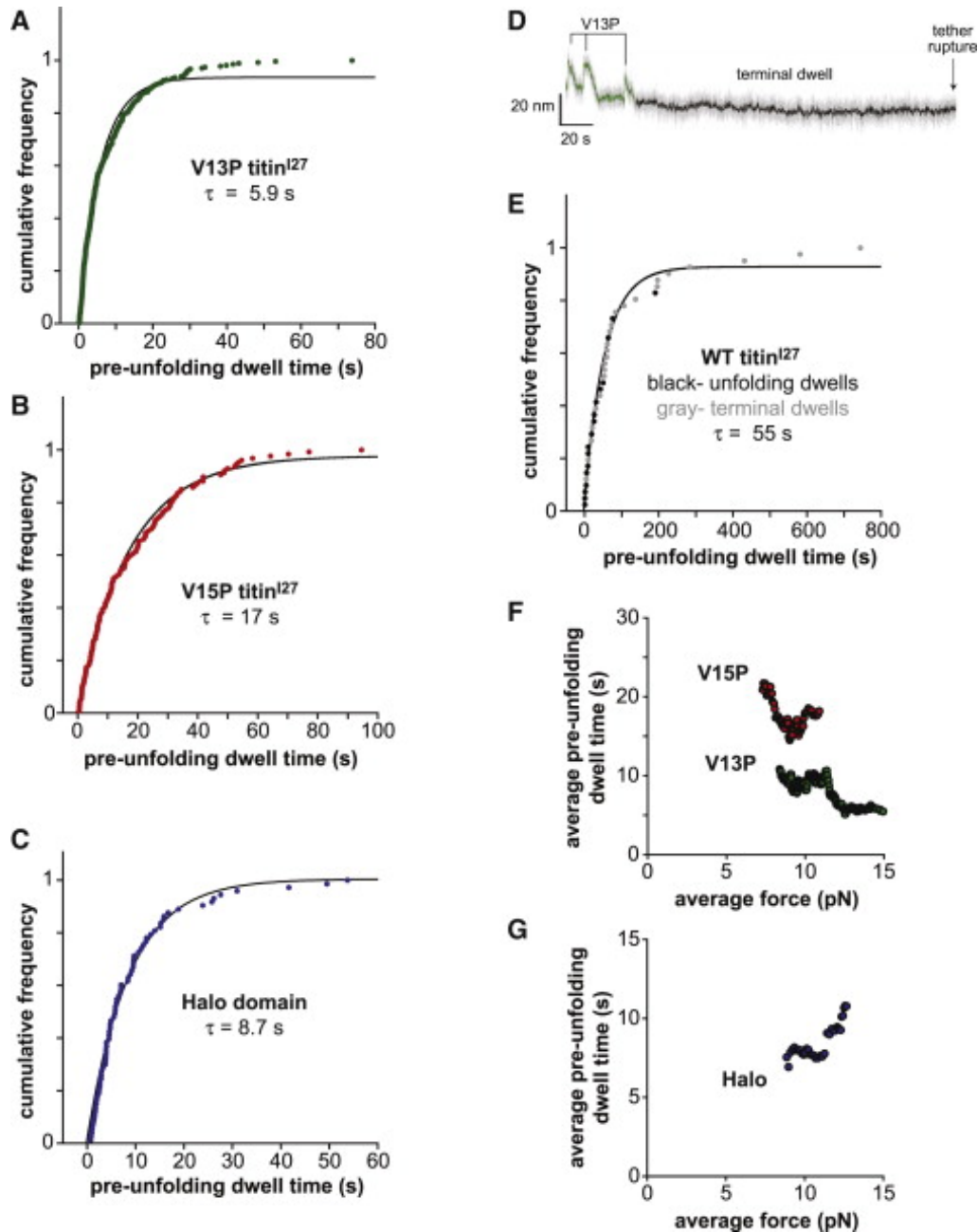


**Figure 2.** ClpXP unfolding of domains in multi-domain substrates. (A-C) Distributions of pre-unfolding dwell times for the V13P, V15P, and Halo domains. In each plot, the solid line is a non-linear-least-squares fit to  $y=A*(1-\exp(-t/t_{unf}))$ . (D) For the Halo-WT-V13P-V13P-V13P-ssrA substrate, long “terminal” dwells were often observed following unfolding and translocation of the V13P titin domains. (E) ClpXP unfolding of wild-type titin<sup>I27</sup> domains. Black symbols are pre-unfolding dwells; gray symbols are “terminal” dwells. The line is a fit to  $y=A*(1-\exp(-t/t_{unf}))$ . (F) Plots of average force versus average pre-unfolding dwell times (calculated over a moving 50-point window) for the V13P and V15P domains. (G) Plot of average force versus average pre-unfolding dwell times (calculated over a moving 40-point window) for the Halo domain. See also Figs. S1, S4,

and S7.

### **Pre-unfolding dwell times depend on substrate stability**

The pre-unfolding dwell represents the time that ClpXP pulls on a native protein domain before denaturation occurs. Pre-unfolding dwells for the first unfolding event in each trajectory were not quantified, as recording began after some attempted unfolding, unfolding, or translocation by ClpXP had occurred. For example, the second and fourth traces in Fig. 1D contain just three titin unfolding events and one Halo unfolding event. Because there are four titin domains in the multi-domain substrate, one V15P or V13P domain must have been unfolded and translocated before these traces began.

ClpXP unfolding of a protein domain typically requires many ATP-hydrolysis events (Kenniston et al., 2003). If enzymatic unfolding occurs by a single pathway and one rate-limiting kinetic step, then pre-unfolding dwells should be exponentially distributed. Multiple unfolding pathways with one rate-limiting step would give dwells distributed as a sum of exponentials, whereas multiple kinetic steps with similar time constants would give a gamma distribution of dwell times. For ClpXP unfolding of V13P (N = 278 events), V15P (N = 127 events), and Halo (N = 73 events), the pre-unfolding dwell distributions fit well to single exponentials ( $R^2 \geq 0.987$ ), with average unfolding times ( $t_{\text{unf}}$ ) of 5.9, 17, and 8.7 s, respectively (Figs. 2A-2C). Only 17 WT unfolding events, some of which may be ClpXP independent (see Supplemental Results), were observed in ~200 experiments, indicating that most experiments terminated before WT unfolding. Indeed, some Halo-WT-V13P-V13P-V13P-ssrA traces contained three V13P unfolding events, a

long terminal dwell, and rupture of the bead-bead tether before ClpXP could unfold the WT domain (Fig. 2D). Including WT pre-unfolding dwells and these terminal dwells, which represent a lower bound of the pre-unfolding dwell, gave an exponential distribution with  $t_{\text{unf}} \sim 55$  s ( $N = 41$ ; Fig. 2E). Fitting just the WT pre-unfolding dwells gave a  $t_{\text{unf}}$  about half this value, which was unrealistically small given the distribution of terminal dwells. Rates of ClpXP unfolding in the order  $V13P > V15P > WT$  are consistent with the relative stabilities of these domains (Li et al., 2000; Kenniston et al., 2003). Thus, destabilizing mutations proximal to the site of ClpXP pulling result in faster enzymatic denaturation. The exponential distribution of pre-unfolding dwells for these proteins indicates that one kinetic step is largely rate limiting for ClpXP unfolding, a finding supported by inspection of the randomness of the process (see Supplemental Results). Models with parallel faster and slower exponential processes improved the residuals of the V13P and V15P fits modestly (Fig. S1), consistent with the possibility of two unfolding pathways (see Discussion).

Force has opposing effects, reducing ClpXP activity but also destabilizing domains in the substrate to a degree that depends on the distance to the unfolding transition state (Carrion-Vazquez et al., 1999). We ranked pre-unfolding dwells by force, calculated averages over a moving window, and plotted average dwell time against average force (Figs. 2F & 2G). Unfolding of V13P and V15P was faster at higher force (Fig. 2F), suggesting that force destabilizes these titin domains more than it decreases ClpXP activity. By contrast, Halo unfolding was slower at higher force, suggesting that force

destabilizes Halo less than it decreases ClpXP activity, a result consistent with the distance to the transition state being smaller for ClpXP unfolding of Halo than the titin domains. The ratios of ClpXP-dependent to ClpXP-independent unfolding events were  $\sim 20$ ,  $\sim 7$  and  $\sim 1$  for the V13P, V15P and WT domains, respectively, a trend consistent with distances to the unfolding transition state determined from atomic-force microscopy experiments for these domains (Li et al. 2000; see Supplemental Results).

### **Translocation velocity and pausing**

ClpXP translocation typically proceeded monotonically, but pauses longer than 2.5 s were occasionally observed (Fig. 3A). After subtracting these pauses, we calculated average translocation velocities. The V13P, V15P, and WT velocities were similar, as expected because these sequences differ at only one residue position. For 656 pooled titin translocation traces, the mean velocity was  $24 \pm 0.4 \text{ aa s}^{-1}$  ( $4.4 \pm 0.1 \text{ nm s}^{-1}$ ), where the errors are SEM values. For 78 Halo translocation traces, the mean velocity was slower ( $18 \pm 0.8 \text{ aa s}^{-1}$ ;  $3.3 \pm 0.1 \text{ nm s}^{-1}$ ). Thus, the polypeptide sequence has a modest impact on ClpXP translocation velocity, a result consistent with biochemical studies (Barkow et al., 2009). Fig. 3B shows average translocation velocities plotted against average force. Fitting these data gave unloaded translocation velocities of  $29 \text{ aa s}^{-1}$  for titin domains and  $20 \text{ aa s}^{-1}$  for Halo domains.

Pausing occurred with higher probability at some titin and Halo sequences (Fig. 3C, 3D) and was less common during translocation of titin (3.7% of events) than Halo (17% of

events). Sequence dependent pausing could occur either because of direct interactions of the translocating polypeptide with ClpXP or because some sequences have a higher probability of forming transient structure that impedes translocation.

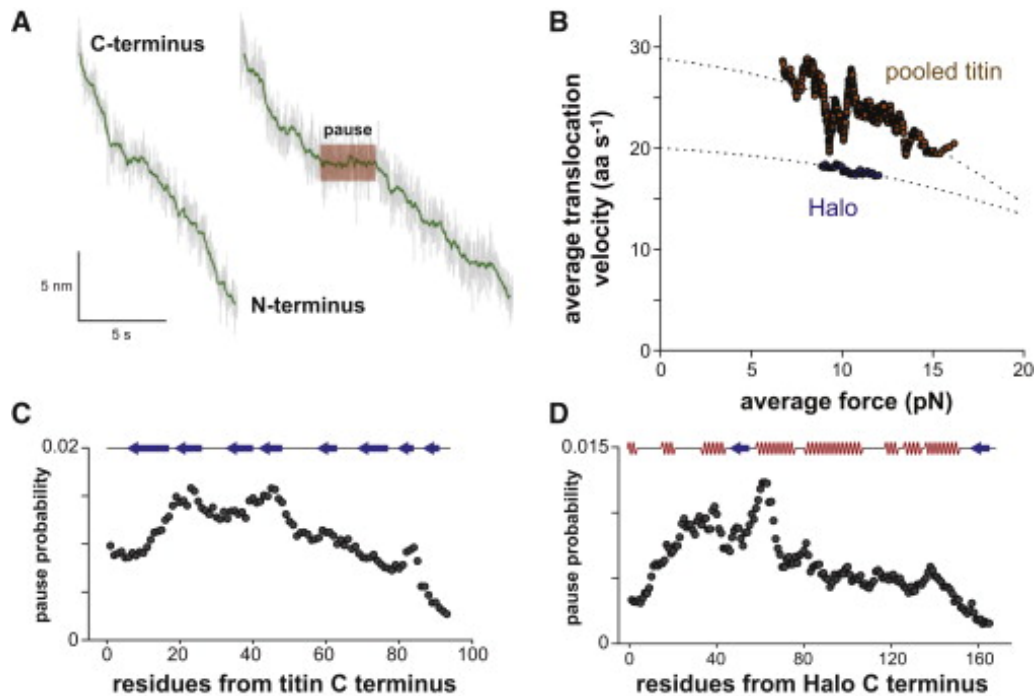


**Figure 3.** Translocation and pausing. (A) The left panel shows a V13P translocation trace proceeding with approximately constant velocity. The right panel shows a V13P translocation trace with a pause. (B) Plots of average force versus average translocation velocity were calculated over a moving 50-point window for the V13P and V15P domains and over a 40-point window for the Halo domain. The lines are fits to a single-barrier Boltzmann equation  $v = v_0 \cdot (1.05) / (1 + 0.05 \cdot \exp(F \cdot 0.7 / kT))$  where  $F$  is the average force and  $kT$  is 4.1 pN·nm at room temperature. (C) Probability of pausing of ClpXP along the length of a titin domain ( $N = 25$ ). (D) Probability of pausing of ClpXP along the length of a Halo domain ( $N = 24$ ). Secondary structure in the native structure is indicated schematically in panels C and D (arrows represent  $\beta$  strands; zigzag lines represent  $\alpha$  helices).

## **Stochastic steps of different size and kinetic complexity contribute to translocation**

Using a chi-squared algorithm (Kerssemakers et al., 2006), we resolved individual physical steps in a subset of translocation traces with good signal to noise (for examples, see Fig. 4A). As reported (Aubin-Tam et al., 2011; Maillard et al., 2011; Sen et al., 2013), the smallest physical steps were  $\sim 1$  nm but many steps were 2-fold, 3-fold, and 4-fold larger (Figs. 4A, 4B). Force had little effect on the average step length ( $\sim 2$  nm; Fig. 4C), and complete translocation of each titin domain ( $\sim 90$  residues) required an average of  $\sim 8$  physical steps (Fig. 4D).

During titin translocation, the dwell times both preceding and following a physical step increased with the size of the step (Fig. 4E). The dwell times for pooled steps of all sizes (Fig. 4F) and for individual steps of different sizes (Fig. S2) were distributed non-exponentially, suggesting that multiple kinetic steps contribute to each physical translocation step. Importantly, there was no strong sequential pattern of step sizes (Fig. 4G). In the trajectories shown in Fig. 4A, for example, the order of steps was 1-2-1-1-1-2-3-3-1-1 for the leftmost trace, 3-2-2-2-3-4 for the center trace, and 1-1-1-1-1-2-2-3-2-2-1-1 for the rightmost trace. Despite the absence of a clear pattern, 1 nm steps had a higher probability of being preceded or followed by another 1 nm step compared to longer steps, and steps of 2-4 nm also tended to be preceded and followed by longer steps (Fig. 4G). These results support a stochastic mechanism of subunit firing with



some degree of motor memory. ClpXP translocation of the Halo domain also showed a distribution of steps ranging from  $\sim 1$ -4 nm (Fig. S3).

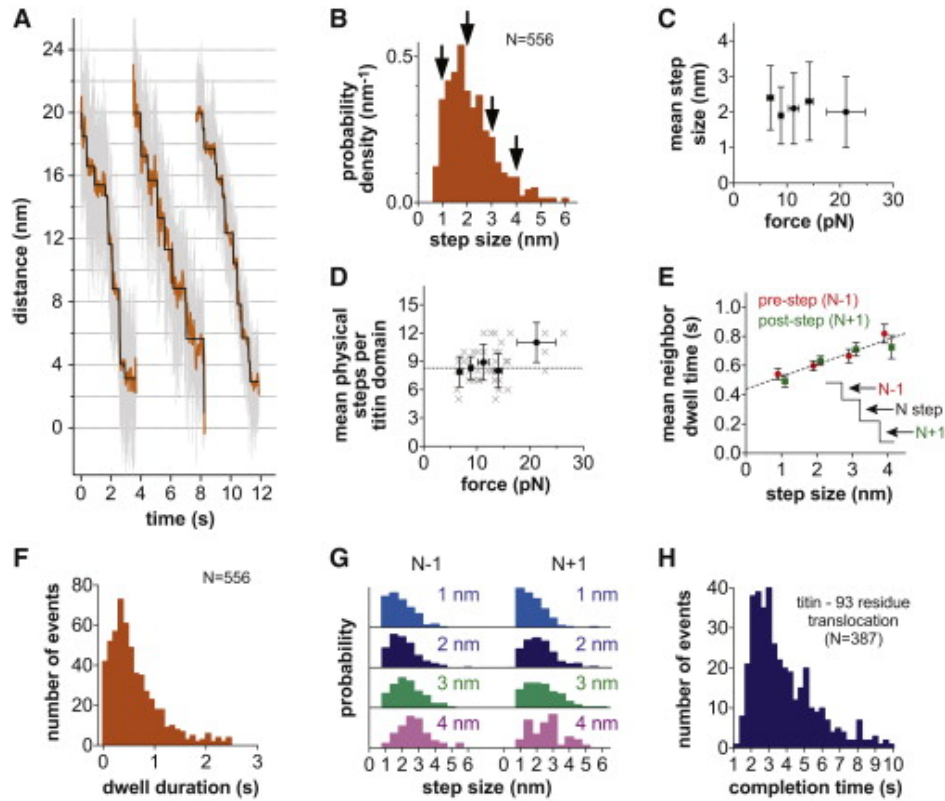


**Figure 4.** Physical steps during titin translocation. (A) Representative stepping in ClpXP translocation trajectories. Raw data were decimated to 500 Hz (gray) or 50 Hz (orange). Chi-square fits to the 50 Hz data are shown in black (Kerssemakers et al., 2006). (B) Distribution of physical steps sizes during titin translocation. (C) Mean physical step size during titin translocation as a function of force. X- and Y-error bars are  $\pm 1$  SD (N = 70-221). (D) Mean number of physical steps required to translocate an 89-residue titin domain and 4-residue linker as a function of force (black squares). X- and Y-error bars are  $\pm 1$  SD (N = 6-20). Gray X's are step numbers from individual translocation trajectories. (E) Mean dwell times  $\pm$  SEM (N = 45-236) before (red) or after (green) a physical step of  $\sim 1$ ,  $\sim 2$ ,  $\sim 3$ , or  $\sim 4$  nm (pre- and post-step values are offset slightly on the x-axis for clarity). (F) Distribution of dwell times preceding steps of all sizes during titin translocation. (G) Occurrence of steps of different size either before (N-1) or after (N+1) physical steps of 1-4 nm. (H) Distribution of times required to complete translocation of 89-residue titin domains and subsequent 4-residue linkers after subtracting pauses. See also, Figs. S2, S3, S5, S6, and S8.

To investigate mechanism independently of the detection of individual steps, we calculated times from the beginning to the end of translocation of V13P and V15P domains followed by the 4-residue linker (93 total residues;  $N = 387$ ) and subtracted any pauses. The histogram of completion times showed multiple peaks (Fig. 4H), supporting populations of faster and slower moving enzymes, a finding consistent with our observation that ClpXP has an increased probability of taking short steps after short steps and *vice versa*.

**Unfolding, translocation, and pausing by a hobbled ClpX motor.** To determine the effects of eliminating ATP hydrolysis in multiple ClpX subunits, we used a variant containing two subunits with ATPase-defective R370K sensor-II mutations (R), two wild-type subunits (W), and two subunits with ATPase-defective E185Q Walker-B mutations (E) in the order RWERWE. The ATPase defective subunits in this ClpX variant, which supports degradation of *ssrA*-tagged V13P, V15P, and WT titin substrates at 15-30% of wild-type ClpXP rates, can still bind and release nucleotide (Joshi et al., 2004; Hersch et al., 2005; Martin et al., 2005). In optical-tweezer experiments, we observed RWERWE ClpXP unfolding and translocation of V13P domains in Halo-V13P-V13P-V13P-V13P-*ssrA* (Fig. 5A) at forces up to 10.4 pN, whereas the wild-type enzyme was active at forces as high as 26 pN. An exponential fit of pre-unfolding dwell times for RWERWE ClpXP gave a  $t_{\text{unf}}$  of 50 s ( $N = 19$ ; Fig. 5B), corresponding to ~8-fold slower unfolding than by ClpXP with six active subunits. In experiments using Halo-V15P-V15P-V15P-V15P-*ssrA* or Halo-WT-WT-WT-WT-*ssrA*, we detected no RWERWE ClpXP unfolding.

Thus, preventing ATP hydrolysis in four ClpX subunits dramatically slows the rate of unfolding of V13P, the least stable of the three titin-domain variants tested, and makes enzymatic unfolding of the V15P and WT domains too slow to detect under the forces used for optical trapping.

For V13P translocation by RWERWE ClpXP, the average translocation velocity after removing pauses was  $5.7 \pm 0.5 \text{ aa s}^{-1}$ , a rate  $\sim 4$ -fold slower than ClpXP. Pauses defined as dwells longer than 7.5 s were present in  $\sim 45\%$  of RWERWE traces, whereas pauses defined as dwells longer than 2.5 s were present in fewer than 4% of wild-type ClpXP traces. Thus, a ClpX ring with just two active subunits pauses more frequently and for longer times than a ring with six active subunits. The dwells between RWERWE ClpXP translocation steps were substantially longer than between ClpXP translocation steps (Figs. 5C, 5D). Strikingly, however, individual physical steps in RWERWE ClpXP translocation traces also ranged from  $\sim 1$ -4 nm (Figs. 5C, 5D). We conclude that large physical steps do not require ATP hydrolysis in more than two ClpX subunits.

**Commitment is a slow step in solution degradation.** Previous studies show that ClpP proteolysis is not a slow step in degradation (Thompson and Maurizi, 1994; Kenniston et al., 2003). How well do average times of unfolding ( $t_{\text{unf}}$ ) and translocation ( $t_{\text{trans}}$ ) determined in single-molecule experiments predict average degradation times determined at substrate saturation ( $t_{\text{deg}} = 1/V_{\text{max}}$ ) in solution? If the average commitment time ( $t_c$ ) is defined to satisfy the equation  $t_c + t_{\text{unf}} + t_{\text{trans}} = t_{\text{deg}}$ , then  $t_{\text{unf}} + t_{\text{trans}} \approx t_{\text{deg}}$  only

when  $t_c$  is small compared to  $t_{\text{unf}} + t_{\text{trans}}$ . For six substrates of varying stability, a plot of  $(t_{\text{unf}} + t_{\text{trans}})$  against  $t_{\text{deg}}$  gave a linear correlation with a slope of  $\sim 0.25$  (Fig. 6A), indicating that solution degradation is  $\sim 4$ -times slower than expected from single-molecule unfolding and translocation. Although differences in conditions between solution and single-molecule experiments could account for some variation (see Fig. 6A legend), this result suggests that  $t_c$  is the slow step in solution degradation or that  $\sim 75\%$  of ClpXP enzymes are inactive, as calculation of  $V_{\text{max}}$  assumes 100% activity. To distinguish between these possibilities, we monitored single-turnover binding and unfolding of GFP-ssrA by a 20-fold molar excess of ClpXP (5- to 20-fold excess over  $K_M$ ) at a series of temperatures and fit the exponential trajectories to determine  $t$  values (Fig. 6B). We also performed steady-state degradation at each temperature to determine  $t_{\text{deg}}$  (Fig. 6C),  $K_M$  for protein substrate (Fig. 6D), and measured rates of ATP hydrolysis in the presence of saturating GFP-ssrA (Fig. 6E). To calculate fractional activity, we added the time expected for GFP translocation to the single-turnover  $t$  values for binding/unfolding and divided this time by  $t_{\text{deg}}$ . The fractional ClpXP activity was  $\sim 0.4$  at 15 °C and increased to  $\sim 0.9$  at 37 °C (Fig. 6F). The latter result indicates that ClpXP is  $\sim 90\%$  active, a result consistent with previous studies (Hersch et al., 2005; Shin et al., 2009). Lower “activity” at lower temperatures may be a consequence of more ClpXP enzymes assuming a conformation that does not support substrate binding or activity.

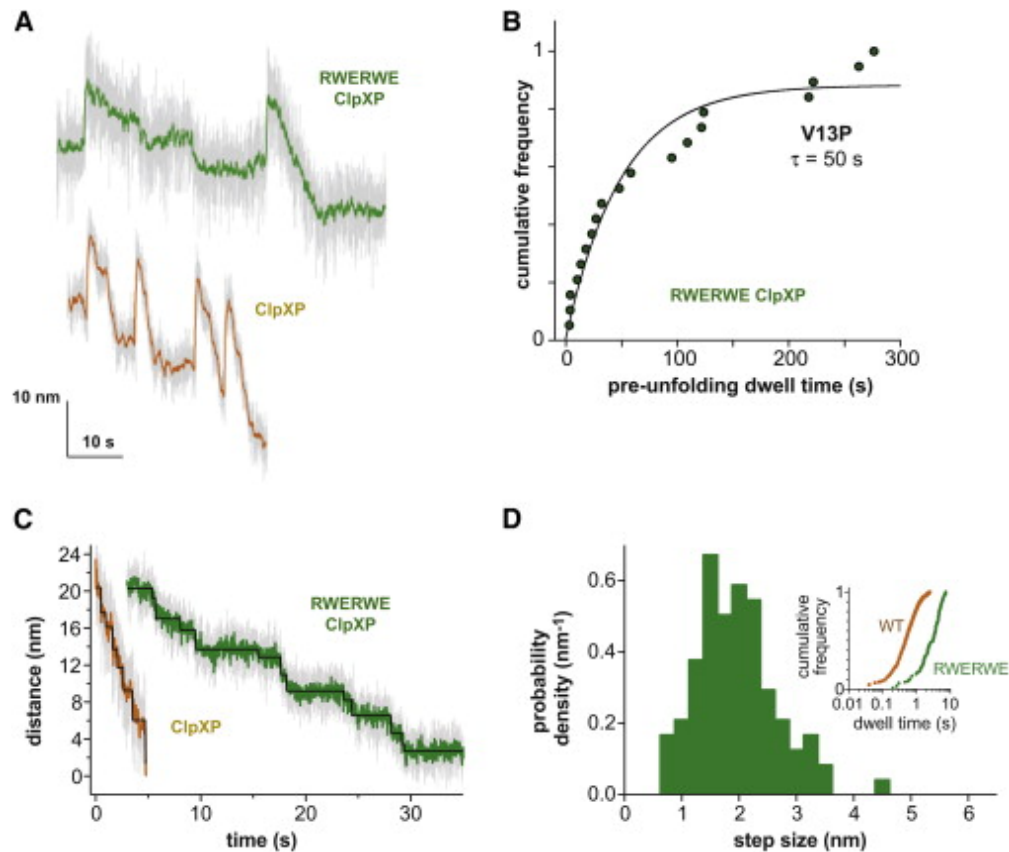


**Figure 5.** Unfolding and translocation by RWERWE ClpXP. (A) V13P unfolding and translocation traces for RWERWE ClpXP (top) and ClpXP with six active subunits (bottom). (B) Distributions of RWERWE ClpXP pre-unfolding dwell times for the V13P domain. The line is a non-linear-least-squares fit to  $y = A*(1-\exp(-t/t_{unf}))$ . (C) Representative stepping in titin V13P translocation by ClpXP (orange) and RWERWE ClpXP (green). Decimation and fits (black) are described in Fig. 4A. (D) Distribution of RWERWE physical step sizes. Inset- Cumulative frequency distributions of dwell times preceding steps for ClpXP (orange) or RWERWE ClpXP (green). See also Fig. S8.

The time required for ClpXP unfolding of pre-engaged GFP in solution is  $\sim 6$  s at  $30^\circ\text{C}$  (Martin et al., 2008a). Subtracting this time from the 34 s required to bind and unfold GFP in our single-turnover experiment at  $30^\circ\text{C}$  yields a  $t_c$  of 28 s, which is  $\sim 4.5$ -fold longer than the pre-engaged unfolding time. As  $t_{deg}$  is substantially longer than  $t_{unf} + t_{trans}$  even for substrate proteins with marginal stability (Fig. 6A),  $t_c$  represents much of the time required for ClpXP degradation and appears to increase in proportion to substrate

stability. For ClpXP degradation of wild-type titin<sup>I27</sup> substrates, cycles of binding, attempted engagement and/or unfolding, and substrate release contribute to the time needed for degradation (Kenniston et al., 2005). The linearity of the Fig. 6A plot suggests that similar cycles of substrate binding and release contribute to the degradation time required for many substrates.

## **DISCUSSION**

### **Domain stability and ClpXP unfolding**

Matouschek and colleagues first reported that the local stability of structural elements adjacent to the degradation tag determined resistance to enzymatic unfolding (Lee et al., 2001). Our results support their model, as we find that mutations that decrease stability by altering hydrogen bonds to the C-terminal  $\beta$ -strand of titin also decrease the average pre-unfolding dwell time in single-molecule ClpXP experiments. However, rates of ClpXP degradation are not always correlated with global stability. For example, ClpXP degrades an *ssrA*-tagged variant of a hyperstable RNase-H ( $\Delta G_u \approx 12$  kcal/mol) faster than it degrades V13P-titin<sup>I27</sup>-*ssrA* ( $\Delta G_u \approx 3$  kcal/mol) (Kenniston et al., 2003; 2004). In RNase-H-*ssrA*, ClpXP initially pulls against a C-terminal helix as opposed to pulling against a  $\beta$ -strand in titin. Lee et al. (2001) speculated that AAA+ proteases might be able to unfold an  $\alpha$ -helix, which can be pulled apart by stepwise unzipping, more easily than a strand in a  $\beta$ -sheet, which requires simultaneous shearing of multiple hydrogen bonds (Fig. S4). In the absence of force, our results suggest that ClpXP unfolds the Halo domain, which has a C-terminal helix, substantially faster than any of

the titin domains, supporting the possibility that helices are inherently easier to unfold than strands in  $\beta$  sheets.

To a first approximation, the pre-unfolding dwell times for the V13P, V15P, and Halo domains were exponentially distributed, supporting one major unfolding pathway and a single rate-limiting kinetic step. Nevertheless, unfolding times were substantially longer than times required for even a burst of power strokes ( $\sim 0.6$  s based on the ATPase rate and translocation dwells), as expected if unfolding requires coincidence between a power stroke and transient stochastic thermal destabilization. Because most protein domains fold cooperatively, ClpXP disruption of even a small number of stabilizing native interactions could result in rapid global unfolding of the remaining structural elements in the domain. At a second level, ClpXP unfolding of V13P fit better to exponential processes acting on less-stable and more-stable populations of similar size (Fig. S1), with enough events ( $N = 262$ ) to make sampling error unlikely. This result is consistent with the existence of two unfolding pathways, which could depend upon which parts of the V13P domain are stochastically destabilized. For example, the N-terminal portion of V13P might be transiently frayed in the more-stable population and the C-terminal transiently region frayed in the less-stable population.

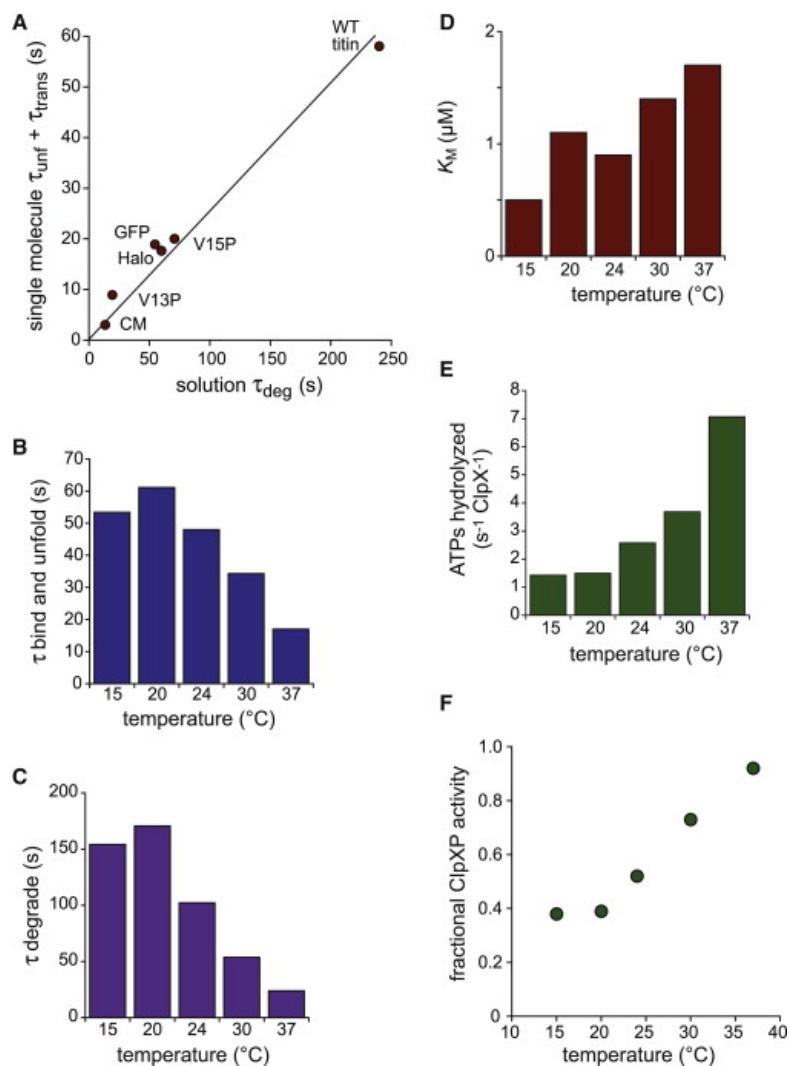


**Figure 6.** Solution degradation times are poorly predicted by single-molecule unfolding and translocation times. (A) Plot of average times required for solution degradation ( $t_{deg}$ ) of titin-ssrA (WT), V15P-titin-ssrA (V15P), V13P-titin-ssrA (V13P), carboxymethylated titin-ssrA (CM), GFP-ssrA (GFP), and Halo-ssrA (Halo) versus  $t_{unf} + t_{trans}$  times from single-molecule experiments (Kim et al., 2000; Kenniston et al., 2003; Sen et al., 2013; this work). Times for titin and GFP degradation were determined at 30 °C, whereas single-molecule experiments and Halo-ssrA degradation were performed at room temperature. Degradation is slower at lower temperatures (see panel C), which would increase the discrepancy between the solution and single-molecule results.  $t_{unf}$  values were determined under load and could be different at zero force, but V13P and V15P  $t_{unf}$  values (Fig. 2E) would not increase 4-fold and the Halo  $t_{unf}$  value appears to decrease (Fig. 2F). (B)  $t$  values for single-turnover binding and unfolding of GFP-ssrA ( $0.5 \mu$ M) by ClpXP ( $10 \mu$ M ClpX $^{\Delta N}$ ;  $20 \mu$ M ClpP) at different temperatures. (C)  $t_{deg}$  values ( $1/V_{max}$ ) at different temperatures determined from Michaelis-Menten plots of steady-state rates of degradation of different concentrations of GFP-ssrA by ClpX $^{\Delta N}$  ( $0.3 \mu$ M) and ClpP ( $0.9 \mu$ M). (D)  $K_M$  values for GFP-ssrA degradation at different temperature (conditions as in



panel C). (E) Rates of ClpXP ATP hydrolysis at different temperatures by ClpX<sup>ΔN</sup> (0.3 μM) in the presence of ClpP (0.9 μM) and GFP-ssrA (20 μM). (F) Fractional activity of ClpXP at different temperatures calculated as  $(t_c + t_{unf} + 5 \text{ s})/t_{deg}$ , where the  $t_c + t_{unf}$  value is taken from panel B and 5 s is the estimated time for translocation of GFP-ssrA.

### **A model for unfolding, different physical step sizes, and motor memory**

We find that a substantial number of physical translocation steps occur in multiples of ~1 nm, in agreement with previous results (Aubin-Tam et al., 2011; Maillard et al., 2011; Sen et al., 2013). Based on structures of ClpX rings, conformational changes larger than 1 nm seem unlikely, and it is commonly assumed that a ~1 nm step involves hydrolysis of one ATP and one power-stroke (Glynn et al., 2009; Aubin-Tam et al., 2011; Maillard et al., 2011; Sen et al., 2013; Stinson et al., 2013). Thus, bursts involving multiple power strokes are likely to drive larger physical steps. For wild-type ClpXP, each power stroke could result either directly or indirectly from hydrolysis of one ATP, as a ClpX hexamer binds a maximum of four ATPs (Hersch et al., 2005). Despite having just two catalytically active subunits, however, RWERWE ClpXP also takes physical steps ranging from ~1-4 nm, raising the possibility that a single ATP-hydrolysis event can generate more than one power stroke. For example, an initial power stroke might be generated by ATP hydrolysis and ADP/P<sub>i</sub> release in one subunit and a subsequent power stroke by ATP dissociation from an inactive subunit in RWERWE ClpX (see below).

Any model of ClpXP function needs to be consistent with structural and biochemical results. For example, subunits in the ClpX hexamer display structural and biochemical

asymmetry, suggesting a large number of different states and nucleotide-bound ring configurations (Baker and Sauer, 2012). Moreover, based on equilibrium and kinetic studies, two subunits in a ClpX hexamer do not appear to bind ATP, two bind ATP weakly, and two bind ATP strongly (Hersch et al., 2005; Stinson et al., 2013). ATP binding to subunits with weak affinity drives conformational changes required for the ClpX ring to hydrolyze ATP and perform mechanical work (Stinson et al., 2013). ATP hydrolysis and coupled mechanical work by ClpX rings cannot depend on a strictly sequential mechanism, as variants with numerous ATPase-inactive subunits still unfold and degrade protein substrates in solution (Martin et al., 2005) and in the single-molecule RWERWE studies here. Moreover, a strictly sequential mechanism should generate a clear sequence of translocation step sizes, which we do not observe. Finally, a model should account for the fact that ATP hydrolysis is substantially slower during ClpXP unfolding of native substrates than during translocation (Kenniston et al., 2003).

The models depicted in Fig. 7A and 7B meet the criteria described above and provide a quantitative framework for understanding ClpXP unfolding and translocation. ClpX rings are designated as active (X) or inactive (iX) with the number of bound ATPs specified by a trailing number. Thus, X4 is an active ring with four ATPs, and iX2 is an inactive ring with two ATPs. X3 and X4 rings are active. In agreement with biochemical studies (Stinson et al., 2013), all other rings are inactive and must bind additional ATP and/or change conformation to become an active X4 or X3 ring. When a natively folded protein domain cannot enter the axial channel of an X4 or X3 ring, ATP hydrolysis and product

release result either in a futile power stroke or in a power stroke that causes unfolding (Fig. 7A). For simulations with the kinetic constants shown, the rates of these processes, conformational changes, and ATP-binding steps result in single-exponential unfolding kinetics ( $R^2 = 0.999$ ) and a  $t_{\text{unf}}$  of 6 s, a value close to  $t_{\text{unf}}$  for V13P titin. Decreasing just the rate constant for unfolding in the model produces longer pre-unfolding dwells, as we observe for the Halo, V15P titin, and WT titin domains. The model also predicts hydrolysis of an average of  $\sim 5$  ATPs for each V13P domain that ClpXP unfolds and higher ATP consumption in proportion to the increased unfolding times for more stable domains, as observed experimentally (Kenniston et al., 2003).

Once unfolding is successful, additional cycles of ATP hydrolysis drive translocation of the polypeptide chain as diagrammed in Fig. 7B. Again, only X4 and X3 rings are active. From the X4 ring, physical steps of 1-4 nm are taken depending upon which ATP-bound subunit hydrolyzes ATP or fires first. For example, initial firing of low-affinity subunit **a** results in a 1 nm step, initial firing of low-affinity subunit **b** results in a 2 nm step, and so on (Fig. 7C). From the X3 ring, firing of the **b** subunit results in a 1 nm step, whereas firing of the **c** and **d** subunits result in steps of 2 and 3 nm, respectively. For steps of 2, 3, or 4 nm, we assume that 2, 3, or 4 ATPs are hydrolyzed and/or released in rapid succession, generating a burst of power strokes that are not experimentally resolved. Simulations using the rate constants in Fig. 7B produce step-dwell distributions (Fig. S2) and step-size distributions close to the experimental distributions (Fig. S5). Step memory, which depends on the rates at which the X3 ring takes additional steps or

recycles to X4, was also recapitulated (Fig. S6), but to a smaller extent than observed. In simulated data, for example, 38% of all 1 nm steps were followed by a second 1 nm step, whereas this value was 41% in the experimental data. In the absence of memory, only 29% of the next steps would also be 1 nm. Sen et al. (2013) reported almost complete loss of 4 nm steps at ATP concentrations near  $K_M$ . At low ATP concentrations, our model predicts that the population of X3 rings would increase substantially compared to X4 rings, reducing the average step size and fraction of 4 nm steps. The ATPase rate in our model is effectively determined by the slow conformational rearrangements needed to generate active X4 and X3 rings ( $2.2 \text{ s}^{-1}$  for translocation;  $0.5 \text{ s}^{-1}$  for unfolding), predicting  $\sim 4$ -fold faster ATP hydrolysis during translocation than unfolding, as is experimentally observed during ClpXP degradation of native and denatured titin substrates (Kenniston et al., 2003). Thus, our model accounts for a broad range of experimental results. We were unable to match the experimental results using models in which ClpX conformational changes precede rather than follow ATP binding or in which X4 rings are the only active species.

### **Stochastic AND coordinated ATP hydrolysis**

In our model, initial ATP hydrolysis in the X4 or X3 rings is probabilistic, as first proposed based on studies of ClpX rings with mixtures of active and inactive subunits (Martin et al., 2005). Contrary to arguments by Smith et al. (2011), a probabilistic or stochastic model does not imply that subunits act independently. Indeed, Martin et al. (2005) found that ATP-hydrolysis activity was not strictly proportional to the number of

ATPase active subunits and provided strong evidence that directional communication between neighboring subunits regulates ATP hydrolysis and mechanical activity. In crystal structures of hexameric ClpX rings, the nucleotide-binding pockets in each subunit that can bind ATP (loadable subunits) vary slightly (Glynn et al., 2009; Stinson et al., 2013), providing a basis for differential nucleotide affinities and for different probabilities of which subunit fires first. It is also possible, however, that interactions with the protein substrate determine which subunit fires first (Martin et al., 2005). For example, GYVG loops in the axial pore of ClpX are known to contact the *ssrA* tag and translocating substrates and to influence ATP-hydrolysis rates. Thus, an ATP-bound subunit whose pore loop was in direct contact with a translocating polypeptide or the *ssrA* tag might have a higher probability of firing first (Martin et al., 2008b; 2008c), and the highly variable chemical and conformational heterogeneity of an unfolded polypeptide chain could determine the stochastic nature of initial firing.

Following stochastic firing of a specific subunit in the ClpX ring, whether and how many additional subunits fire rapidly will depend on subunit-subunit communication. Although the details of such communication remain to be deciphered, we suggest one possibility. For example, firing of a given subunit might cause ATP-bound counter-clockwise subunits to fire or release nucleotide, so that initial firing in the **a**, **b**, **c**, or **d** subunits in X4 would result in hydrolysis/release of 1, 2, 3, or 4 ATPs and translocation steps of 1, 2, 3, or 4 nm, and initial firing of the **b**, **c**, or **d** subunits in X3 would result in hydrolysis/release of 1, 2, or 3 ATPs and physical steps of 1, 2, or 3 nm (Fig. 7C). Thus,

a physical translocation step that began with a stochastic ATP-hydrolysis event could be followed by coordinated hydrolysis/release events, which could be programmed sequentially or stochastically. The choice of counter-clockwise versus clockwise propagation in the model is arbitrary.

With minor modifications, this subunit-subunit communication model can also explain how RWERWE ClpXP could take steps of ~3 nm or larger using only two hydrolytically active wild-type subunits in the ClpX ring. As shown in Fig. 7D, multiple configurations of an X4 ring are possible for RWERWE ClpX. When W subunits occupy both the **a** and **d** positions (Fig. 7D, left), initial firing of the **a** subunit could generate a 1 nm step, whereas initial firing of the **d** subunit could yield a 4 nm step, with ATP release from inactive subunits generating some power strokes. By contrast, RWERWE X4 configurations with wild-type subunits at the **b** or **c** positions (Fig. 7D, center and right) could result in 2 or 3 nm steps. Is it energetically feasible for ATP release to generate a power stroke? The highest force at which we recorded RWERWE ClpXP activity was ~10 pN. To drive a ~1 nm movement against this force requires ~1.5 kcal/mol (~2.5 kT) of energy. At the 2 mM ATP concentrations used for our experiments, a conformational change in the ATP-binding pocket that weakened affinity to ~30 mM would allow ATP dissociation to generate a favorable free-energy change of ~1.6 kcal/mol ( $\Delta G = -RT \ln(30 \text{ mM}/2 \text{ mM})$ ), making it plausible that ATP release drives a power stroke. ATP-loadable and unloadable subunits in the ClpX ring interconvert during function (Stinson et al., 2013), and thus the affinity of a given subunit for ATP could become substantially

weaker as a consequence of structural changes in neighboring subunits. Why are the dwell times between physical steps in RWERWE ClpXP translocation so much longer than in wild-type ClpXP translocation? The simplest possibility is that the presence of catalytically inactive R or E subunits at ring positions poised to fire requires a slow ring-resetting reaction.

### **Alternative models**

Although the models in Fig. 7 explain our single-molecule results and are consistent with a wide range of observations, related models may do so equally well. For example, we model the active ClpX ring with five loadable subunits and one unloadable subunit (Stinson et al., 2013). However, models that allow other ratios of loadable to unloadable subunits could work equally well. Similarly, we assume that only four ATPs bind to the ClpX ring based on biochemical results (Hersch et al., 2005), but the results could also be fit if ATP bound to each loadable subunit. The modeled arrangement of high-affinity and low-affinity subunits in the ClpX ring is also speculative.

In a very different model proposed by Sen et al. (2013), the number of ATPs bound to the ClpX ring solely determines the size of the subsequent physical step, which always ends with a nucleotide-free ClpX ring. Thus, they suggest that a 4 nm step is taken if four ATPs are initially bound to the ClpX ring, a 3 nm step is taken if three ATPs are

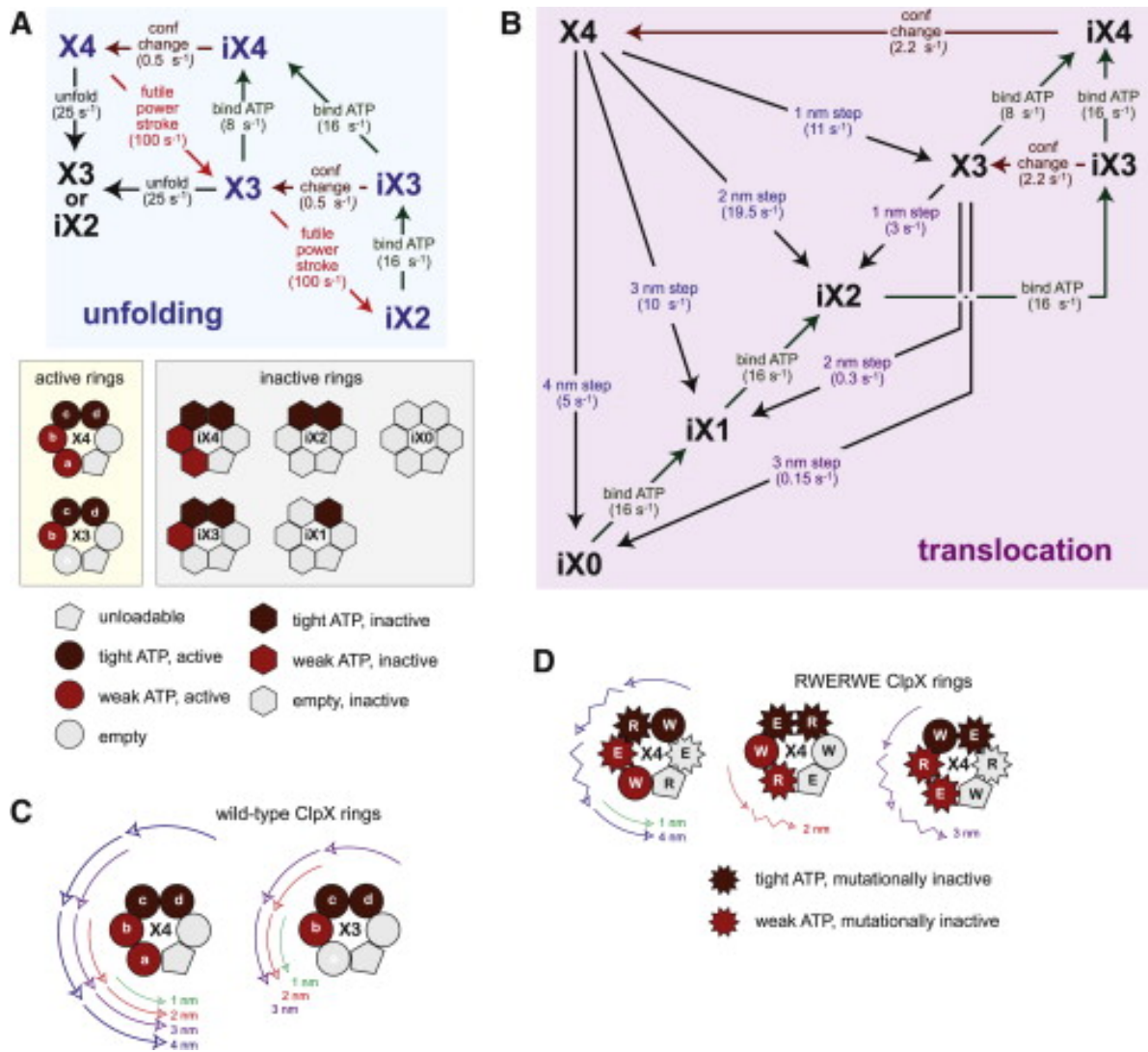


**Figure 7.** Mechanochemical models for ClpXP function. X4 and X3 rings are hydrolytically and mechanically active. iX3, iX2, iX1, and iX0 rings are inactive. Numbers after the X are bound ATPs. In the cartoons of the ClpX hexamer, dark red subunits bind ATP tightly, red subunits bind ATP weakly, and light gray subunits do not bind ATP. (A) Unfolding model. ATP hydrolysis in the X4 or X3 rings results in an unfolding power stroke, which allows translocation to begin, or in a futile power stroke. ATP-binding reactions are represented by green arrows and conformational changes by dark red arrows. For simplicity, ATP binding to iX0 or iX1 rings is not shown in this panel, ATP-dissociation reactions are not included, and different configurations of nucleotide-bound subunits in the X3 ring are not considered. Pseudo first-order rate constants for ATP-association reactions are for saturating concentrations of ATP. The mechanical stability of a native protein determines the rate of the unfolding reaction; other rates are determined by the properties of ClpXP. The rate constants in parenthesis give exponential unfolding kinetics ( $t_{\text{unf}} \sim 6$  s). (B) Translocation model. Depending on which ATP-bound subunit in the X4 or X3 rings hydrolyzes ATP first, physical translocation



steps of 1, 2, 3, or 4 nm are taken (black arrows). A physical step of  $N$  nm is associated with  $N$  hydrolysis/release events. Numbers in parentheses are rate constants that were adjusted to provide a reasonable fit to experimental data. (C) In the cartoons shown, initial ATP hydrolysis in subunits of X4 or X3 rings (labeled d, c, b, or a) result in very fast ATP hydrolysis/release events that generate power strokes (arrows) in the ATP-bound counter-clockwise subunits, generating physical translocation steps of 4, 3, 2, or 1 nm, respectively. (D) As shown on the left, if wild-type (W) subunits occupy the d and a positions in X4 rings of RWERWE ClpX, then translocation steps of 1 nm (subunit a fires first) or 4 nm (subunit d fires first) are taken. When subunit d fires first, ATP is released from the counter-clockwise inactive c (R) and b (E) subunits to generate power strokes (crooked arrows). If wild-type (W) subunits occupy the b or c positions in the X4 ring (center and right, respectively), then initial hydrolysis in these subunits results in steps of 2 or 3 nm, respectively, again with ATP release from counter-clockwise inactive subunits generating power strokes (crooked arrows). See also Figs. S2, S5, and S6.

bound, and a 2 nm step is taken if two ATPs are bound. Their model excludes the possibility of 1 nm steps. In conflict with biochemical experiments (Stinson et al., 2013), the Sen model requires ClpX rings with ATP bound only to two high-affinity subunits to be active. It also fails to account for the motor memory we observe or to explain why a broad mixture of physical-step sizes is observed at saturating concentrations of ATP. Sen et al. (2013) propose that  $P_i$  release is the force-sensitive step coupled to each power stroke, rather than ATP hydrolysis, ADP release, or ATP binding. In our view, the chemical step responsible for power strokes remains in question, as the  $P_i$ -release model depends upon untested assumptions and fails to account for our finding that RWERWE ClpXP can take steps of  $\sim 3$  nm or longer.

### **Importance of large and small step sizes**

What role do large physical translocation steps play in ClpXP degradation? As a single 4 nm step takes  $\sim 35\%$  as much time as four 1 nm steps, bigger physical steps may

simply allow faster translocation and thus faster degradation. We note, however, that translocation may represent a small fraction of the time required for degradation of many proteins. Another possibility is that a kinetic burst of power strokes is better able to unfold certain proteins, for example those with larger distances to the unfolding transition state. If large translocation steps are beneficial, then why has ClpXP evolved to take small steps as well? Small steps may allow ClpX to maintain a tighter grip on the substrate because more subunits are ATP bound (Nager et al., 2011), allowing more efficient transfer of force and increasing the probability of unfolding certain proteins.

### **Lessons for solution degradation**

For multiple substrates, ClpXP degradation is substantially slower than predicted based on single-molecule rates of unfolding and translocation (Fig. 6A), indicating that commitment is the slowest step in solution degradation. Indeed, experiments suggest that native titin substrates are bound and released many times before being unfolded by ClpXP (Kenniston et al., 2005). Two factors can affect commitment times for ClpXP. First, the SspB adaptor, which binds both to the *ssrA* tag and to ClpX, increases  $V_{\max}$  for protein degradation (Levchenko et al., 2000; Flynn et al., 2001; Wah et al., 2002). If commitment is the slow step in degradation at substrate saturation, then SspB must make this step faster. Consistently, SspB reduces the time required for binding and unfolding in single-turnover experiments. For example, in single-turnover experiments at 30 °C, the time required for ClpXP binding and unfolding of GFP-*ssrA* is ~34 s in our experiment but ~17 s with SspB present (Martin et al., 2008a). Thus, SspB is likely to

increase the probability of unfolding by increasing the average number of ClpXP unfolding attempts that occur before substrate dissociation and the need for rebinding. Second, the length of polypeptide bound in the axial pore of ClpXP influences commitment. For example, this length is ~15 residues for ssrA-tagged titin, Halo, and GFP substrates but 35-40 residues for the non-tagged domains of multi-domain substrates, including those in single-molecule experiments (Lee et al., 2001; Kenniston et al., 2005; Martin et al., 2008a). In single-turnover experiments performed in the presence of SspB at 30 °C, ClpXP degraded GFP followed by an unstructured C-terminal titin-ssrA domain almost twice as fast as GFP-ssrA and at rates similar to those observed for single-molecule unfolding (Martin et al., 2008a; Maillard et al., 2011; Sen et al., 2013). From a mechanistic perspective, a longer region of polypeptide in the axial pore of ClpXP should allow a tighter grip by the enzyme and thus reduce the probability of dissociation following a failed unfolding attempt. If longer unstructured degrons can speed degradation and result in a lower net cost in terms of ATP hydrolysis, then why are relatively short degrons used so often in biological systems? One possibility is that protein degradation typically occurs in energy-rich cellular environments and that longer degrons would open the possibility for truncation of the degron by non-specific proteases, preventing targeted degradation of the proper substrates by ClpXP and other AAA+ proteases.

## EXPERIMENTAL PROCEDURES

Complexes of ClpXP with multi-domain substrates containing an N-terminal Halo domain, which was covalently linked to biotinylated double-stranded DNA, were tethered between two laser-trapped beads as described (Aubin-Tam et al., 2011). Briefly, DNA-linked substrates were tethered to a 1- $\mu\text{m}$  streptavidin-coated polystyrene bead that was loosely bound to the surface of a glass cover slip via a DNA-tethered glass-binding peptide aptamer. Biotinylated ClpXP was attached to a 1.26- $\mu\text{m}$  streptavidin-coated polystyrene bead, which was trapped and brought into the vicinity of the bead containing the DNA-linked substrate. Upon substrate recognition by ClpXP, as determined by inter-bead tension, the laser trap for the substrate bead was turned on and the cover slip was moved to rupture the aptamer-glass attachment, resulting in tethering the ClpXP-substrate complex between two laser-trapped beads (Fig. 1C). Experiments were performed at room temperature (18-22 °C), using 2 mM ATP and ATP-regeneration and oxygen-scavenging systems (Aubin-Tam et al., 2011).

Data acquisition was carried out as described (Aubin-Tam et al., 2011). Custom MATLAB scripts were used to calculate inter-bead distances, measure the magnitude of unfolding distances, and measure the time elapsed from the end of one translocation event to the next unfolding event, which represents the pre-unfolding dwell time. Translocation events in each trace were separated and fit with a linear equation to determine the average translocation velocity. We developed a pause-detecting MATLAB script in which the translocation data is smoothed to decrease environmental noise, and

then differentiated to determine the instantaneous velocity. Pauses were identified as time periods in which this velocity remained at or below zero for longer than 2.5 s for ClpXP translocation or 7.5 s for RWERWE ClpXP translocation.

Additional experimental procedures are documented in the Supplement below.

## REFERENCES

- Aubin-Tam, M-E., Olivares, A.O., Sauer, R.T., Baker, T.A., and Lang, M.J. (2011). Single-molecule protein unfolding and translocation by an ATP-fueled proteolytic machine. *Cell* *145*, 257–267.
- Baker, T.A., and Sauer, R.T. (2012). ClpXP, an ATP-powered unfolding and protein-degradation machine. *Biochim. Biophys. Acta* *1823*, 15–28.
- Barkow, S.R., Levchenko, I., Baker, T.A., and Sauer, R.T. (2009). Polypeptide translocation by the AAA+ ClpXP protease machine. *Chem. Biol.* *16*, 605–612.
- Carrion-Vazquez, M., Oberhauser, A.F., Fowler, S.B., Marszalek, P.E., Broedel, S.E., Clarke, J., and Fernandez, J.M. (1999). Mechanical and chemical unfolding of a single protein: a comparison. *Proc. Natl. Acad. Sci. USA.* *96*, 3694–3699.
- Glynn, S.E., Martin, A., Nager, A.R., Baker, T.A., and Sauer, R.T. (2009). Structures of asymmetric ClpX hexamers reveal nucleotide-dependent motions in a AAA+ protein-unfolding machine. *Cell* *139*, 744–756.
- Joshi, S.A., Hersch, G.L., Baker, T.A., and Sauer, R.T. (2004). Communication between ClpX and ClpP during substrate processing and degradation. *Nat. Struct. Mol. Biol.* *11*, 404–411.
- Kenniston, J.A., Baker, T.A., Fernandez, J.M., and Sauer, R.T. (2003). Linkage between ATP consumption and mechanical unfolding during the protein processing reactions of an AAA+ degradation machine. *Cell* *114*, 511–520.
- Kenniston, J.A., Burton, R.E., Siddiqui, S.M., Baker, T.A., and Sauer, R.T. (2004). Effects of local protein stability and the geometric position of the substrate degradation tag on the efficiency of ClpXP denaturation and degradation. *J. Struct. Biol.* *146*, 130–140.
- Kenniston, J.A., Baker, T.A., and Sauer, R.T. (2005). Partitioning between unfolding and release of native domains during ClpXP degradation determines substrate selectivity and partial processing. *Proc. Natl. Acad. Sci. USA* *102*, 1390–1395.
- Kerssemakers, J.W., Munteanu, E.L., Laan, L., Noetzel, T.L., Janson, M.E., and Dogterom, M. (2006). Assembly dynamics of microtubules at molecular resolution. *Nature* *442*, 709–712.
- Kim, Y.I., Burton, R.E., Burton, B.M., Sauer, R.T., and Baker, T.A. (2000). Dynamics of substrate denaturation and translocation by the ClpXP degradation machine. *Mol. Cell* *5*, 639–648.

Lee, C., Schwartz, M.P., Prakash, S., Iwakura, M., and Matouschek, A. (2001). ATP-dependent proteases degrade their substrates by processively unraveling them from the degradation signal. *Mol. Cell* *7*, 627–637.

Levchenko, I., Seidel, M., Sauer, R.T., and Baker, T.A. (2000). A specificity-enhancing factor for the ClpXP degradation machine. *Science* *28*, 2354–2356.

Li, H., Carrion-Vazquez, M., and Fernandez, J.M. (2000). Point mutations alter the mechanical stability of immunoglobulin modules. *Nat. Struct. Biol.* *7*, 1117–1120.

Maillard, R.A., Chistol, G., Sen, M., Righini, M., Tan, J., Kaiser, C.M., Hodges, C., Martin, A., and Bustamante, C. (2011). ClpX(P) Generates Mechanical Force to Unfold and Translocate Its Protein Substrates. *Cell* *145*, 459–469.

Martin, A., Baker, T.A., and Sauer, R.T. (2005). Rebuilt AAA + motors reveal operating principles for ATP-fuelled machines. *Nature* *437*, 1115–1120.

Martin, A., Baker, T.A., and Sauer, R.T. (2008a). Protein unfolding by a AAA+ protease is dependent on ATP-hydrolysis rates and substrate energy landscapes. *Nat. Struct. Mol. Biol.* *15*, 139–145.

Martin, A., Baker, T.A., and Sauer, R.T. (2008b). Pore loops of the AAA+ ClpX machine grip substrates to drive translocation and unfolding. *Nat. Struct. Mol. Biol.* *15*, 1147–1151.

Martin, A., Baker, T.A., and Sauer, R.T. (2008c). Diverse pore loops of the AAA+ ClpX machine mediate unassisted and adaptor-dependent recognition of ssrA-tagged substrates. *Mol. Cell* *29*, 441–550.

Nager, A.R., Baker, T.A., and Sauer, R.T. (2011) Stepwise unfolding of a  $\beta$ -barrel protein by the AAA+ ClpXP protease. *J. Mol. Biol.* *413*, 4–16.

Sauer, R.T., and Baker, T.A. (2011). AAA+ proteases: ATP-fueled machines of protein destruction. *Annu. Rev. Biochem.* *80*, 587–612.

Sen, M., Maillard, R.A., Nyquist, K., Rodriguez-Aliaga, P., Pressé, S., Martin, A., and Bustamante, C. (2013). The ClpXP protease unfolds substrates using a constant rate of pulling but different gears. *Cell* *155*, 636–646.

Shin, Y., Davis, J.H., Brau, R.R., Martin, A., Kenniston, J.A., Baker, T.A., Sauer, R.T., and Lang, M.J. (2009). Single-molecule denaturation and degradation of proteins by the AAA+ ClpXP protease. *Proc. Natl. Acad. Sci. USA* *10*, 19340–19345.

Smith, D.M., Fraga, H., Reis, C., Kafri, G., and Goldberg, A.L. (2011). ATP binds to proteasomal ATPases in pairs with distinct functional effects, implying an ordered reaction cycle. *Cell* *144*, 526–538.

Stinson, B.M., Nager, A.R., Glynn, S.E., Schmitz, K.R., Baker, T.A., and Sauer, R.T. (2013) Nucleotide binding and conformational switching in the hexameric ring of a AAA+ machine. *Cell* 153, 628–639.

Thompson, M.W., and Maurizi, M.R. (1994). Activity and specificity of *Escherichia coli* ClpAP protease in cleaving model peptide substrates. *J. Biol. Chem.* 269, 18201–18208.

Wah, D.A., Levchenko, I., Baker, T.A., and Sauer, R.T. (2002) Characterization of a specificity factor for an AAA+ ATPase: assembly of SspB dimers with ssrA-tagged proteins and the ClpX hexamer. *Chem. Biol.* 9, 1237–1245.



## SUPPLEMENTAL RESULTS

**Randomness calculations.** The number of rate-limiting steps required for unfolding can be assessed by a randomness parameter ( $r$ ) that measures the dwell-time variance divided by the average dwell time squared (Svoboda et al., 1994; Schnitzer and Block, 1997; Floyd et al. 2010). An  $r$  value of  $\sim 1$  is expected for an exponential process with a single rate-limiting kinetic step, a value of  $\sim 1/n$  is expected for  $n$  sequential reactions with similar time constants, and a value  $>1$  is expected for reactions involving two populations and time constants (Fig. S7). For ClpXP pre-unfolding dwells, the  $r$  values were 1.50 (V13P), 0.95 (V15P), and 1.24 (Halo). To estimate likely errors, we performed trials in which half of the dwell times from each data set were randomly removed, calculated  $r$  values, and then determined an average  $\pm 1$  SD for a set of 10 independent trials, yielding values of  $1.44 \pm 0.16$  (V13P),  $0.91 \pm 0.19$  (V15P), and  $1.31 \pm 0.25$  (Halo). For V13P unfolding, the lower error bound of the randomness parameter was substantially above 1, as expected for a reaction with two populations, in agreement with the better fit of these data by exponential processes operating on two populations (Fig. S1). For ClpXP unfolding of V15P and Halo, the fits and randomness values indicate that a single predominant kinetic step is rate limiting.

**ClpX-independent unfolding.** The protein substrate is under tension and destabilized in the optical trap. Thus, spontaneous unfolding of any domain in a substrate is possible, whereas ClpXP can only unfold a domain that is directly engaged. Unfolding

transitions followed by translocation were classified as ClpXP-dependent and those not followed by translocation as ClpXP-independent. When we divided the number of ClpXP-dependent unfolding events by the number of ClpXP-independent events, the ratio was  $\sim 20$  for the least stable V13P domain (188 experiments),  $\sim 7$  for the more stable V15P domain (121 experiments), and  $\sim 1$  for the most stable WT domain (129 experiments). If experimental tension unfolded a domain proximal to ClpXP, then translocation could potentially ensue, but the probability of such events is only significant for the WT domain.

Why does ClpXP accelerates domain unfolding above the destabilizing influence of the experimental load in the order V13P > V15P > WT. One possibility is that ClpXP pulls only from the C-terminus, whereas experimental tension pulls from both termini and thus changes the unfolding pathway. Distances between the native structure and the unfolding transition state may also explain these results. Force accelerates kinetic reactions along the direction of applied load with an exponential dependence:  $\exp(Fd/kT)$ , where  $F$  is the force,  $d$  is the distance between the native structure and the unfolding transition state, and  $kT$  is 4.1 pN·nm under our experimental conditions. In our experimental dumbbell geometry (Fig. 1C), mechanical force applied by the traps acts on both motor-dependent and motor-independent events. The actual force applied to a ClpXP engaged substrate includes the mechanical load across the system and a transient pulling force from the ClpX power stroke. All substrate domains are under tension applied by the traps and are therefore subject to ClpXP-independent mechanical

unfolding. However, unfolding is accelerated further by intermittent ClpXP pulling applied to the engaged domain with a force that we estimate to be ~20 pN. As noted above, the unfolding rate is exponentially weighted by the distance to the unfolding transition state. Using distances to the unfolding transition states of the V13P (0.6 nm), V15P (0.45 nm), and WT (0.25 nm) domains measured in AFM experiments (Li et al., 2000) and assuming ClpXP additionally applies 20 pN of force, ClpXP would be expected to accelerate the unfolding rates of the V13P, V15P, and WT domains by factors of 19 ( $\exp(20 \text{ pN} \cdot 0.6 \text{ nm} / 4.1 \text{ pN} \cdot \text{nm})$ ), 9 ( $\exp(20 \text{ pN} \cdot 0.45 \text{ nm} / 4.1 \text{ pN} \cdot \text{nm})$ ), and 3 ( $\exp(20 \text{ pN} \cdot 0.25 \text{ nm} / 4.1 \text{ pN} \cdot \text{nm})$ ), respectively. The observed ratios of ClpXP-dependent to ClpXP-independent events for these domains were 20, 7, and 1. We note that sampling errors, especially for the WT domain, and the possibility that the unfolding transition state for ClpXP-dependent unfolding is different from that for ClpXP-independent unfolding make it unlikely that the calculated and observed ratios would be exactly the same.

## SUPPLEMENTAL DISCUSSION

**Conformational switching.** Conformational switching between ATP loadable and unloadable subunits in the ClpX ring, with concomitant changes in the identities of the subunits that bind ATP with high and low affinity, appears to be required for robust mechanical activity (Stinson et al., 2013). How can this requirement be rationalized in terms of the models shown in Fig. 7? One possibility is that conformational switching is

directly involved in force generation for every power stroke. Another possibility is that the products of ATP hydrolysis are not properly ejected after some unfolding attempts or translocation steps. Loadable-unloadable conformational switching might eject these products and redefine the ATP affinities of individual subunits to reset the ClpX ring and allow resumption of translocation or unfolding attempts (Stinson et al., 2013). Pausing during ClpXP translocation may arise in this manner, with the greater pausing propensity of RWERWE ClpXP resulting from the presence of catalytically inactive subunits, which increase the probability that a translocation step finishes with a ring conformation that must be reset before activity resumes.

## **SUPPLEMENTAL EXPERIMENTAL METHODS**

**Protein expression and purification.** SsrA-tagged protein substrates, *E. coli* ClpP, and single-chain hexamers of wild-type ClpX<sup>ΔN</sup> or RWERWE ClpX<sup>ΔN</sup> with a C-terminal biotinylation site were cloned, expressed, and purified as described (Kim et al., 2000; Kenniston et al., 2003; Martin et al., 2005; Aubin-Tam et al., 2011; Stinson et al., 2013). In multi-domain substrates, the linker between the Halo domain and the adjacent titin domain had the sequence ISGEPTTEDLYFQSDNAIAPRM; all additional titin domains were connected by the sequence GTRM. The C-terminal sequence of each multi-domain substrate was KVKELGH<sub>6</sub>GAANDENYALAA, where the ssrA tag that targets the substrate to ClpXP is underlined.

**Step-finding in translocation traces.** Data collected at a 3 kHz sampling frequency were decimated to 50 Hz (i.e., filtered using a third-order Chebyshev Type I low-pass filter and resampled to 50 Hz). To find steps in the decimated data, we used a MATLAB implementation of the chi-squared minimization method of Kerssemakers et al. (2006) provided by J. Kerssemakers (TU Delft), which has been shown to outperform the Student's t-test and other step-finding algorithms (Carter et al., 2008). The chi-squared method requires input of the number of steps to fit within a given trace, which we estimated by taking the pair-wise distribution of decimated data subjected to a step-smoothing algorithm based on L1-regularization with independent noise (Little et al., 2011; <http://www.maxlittle.net>). Because the chi-squared algorithm does not require a minimum detectable step size to be set, a threshold of 0.75 nm was selected. Steps smaller than this threshold, including backward steps or slips, were combined with previous and following steps by adding the dwell-weighted average ( $S_{avg}$ ) of a small step (S) to the previous step (S-1) and subtracting  $S_{avg}$  from the following step (S+1). The dwell-weighted average is defined as:

$$S_{avg} = S \cdot (d_{S+1}) / (d_S + d_{S+1})$$

where  $d_S$  is the dwell preceding a small step and  $d_{S+1}$  is the dwell following a small step. A custom MATLAB script was written to automate this iterative process.

**Accuracy of the step-finding algorithm.** The chi-squared method has been found to be as good or better than other step-finding algorithms (Carter et al. 2008; Aggrawal et

al. 2012), but we sought to test its accuracy in detecting steps in data with noise comparable to the smallest steps, as observed in our ClpXP translocation traces (SD  $\sim$ 1 nm). Two tests were employed. First, translocation traces consisting of a mixture of 1 to 4 nm steps were simulated using the Gillespie stochastic simulation method (Gillespie 1977) with a kinetic time constant of 0.2 s for all steps. 1-nm noise (SD) was added to the simulated traces, and steps were detected using the chi-squared algorithm (for examples, see Fig. S8 A-C). For fitting, we initially overestimated the number of steps by 5%, then eliminated steps less than 0.75 nm and combined them with adjacent steps as described above. 84% of 4734 simulated steps were correctly identified in the fits. As might be expected, the accuracy of detection of the 1-nm steps was lowest ( $\sim$ 40%), whereas longer steps were better identified (Fig. S8D). Based on these results, ClpXP may take a higher proportion of 1-nm steps than detected in our experimental data, but this would not change any of our major conclusions.

As an independent method of assessing step-finding accuracy, we generated  $\sim$ 1-nm stepping traces by moving a 1- $\mu$ m polystyrene bead (Spherotech, IL, USA) stuck to a glass cover slip using a nanopositioning piezo stage (Physik Instrumente Model# P-517.3CD, 1-nm positioning resolution). Data were collected similarly to ClpXP data (3 kHz sampling frequency) and further down sampled to 300 Hz to achieve a noise level of SD  $\sim$ 0.7 nm (Fig. S8 F). Fitting using the chi-squared algorithm identified steps with a mean size close to 1 nm (Fig. S8 F inset).

**Simulations.** The kinetics of domain unfolding by ClpXP were simulated using the reactions shown in Fig. 7A plus ATP-binding steps to generate the iX1 and iX2 species using the program Tenua 2.0 (Daniel Wachsstock; <http://bililite.com/tenua/>), which derives and numerically solves differential equations for the concentrations of each reaction species. The kinetics and step distributions in translocation trajectories for a single molecule of ClpXP were simulated using the Gillespie-direct Monte Carlo algorithm implemented in the program Edinburgh Dizzy (2000 s; 100000 result points sampled at 50 Hz; stochastic ensemble size of 1) using the reactions shown in the Fig. 7B model. For both types of simulations, individual rate constants were varied until reasonable agreement between the simulated and observed kinetics were obtained. 10% changes in the rate constants shown in Figs. 7A and 7B still match the experimental results reasonably well; 50% changes resulted in substantial differences between the simulated and experimental results.

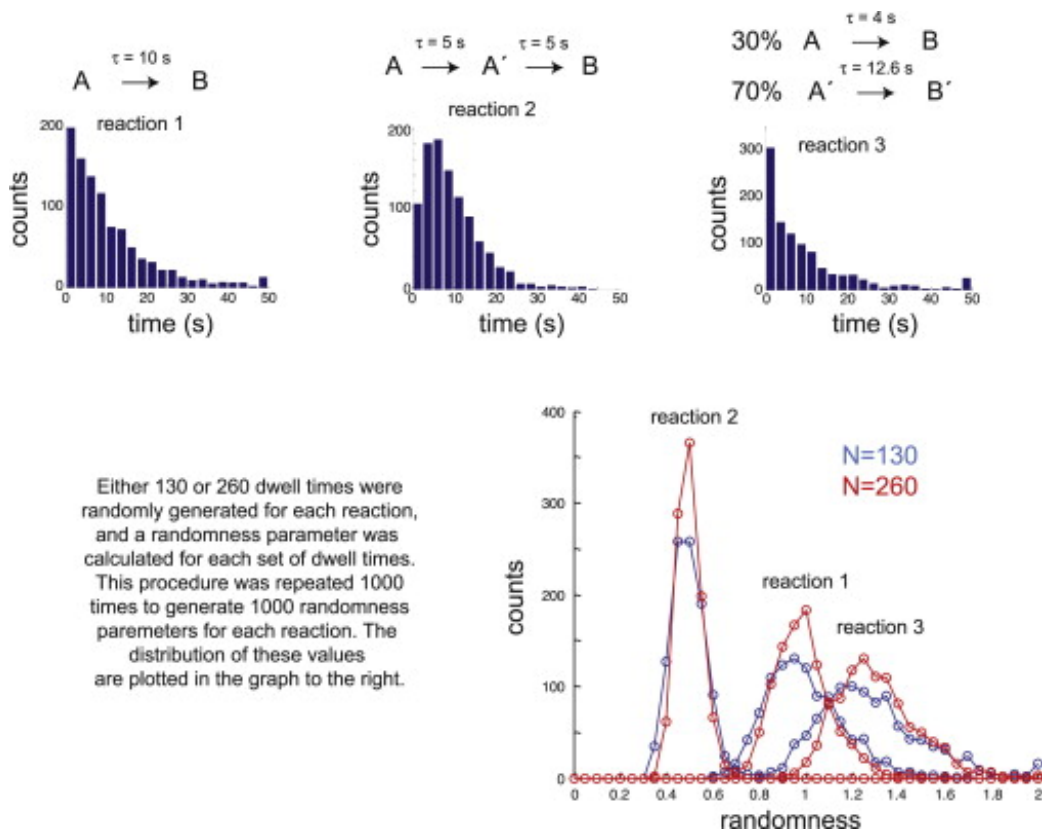


**Figure S1.** Randomness Simulations, Related to Figure 2. Simulation of time courses and randomness parameters for a simple unimolecular process (reaction 1), for two sequential steps with the same time constant (reaction 2), and for a heterogeneous process with two reactions and time constants (reaction 3). The top portion of the figure shows simulations of time courses for each type of reaction. The bottom portion of the figure shows the distribution of randomness parameters calculated for each type of reaction from distributions of dwell times (1000 trials) simulated randomly for 130 or 260 events.



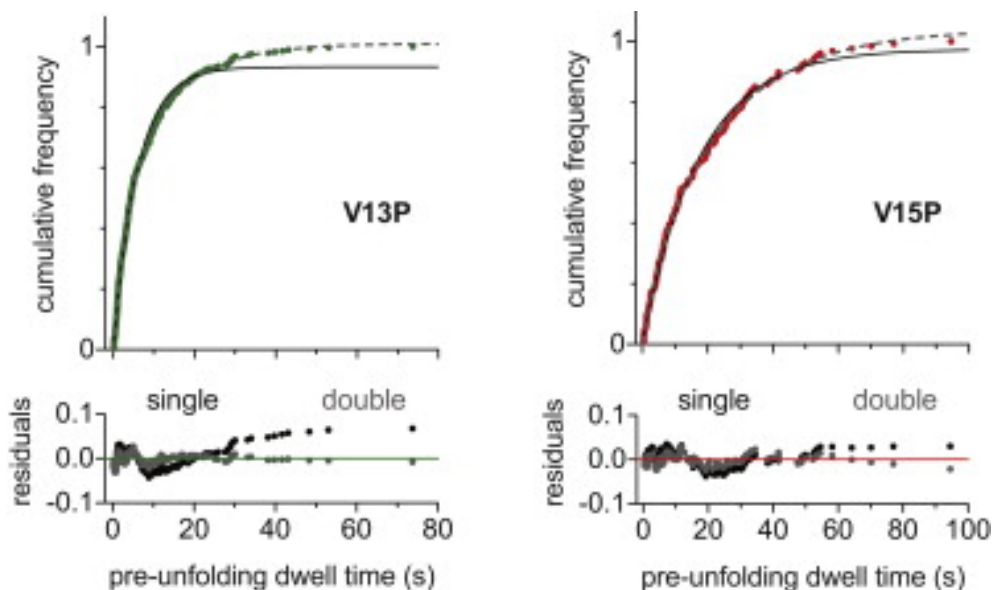


**Figure S2.** Single and Double Exponential Fits of Preunfolding Dwell Times, Related to Figure 2. Plots of cumulative frequency versus ClpXP pre-unfolding dwell times for titin<sup>V13P</sup> (green symbols) and titin<sup>V15P</sup> domains (red symbols). Although single exponentials fit the data reasonably well (black solid lines, top panels), a double exponential function,  $y = \text{amplitude}_1 * (1 - \exp(-t/\tau_{\text{unf1}})) + \text{amplitude}_2 * (1 - \exp(-t/\tau_{\text{unf2}}))$  (gray dashed lines, top panels), fits the data better (residual plots shown in bottom panels). For V13P,  $\tau_{\text{unf1}} = 3.6 \pm 0.2$  s (48% amplitude<sub>1</sub>) and  $\tau_{\text{unf2}} = 13.1 \pm 1.1$  s (52% amplitude<sub>2</sub>). For V15P,  $\tau_{\text{unf1}} = 5.3 \pm 0.9$  s (16% amplitude<sub>1</sub>) and  $\tau_{\text{unf2}} = 24.4 \pm 1.3$  s (84% amplitude<sub>2</sub>). Double-exponential fitting of Halo unfolding resulted in equal time constants for  $\tau_{\text{unf1}}$  and  $\tau_{\text{unf2}}$  (8.7 s), which were identical to a single-exponential fit of the data.

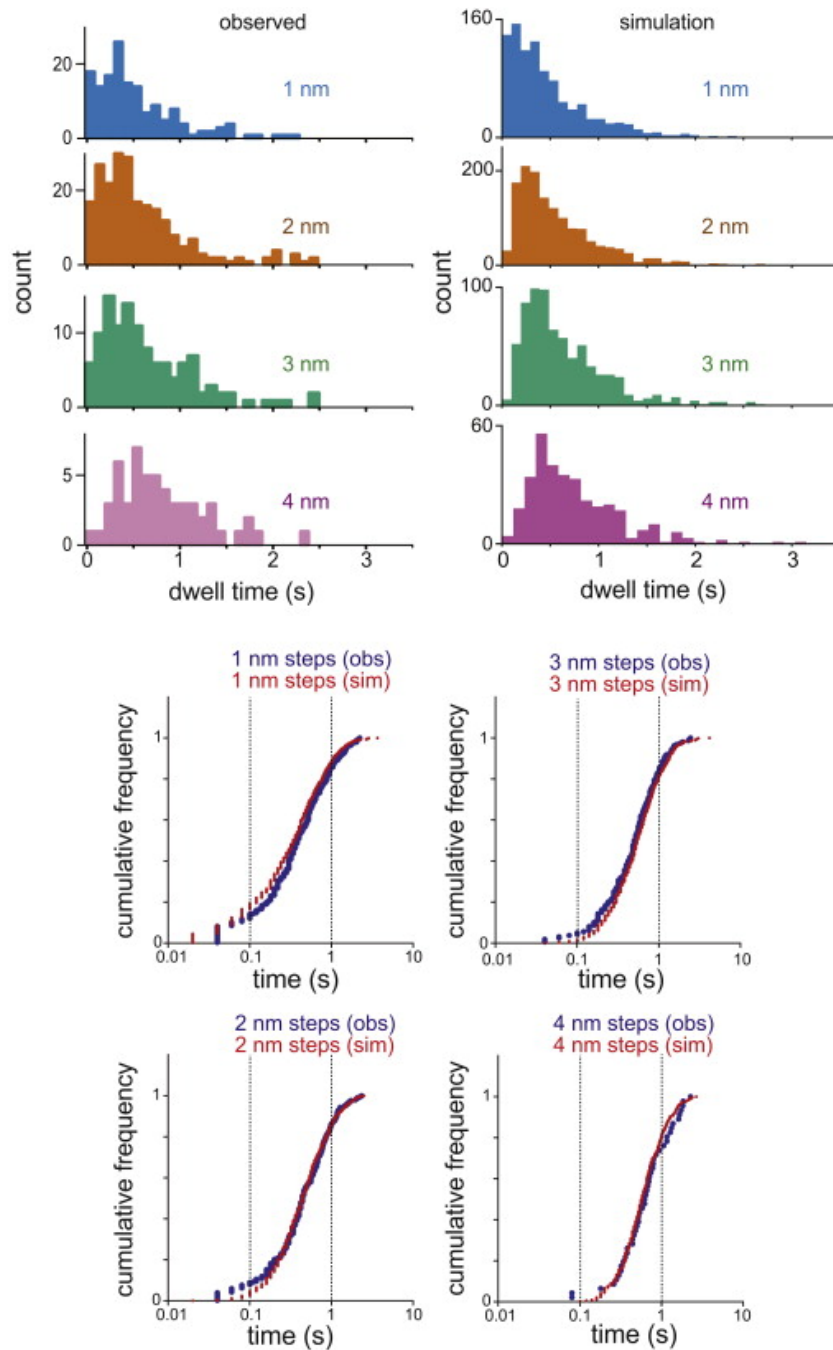


**Figure S3.** Experimental and Simulated Prestep Dwell Distributions, Related to Figures 4 and 7. Distribution of dwell times before physical steps of different sizes from experiments (observed; left panel on top; blue symbols on bottom) or a simulation using the model and rate constants shown in Figure 7B (right panel on top; red symbols on bottom).

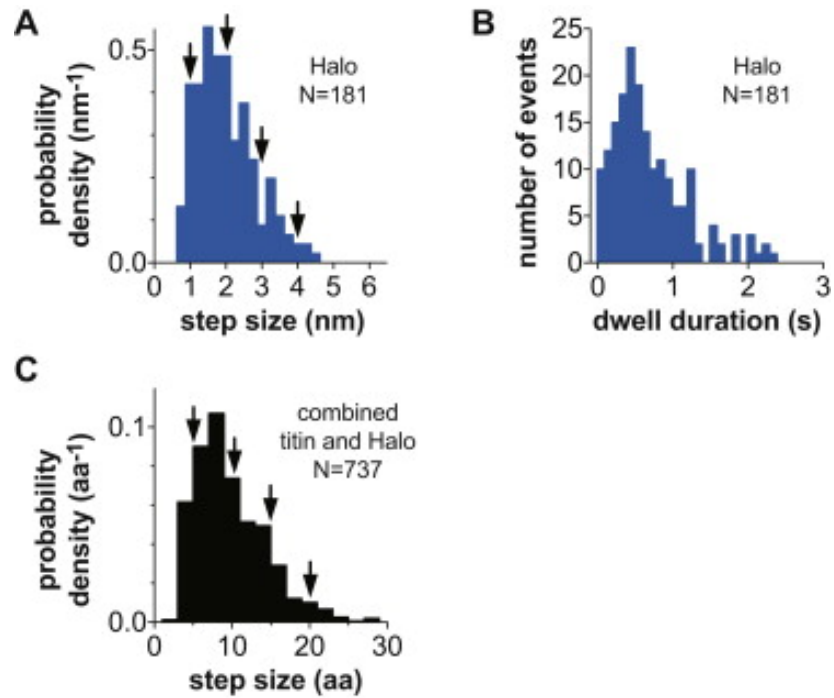
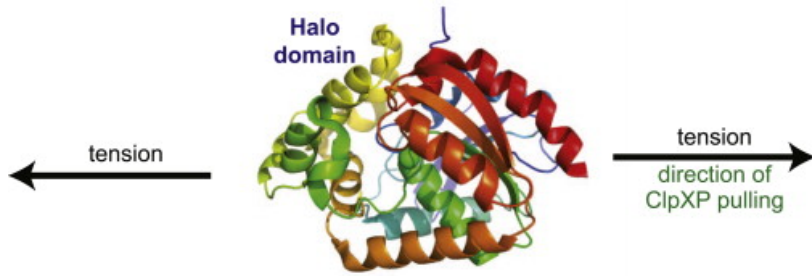


**Figure S4.** Distributions of ClpXP translocation step sizes and dwell durations (related to Fig. 4). (A) Probability-density distribution of individual physical-step sizes during Halo translocation. Arrows show positions of 1, 2, 3, and 4 nm steps. (B) Distribution of dwell durations preceding individual steps for Halo translocation. (C) Distribution of physical-step sizes during combined titin and Halo translocations calculated in units of amino acids (aa).



titin<sup>I27</sup> - ClpXP pulling produces a force that attempts to shear the hydrogen bonds that keep the C-terminal strand (red) in the native  $\beta$  sheet.



Halo - pulling produces a force that would allow unzipping of the C-terminal helix (red) a few residues at a time.

**Figure S5.** ClpXP Unfolding of the C-Terminal Elements of Secondary Structure in the Titin<sup>I27</sup> or Halo Domains, Related to Figure 2.

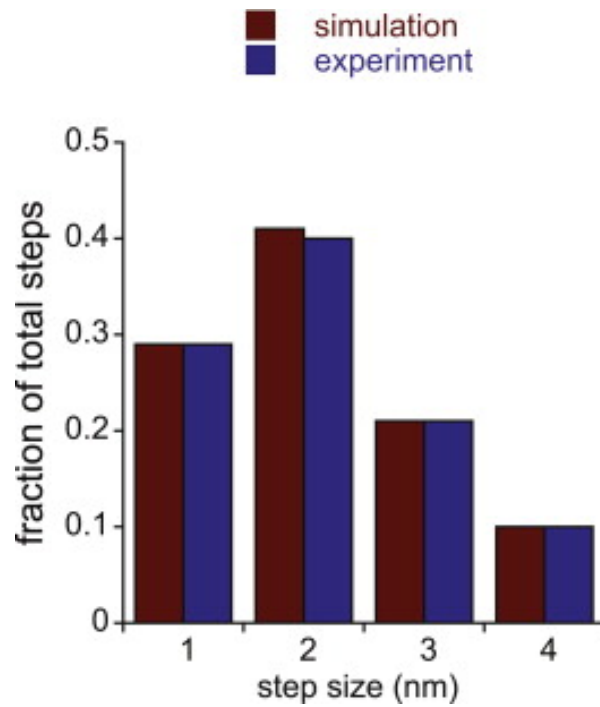


**Figure S6.** Experimental and Simulated Distributions of Translocation Step Sizes, Related to Figures 4 and 7. Comparison of step-size distributions calculated from titin translocation experiments (red bars) and from a simulation performed using the model and rate constants shown in Figure 7B (blue bars).

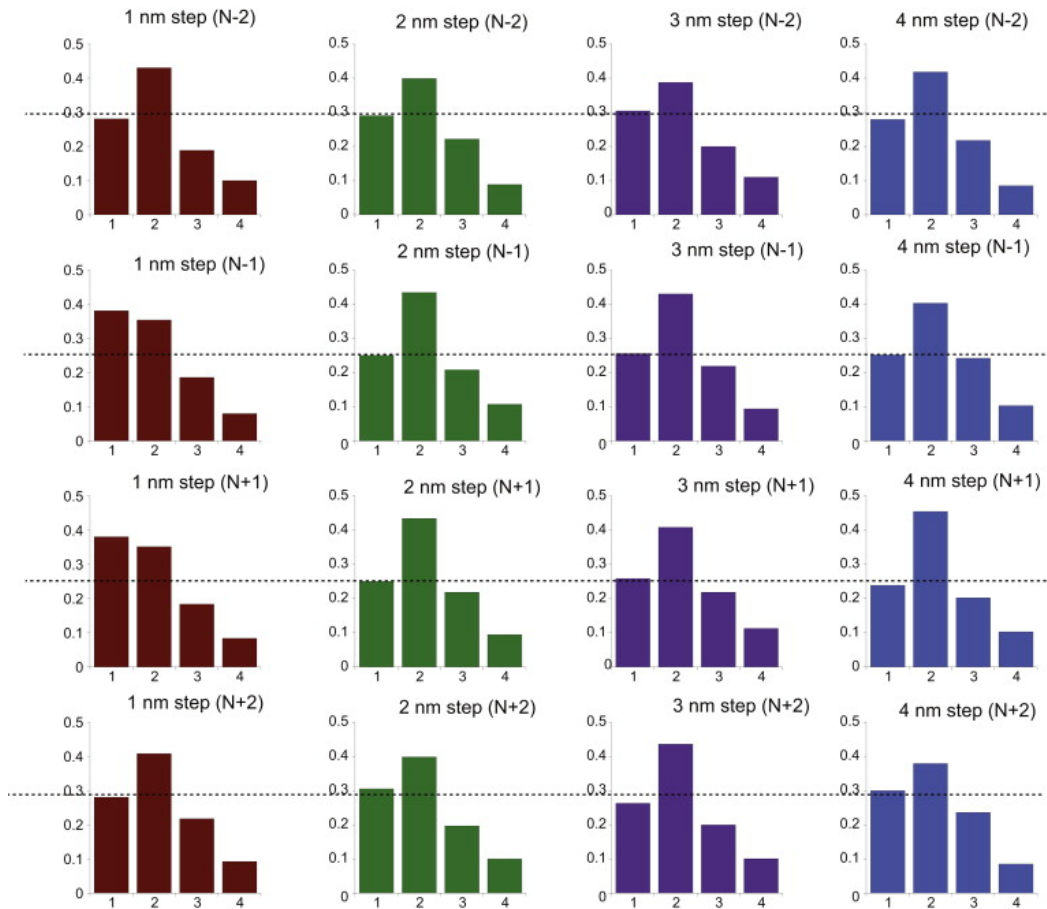


**Figure S 7.** Observed and Simulated Memory in Translocation Stepping, Related to Figures 4 and 7. A simulation performed using the model and rate constants shown in Figure 7B predicts that 1 nm steps are more probable after 1 nm steps than after steps of 2-4 nm. For example, before or after a 1 nm step, the probability of another 1 nm step is 0.38, whereas before or after 2-4 nm steps, the probability of a 1 nm step is ~0.25. Although these results match the trend seen in experiment data (Figure 4G), the simulation under predicts the degree of step memory in the experimental data.

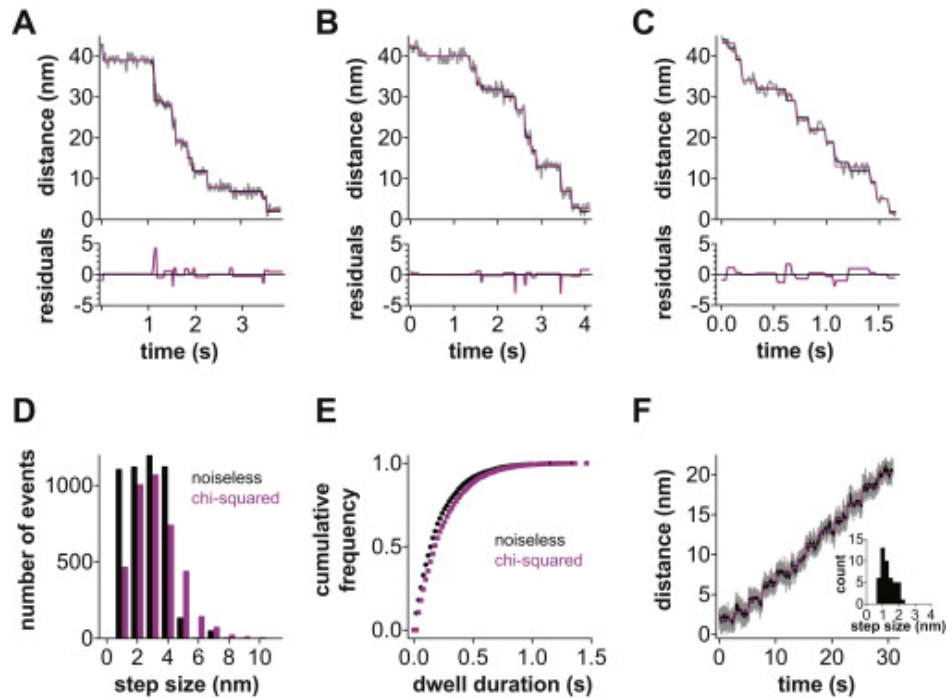


**Figure S8.** Controls for Accuracy of Translocation-Step Detection, Related to Figures 4 and 5. (A–C) Simulated stepping traces were used to test the chi-square step-finding algorithm. Simulations contained a mixture of 1-4-nm steps ( $\tau = 0.2$  s; data sampled at 50 Hz), to which random noise of 1 nm (SD) was added. The top panels show the noise-free simulated data in black, the simulated data plus noise in gray, and the chi-square fits to the simulated data plus noise in magenta. The bottom panels show the residuals of the chi-square fits to noise-free simulated data. (D) Comparison of the number of simulated steps of different sizes and the number of steps detected. (E) Pre-step dwell distributions of noise-free simulated steps (black) and steps found in simulated steps with added noise using the chi-square method (magenta). Single-exponential fits gave  $\tau$  values of 0.203 s ( $R^2 \geq 0.999$ ) for the noise-free data and 0.239 s ( $R^2 \geq 0.998$ ) for the data with added noise. (F) Piezo stage-driven  $\sim 1$ -nm movements of a stuck bead were used to test the accuracy of the chi-square step finder. Data were collected at 3 kHz, down sampled to 300 Hz (gray) to mimic the noise level observed in ClpXP translocation traces, and steps were determined using the chi-square algorithm (fit shown in magenta). Data shown in black represents a portion of the piezo-stage movements and were decimated to 30 Hz for clarity. The inset shows the distribution of all fitted step sizes with a mean of  $1.3 \pm 0.06$  nm (SEM,  $N = 46$ ).

## SUPPLEMENTAL REFERENCES

Aggarwal, T., Materassi, D., Davison, R., Hays, T., Salapaka, M. (2012). Detection of steps in single molecule data. *Cell. Mol. Bioeng.* 5, 14-31.

Carter, N.J., Cross, R.A. (2005). Mechanics of the kinesin step. *Nature* 435, 308–312.

Carter, B.C., Vershinin, M., and Gross, S.P. (2008). A comparison of step-detection methods: How well can you do? *Biophys. J.* 94, 306–319.

Floyd, D.L., Harrison, S.C., van Oijen, A.M. (2010). Analysis of kinetic intermediates in single-particle dwell-time distributions. *Biophys. J.* 99, 360-366.

Gillespie, D.T. (1977). Exact stochastic simulation of coupled chemical reactions. *J. Phys. Chem.* 81, 2340–2361.

Little, M.A., Steel, B.C., Bai, F., Sowa, Y., Bilyard, T., Mueller, D.M., Berry, R.M., and Jones, N.S. (2011). Steps and bumps: Precision extraction of discrete states of molecular machines. *Biophys. J.* 101, 477–485.

Schnitzer, M.J., and Block, S.M. (1997). Kinesin hydrolyses one ATP per 8-nm step. *Nature* 388, 386–390.

Svoboda, K., Mitra, P.P., and Block, S.M. (1994). Fluctuation analysis of motor protein movement and single enzyme kinetics. *Proc. Nat. Acad. Sci. USA* 91, 11782–11786.



## CHAPTER 3

### **Direct visualization of nucleotide turnover during protein degradation by a AAA+ molecular machine**

#### **ABSTRACT**

Single molecule techniques such as optical trapping and fluorescence have been widely used to investigate biophysical properties of molecular motors, proteins, and biomolecules (*e.g.* nucleic acids, biopolymers, etc.). Experiments combining optical force-fluorescence spectroscopy provide an unprecedented ability to directly visualize protein dynamics during specific parts of the mechanochemical cycle of enzymatic processes. However, these technically challenging methods have proven difficult to implement, particularly for molecular motors. Here we develop a single molecule surface tethered optical trapping assay to track mechanical activity during protein degradation by the ClpXP protease, a model AAA+ molecular machine. Using an analogue of the ATP nucleotide, we present a method to directly visualize nucleotide binding during unfolding and translocation using TIRF microscopy. This coincident, interlaced force-fluorescence approach provides a framework for the next-generation of single molecule studies on ClpXP and other AAA+ motors.

## INTRODUCTION

Much like the machines we encounter in everyday life, cells across all lifeforms employ enzymes that function like molecular machines to carry out a diverse set of tasks vital to many elemental cellular processes (Hwang, et al. 2013). Molecular machines from the AAA+ superfamily of enzymes use the power of ATP binding and hydrolysis as chemical fuel to generate mechanical forces and produce work (Hanson, et al. 2005). While AAA+ ATPases are involved in transcription (Kakihara, et al. 2012), protein folding (Hayer-Hartl, et al. 2016), and cargo transport (Cho, et al. 2014), a well studied AAA+ model enzyme, ClpXP, is responsible for proteolysis.

The AAA+ ClpX unfoldase binds the ClpP peptidase in the presence of nucleotide and recognizes molecular labels that guide an unneeded protein to destruction. Upon binding a labeled protein substrate, the ClpX ring undergoes conformational changes that ultimately result in protein denaturation by pulling the folded protein through its narrow pore. Upon successful unfolding, the polypeptide is translocated into ClpP which catalytically degrades the polypeptide into short amino acid sequences that can then be recycled or disposed of (Baker, et al. 2012).

The ClpX ring is made up of six subunits, identical in sequence, that self assemble to form a central pore for substrate processing (Figure 1A). Each subunit has a large and a small domain, which are connected by an unstructured loop where nucleotide binding occurs. This loop is conserved in enzymes belonging to the AAA+ superfamily of motors

(Hanson, et al. 2005), and in the case of ClpX, subunit rotation about this hinge generates two main types of subunit structures (Glynn, et al. 2010). The majority of the time, subunits adopt a loadable conformation (L subunit) in which the nucleotide binding pocket remains accessible. This binding pocket gets abolished in unloadable subunits (U subunit, Fig 1A), preventing nucleotide binding.

Recently, single molecule experiments on the ClpXP model enzyme have advanced our understanding of this molecular motor, and together with biochemical and structural studies have led to a working model for the function of ClpXP. However, the next generation of single molecule studies on this, and other AAA+, motors may require the simultaneous combination of single molecule techniques to elucidate the structure-function relationship of these enzymes (Cordova, et al. 2014). Here we develop and apply a combined force-fluorescence assay to directly visualize nucleotide binding during specific portions of the ClpXP degradation cycle. Our results set the stage for the next generation of single molecule experiments for the model system ClpXP, and the myriad of other ATPases ubiquitously involved in cellular tasks across all life forms.

## **RESULTS**

### **Motor and Nucleotide Construct Design**

Previous work to monitor nucleotide binding at the single molecule level relied on using nucleotide molecules labeled with fluorescent dyes (Ishijima, et al. 1998) (Funatsu, et al. 1997). However, this approach limits single molecule experiments to abnormally low

concentrations (less than 10 nM) of nucleotide given the large fluorescence background noise observed at concentrations resembling cellular levels of ATP (larger than 1 mM). Therefore, we opted instead to label the ATP molecule with a dark fluorescence quencher, and fluorescently label single ClpXP motors. To monitor nucleotide turnover by the ClpXP protease using single-molecule fluorescence, we introduced the single point mutation K330C in the small domain of a single subunit proximal to the nucleotide binding pocket. This cysteine was then covalently labeled with a maleimide-tetramethylrhodamine (TMR) fluorophore. The choice to use this rhodamine dye was vital to the assay, since it has been shown to be among the most resistant fluorophores to enhanced photobleaching from optical trapping photons and reactive oxygen species in solution (Ferrer, et al. 2009). This is of special concern in our assay as we have three different coincident, directly overlapped, laser beams (fluorescence, trapping, and detection).

To monitor nucleotide binding we synthesized an ATP analogue containing the dark quencher molecule, dabcyplus, covalently linked to the 2' carbon of ATP (Figure 1C). In bulk studies, the hydrolysis rates of ATP-dabcyplus quencher (referred to as ATPQ) by ClpX<sup>TMRP</sup> remained largely unchanged in the presence of substrate compared to those of normal ATP (Figure 1D). Although ClpX is able to hydrolyze ATPQ, the degradation activity for a GFP-ssrA substrate decreased nearly 3-fold compared to that of normal ATP (Figure 1E). A lowered degradation rate is to be expected given the large increase in molecular size between ATP and ATPQ, and the well known tight-fitting interaction

between ClpX subunits and nucleotide. We used these constructs below to characterize their single molecule behavior.

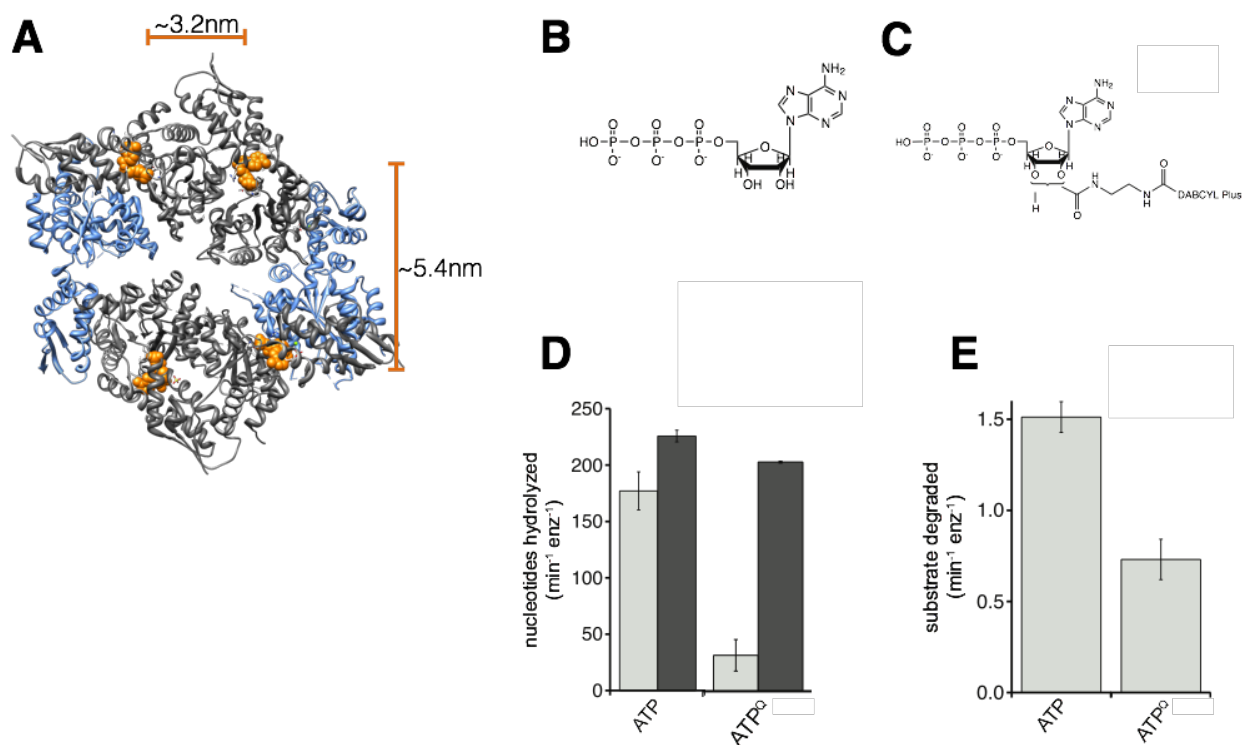


**Figure 1.** Protein degradation in using the ATPQ nucleotide. (A) Crystal structure of the ClpX ring (PDB entry 3HWS) with nucleotide loadable subunits colored in silver, and nucleotide unloadable subunits colored in blue. Bound nucleotides (ATP $\gamma$ S) are shown in orange and the estimated distance between neighboring nucleotides is shown. (B) Structure of the ATP nucleotide and (C) ATPQ nucleotide analogue. (D) Hydrolysis of ATP and ATPQ by ClpX<sup>TMR</sup> (100 nM) in the absence (light gray) and presence (dark gray) of ClpP (300 nM) and an *ssrA*-GFP substrate (10  $\mu$ M). (E) Degradation rates of *ssrA*-GFP substrate by ClpX<sup>TMRP</sup> in the presence of 2 mM ATP or ATPQ. Panels B-E are courtesy of B. Stinson (MIT).

### Tracking mechanical activity from surface tethered ClpXP motors

Previous single molecule studies on the ClpXP motor used a dual trap assay geometry, in which ClpXP motors tethered to a plastic bead are brought in the vicinity of a second bead labeled with a multimeric substrate tagged for degradation (Aubin-Tam, et al.

2011) (Maillard, et al. 2011) (Sen, et al. 2013) (Cordova, et al. 2014) (Iosefson, et al. 2015). In order to combine the optical trapping assay with TIRF based single-molecule fluorescence (smFluorescence), we engineered a surface-tethered assay geometry. To track mechanical degradation using a single optical trap, the ClpX<sup>TMRP</sup> motor was first bound to the surface of a glass coverslip. This was done by binding biotinylated ClpP to a coverslip passivated with polyethylene glycol (PEG) using streptavidin. The surface bound ClpP was then used to bind ClpX<sup>TMR</sup> in the presence of nucleotide. A polystyrene bead functionalized with a multimeric substrate and a terminal ssrA degradation tag was then trapped, brought in the vicinity of the coverslip surface, and ClpXP-substrate connections were actively formed by scanning the microscope stage until substrate recognition occurred. Upon substrate recognition, the displacement of the bead from the center of the optical trap was recorded.

As shown in Figure 2B, using this surface tethered assay geometry, we observed signature ClpXP degradation behavior, evident by the abrupt changes in distance signifying successful protein unfolding, directly followed by constant rate decreases in distance attributed to polypeptide translocation into ClpP (Figure 2A). In the presence of ATP nucleotide, ClpX<sup>TMRP</sup> is able to unfold titin<sup>I27</sup> domains with a V13P mutation (referred to as V13P) and Halo substrates (Figure 2C) at similar rates to those reported in dual trapping assays (Cordova, et al. 2014). Similarly, translocation velocities of V13P, Halo, and a pre-unfolded version V13P (Figure 2B) closely resemble those previously observed (Cordova, et al. 2014) (Iosefson, et al. 2015). These results

validate the new surface tethered assay, and suggest that a ClpXP mutant labeled with a fluorescent tag near the nucleotide binding pocket maintains activity similar to that of wild type ClpXP.

Upon switching nucleotide conditions from saturating ATP (2 mM) to 100  $\mu$ M ATPQ, single molecule degradation behavior was no longer observed. ClpXP mediated substrate recognition of both folded and unfolded protein substrates was commonly observed (middle panel, Figure 2A) but successful protein denaturation or polypeptide translocation could not be achieved at this concentration, or lower. A characteristic part of the protein degradation cycle by ClpXP includes attempted protein denaturation commonly followed by substrate release to prevent stalling the ClpXP machinery if the substrate is too stable to be degraded (Kenniston, et al. 2004). Furthermore, when pulling against the mechanical load from the optical trap, the large majority of substrate recognitions and unfolding attempts lead to unsuccessful degradation and substrate release (Cordova, et al. 2014). This behavior was exacerbated in previous studies using nucleotide analogues like ATP $\gamma$ S (Aubin-Tam, et al. 2011), or ATPQ only as used here, as expected for a ClpXP motor with lowered/slowed-down mechanical output due to an “un-natural” nucleotide molecule. Saturating concentrations of ATPQ, 2 mM, were able to degrade a GFP-ssrA protein in bulk experiments (Figure 1E), yet larger concentrations of ATPQ in a combined force-fluorescence assay yield too fast binding kinetics, and a highly increased background noise signal from inherent light scattering

by the dabcyplus molecule (see fluorescence characterization section below for details).

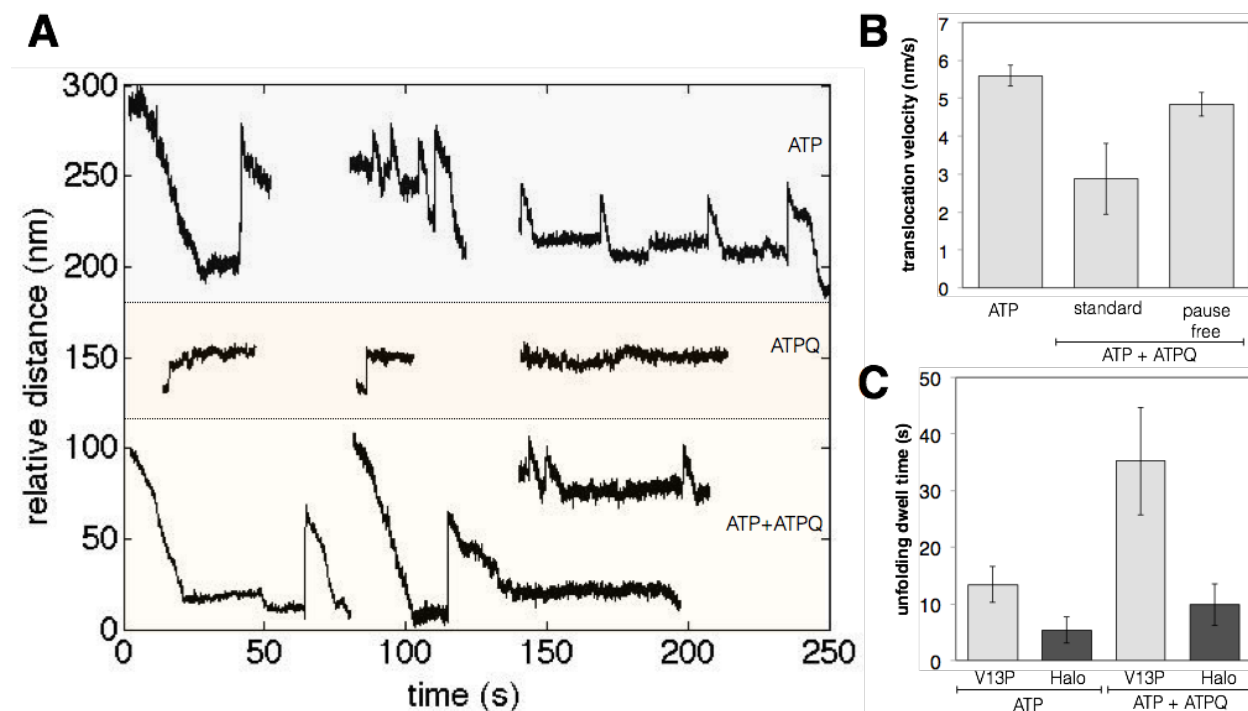


**Figure 2.** (A) Single molecule degradation traces obtained using a surface-tethered optical trapping assay for ClpXP. The three upper traces show ClpX<sup>TMRP</sup> mediated degradation of pre-unfolded titin<sup>I27</sup> (left) and V13P (right) substrates with a terminal Halo domain in the presence of saturating ATP, 100  $\mu$ M ATPQ (middle three traces), and a mixture of 2 mM ATP + 100  $\mu$ M ATPQ (bottom three traces). (B) Translocation velocities calculated from optical trapping trajectories in the presence of ATP only, or a mixture of ATP and ATPQ. Pause free velocities exclude translocation dwells longer than 10 sec observed in the ATP + ATPQ experiments. (C) Unfolding dwell times observed for V13P and Halo substrates in the presence of ATP only, or a mixture of ATP + ATPQ. For (B)-(C), values represent means  $\pm$  SEM.

Single-molecule degradation behavior was regained by using a 1:20 mixture of ATPQ:ATP as shown in the bottom panel of Figure 2A. When using a mixture of nucleotides, single molecule degradation traces show slower translocation rates (Figure 2B),  $3 \pm 0.9$  nm/s (mean  $\pm$  SEM) versus  $6 \pm 0.3$  nm/s with ATP only, which include a



population of long translocation dwells uncommon in traces using ATP only, and are clearly visible at the ~20 sec and 140 sec mark in the bottom panel of Figure 2B. Unfolding dwells times for V13P domains increased from  $13 \pm 3.2$  sec with native ATP to  $35 \pm 9.5$ sec with a mixture of ATP + ATPQ, and from  $5 \pm 2.3$  sec to  $10 \pm 3.7$ sec for Halo domains (Figure 2C). Albeit with slower degradation kinetics compared to native nucleotide, we used these conditions to characterize the nucleotide binding kinetics, below, using smFluorescence, and investigate nucleotide turnover during unfolding and translocation under load in combined force-fluorescence experiments.

### **Characterization of fluorescence quenching upon ATPQ binding**

To characterize the nucleotide binding kinetics of ATPQ in competition with ATP using smFluorescence, we tethered ClpX<sup>TMRP</sup> motors to the surface of a glass coverslip as described above. To enable multiplexed measurements of fluorescent spots on the coverslip surface, an EMCCD camera was used to track fluorescence intensity behavior over time.

For competition experiments between ATP and ATPQ nucleotides, there are three possible ClpX subunit configurations that lead to high fluorescence emission, and one configuration where the fluorescence is expected to be quenched (Figure 3A). When the fluorescently tagged subunit is nucleotide free, binds ATP, or is in an unloadable conformation (U subunit) the fluorescence is expected to be in the “on” state. Alternatively, when an ATPQ molecule binds the tagged subunit, fluorescence is

quenched almost to background level, “off” state, due to the close proximity between ATPQ and the TMR dye. Upon ATPQ, or ADPQ, release the fluorescence emission returns to “on”, unless dye photobleaching occurs during the quenched period.

Representative traces in the presence of ATP only (upper panel, Figure 3B) show stable fluorescence intensity up to the photobleaching of the dye, or fluorescence lifetimes longer than the length of the acquired movie (40 sec). When a mixture of ATP and ATPQ (2 : 0.1 mM) is flowed into the slide, fluorescent traces show multiple levels of emission prior to photobleaching (lower panel, Figure 3B). Crystal structures of the ClpX ring suggest neighboring loadable subunits have a nucleotide-to-nucleotide distance as close as ~3.2nm, and as long as 6.2nm for loadable subunits across the ring (Figure 1A). These distances suggest an ATPQ bound to a neighboring subunit of the fluorescently tagged subunit being imaged can induce FRET-mediated changes in fluorescence intensity of the dye, leading to the multiple intensity levels observed in some traces. In fact, previous ensemble experiments have used FRET between fluorescently tagged ATP analogues to characterize nucleotide affinities to the RPT1 and PAN proteasomes at the bulk level (Kim, et al. 2015). However, the change in intensity from a neighboring subunit is much lower in magnitude, and clearly discernable from ATPQ binding directly to the tagged subunit, which leads to nearly complete quenching of signal (lower panel, Figure 3B). Distributions of the normalized spot intensity in the presence of ATP only (Figure 3C) show a narrow single peak distributed around the normalized intensity value of 1 (i.e. “on” state). This distribution becomes

wider and a new state centered near zero normalized intensity (quenched state) is observed when a mixture of ATP and ATPQ is used. To quantitatively measure nucleotide binding lifetimes we fit the intensity versus time traces using Hidden-Markov modeling (McKinney, et al. 2006), and extracted the dwell times for high and low fluorescence states (see Methods section). In experiments with a mixture of 2 mM ATP and 0.1 mM ATPQ, the average quenched state lifetime, representing the residence time of ATPQ in a ClpX subunit, is  $8.0 \pm 2$  sec (Figure 5). When the amount of ATPQ was lowered to 0.01 mM the residence time remained similar with a value of  $5.2 \pm 1$  sec (Figure 5). To investigate how nucleotide residence times change when unfolding or translocating a protein we used a combined force-fluorescence approach below.

### **Combined force-fluorescence traces**

To combine the optical trapping and smFluorescence experiments we added a confocal TIRF branch to our custom-built optical trapping instrument, similar to that described by Lang and coworkers (Brau, et al. 2006). Specifically, a 532nm fluorescence excitation laser beam was sent through an Acousto-Optic Modulator (AOD) and reflected by a dichroic filter into a 100X objective lens, on an inverted microscope, at the critical angle to achieve objective-side TIRF. The illumination area was overlapped with the position of the optical trap. Fluorescence emission collected through the objective was focused onto a confocal pinhole, aligned such that only photons emitted within a circular area,  $\sim 1.5\mu\text{m}$  in diameter, centered at the trap position are imaged by a Scanning Avalanche Photodiode (SAPD).

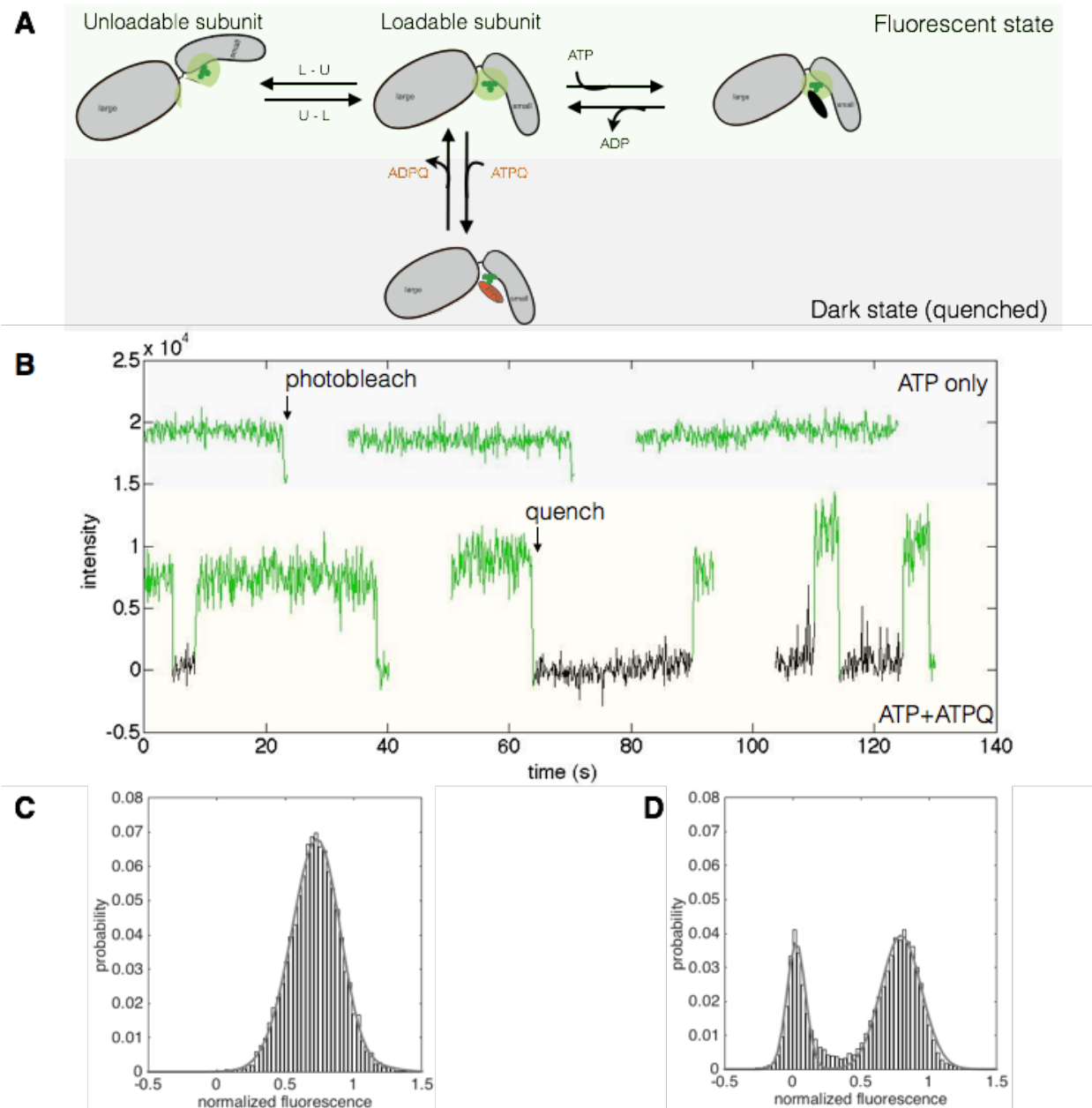


**Figure 3.** (A) In the presence of a mixture of ATP (black disk) and ATPQ (orange disk), a ClpX subunit (made up of a large and small domain) labeled with a TMR dye is expected to exhibit high fluorescence when the subunit is empty (“apo” state), bound to ATP, or in an unloadable conformation. When the subunit binds ATPQ the fluorescence is quenched. (B) Sample fluorescence traces for ClpX<sup>TMRP</sup> motors in the presence of 2 mM ATP (upper panel), and a mixture of 2 mM ATP and 100 μM ATPQ (bottom panel). (C) Histogram of normalized fluorescence intensities for ClpX<sup>TMRP</sup> in the presence of ATP only and a mixture of ATP + ATPQ (D). Fits in gray are to a double Gaussian function.

A separate AOD in the trapping branch of the instrument allowed for the generation of fast, 50 kHz, interlaced pulses of trapping and fluorescence beams, in order to maximize the fluorescence lifetime using interlaced optical force fluorescence (IOFF, (Brau, et al. 2006)). This approach helps prevent the shortened photobleaching times observed in coincident, simultaneous, force-fluorescence experiments (Dijk, et al. 2004) (Ferrer, et al. 2009).

Upon successful substrate recognition by a surface-bound ClpX<sup>TMRP</sup> motor, a computer-automated shutter was opened to illuminate the slide with the excitation laser, and both fluorescence intensity and bead displacement signals were recorded using custom made LabVIEW routines. Combined force-fluorescence experiments in the presence of ATP only, show fluorescence intensity remained constant during degradation of a V13P substrate, and the dye photobleached before the second V13P domain in the substrate was successfully unfolded (Figure 4B).

When a mixture of ATP and ATPQ was added, unfolding dwells were generally long, more than 20sec, when ATPQ turnover was observed as evidenced by quenching and unquenching of fluorescence intensity (Figure 4B), and often lead to substrate release, or tether breakage, which end the experiment. However, when a mixture of ATP and ATPQ was used to monitor translocation of a pre-unfolded titin<sup>I27</sup> substrate, fluorescence signals clearly show high fluorescence emission, with small changes in intensity likely caused by binding/un-binding of ATPQ in a neighboring subunit, and

occasional large magnitude quenching due to ATPQ binding to the subunit being imaged (Figure 4C). Interestingly, for periods of time in which multiple ATPQ nucleotides are bound to the same ClpX ring (~210-220sec mark in Figure 4C), translocation steps dwells are seen to slow down, and resume upon unbinding of ATPQ. Moreover, when only ATP molecules are used during substrate translocation, the fluorescence emission remains constant, without quenching events, and translocation proceeds without pausing (data not shown). This provides real-time visual evidence of how the molecular identity of the nucleotide used as fuel by ClpX, and other ATPases, directly impacts the motor's mechanical output.

Nucleotide binding lifetimes during unfolding were measured to be much longer than during translocation (Figure 5). Compared to nucleotide binding lifetimes in the absence of force and substrate, nucleotide turnover appears to speed up considerably during translocation of an unfolded polypeptide against the optical load of the trap.

## **DISCUSSION**

Here we provide a novel method to directly visualize, in real-time, ATP turnover by a AAA+ model enzyme while simultaneously tracking mechanical protein degradation. These results provide a window into the relative timing of nucleotide transactions during the fundamental portions of the protein degradation cycle. Furthermore, they clearly illustrate the effect of molecular identity of the nucleotide used as fuel, and its impact on motor activity.

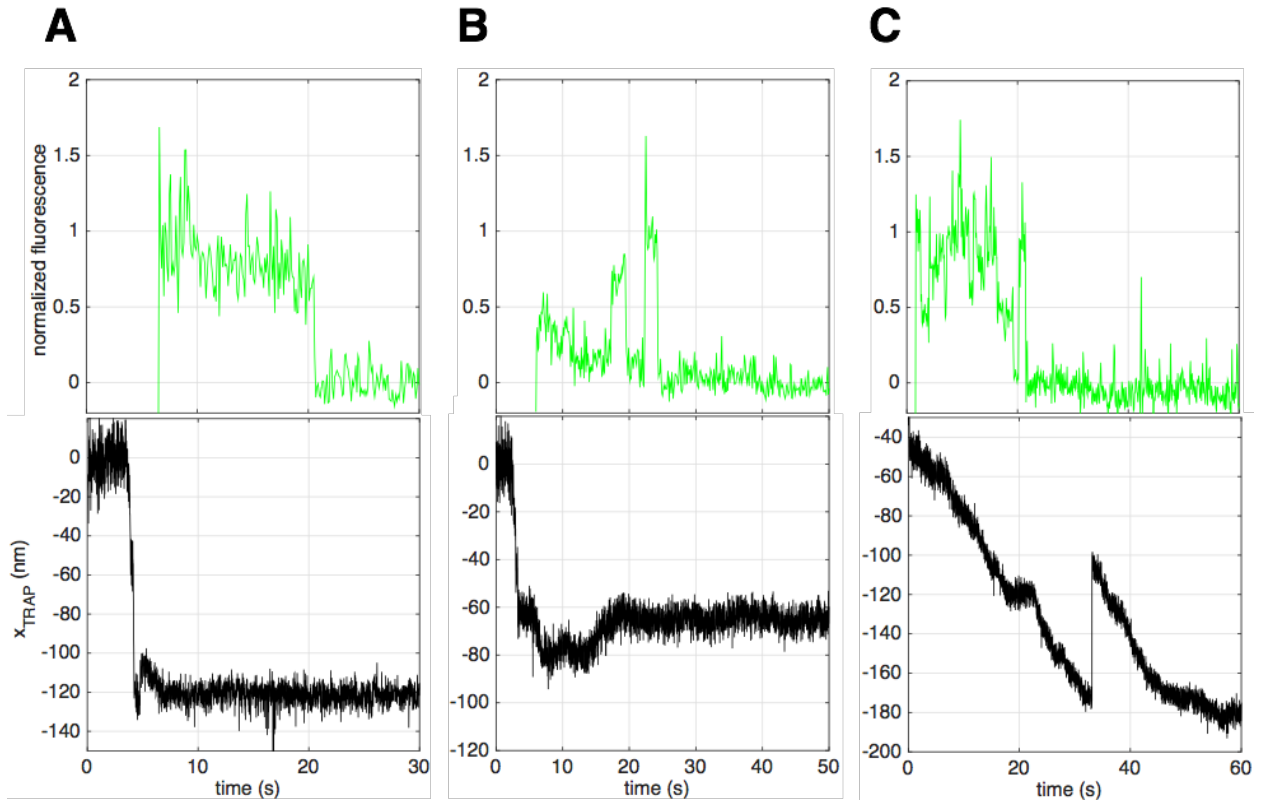


**Figure 4.** Combined force-fluorescence measurements. Mechanical degradation and fluorescence intensity traces for ClpX<sup>TMRP</sup> mediated unfolding of a V13P substrate in the presence of 2 mM ATP only (A), and a mixture of 2 mM ATP and 0.1 mM ATPQ (B-C). In (C) a pre-unfolded titin<sup>I27</sup> substrate was used. Position and intensity data were acquired at 90 Hz, but filtered and plotted at 10 Hz for the fluorescence.

While previous combined force-fluorescence experiments have predominantly focused on nucleic acid structures (Lang, et al. 2004) (Tarsa, et al. 2007) (Hohng, et al. 2007) and their associated enzymes (Comstock, et al. 2015), here we advance the applicability of this method to molecular motors that function on a protein track. As is the case for proteases like ClpXP, a major experimental hurdle lies within the well established degradation mechanism which includes occasional substrate release after failed degradation attempts (Kenniston, et al. 2004). In practice, this translates into having to use an experimental strategy in which the enzyme-substrate complex is

actively formed in real time, unlike previous studies using nucleic acid systems which are dynamic only upon the application of force (*e.g.* DNA shearing, DNA-hairpin transitions) and allow for pre-assembly of the biomolecular system. Here we use a highly automated, computer controlled, routine to actively assemble enzyme-substrate complexes, and carefully control light illumination/exposure to maximize fluorescence lifetimes.

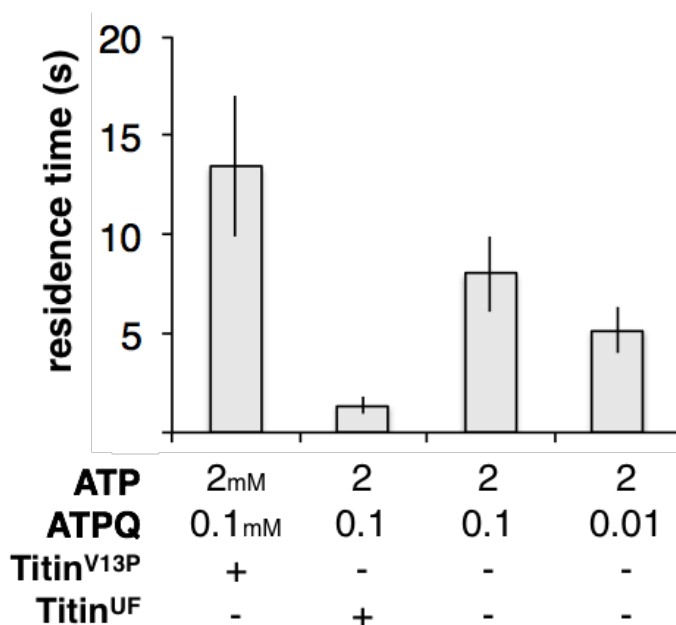


**Figure 5.** Average residence times for ATPQ in a ClpX subunit under different substrate and nucleotide conditions. Values represent means  $\pm$  SEM.

Moreover, by interlacing coincident fluorescence and trapping laser beams at high rates, we have shown the ability to track protein degradation at high resolution using a single-trap apparatus in a surface-tethered assay geometry. By strategically selecting rhodamine fluorophores we observe fluorescence lifetimes during the combined force-



fluorescence experiments on time scales similar to those of cellular tasks performed by molecular motors like ClpXP.

Together, these results set up the next-generation wave of single molecule experiments to investigate the ubiquitous enzymes of the AAA+ superfamily of molecular motors (Olivares, et al. 2016). Such experiments include using smFluorescence techniques like FRET (Tarsa, et al. 2007), or TMR/TMR quenching (Zhou, et al. 2011), to investigate whether large conformational changes in a single ClpX subunit coincide with successful protein denaturation. Also, similar strategies to the dark quencher assay studied here could be used to investigate substrate engagement by the ClpX ring, as well as to characterize substrate processing through the ClpXP pore-channel.

## **METHODS**

### **Single molecule fluorescence measurements**

Surface tethered ClpX<sup>TMRP</sup> motors were assembled on a PEG coated slide to prevent non-specific adsorption onto the glass coverslip surface. PEGylation of coverslips was done using a slightly modified version of the method described by previously reported (Jang and Nam 2008). Single molecule fluorescence only measurements were carried out on a custom-built instrument using a 532nm illumination laser (Coherent, Inc). Excitation light at ~3mW was sent into the back aperture of a 100X 1.49NA objective (Olympus), mounted on a modified inverted microscope (Nikon), at a critical angle for TIR. Fluorescence emission was collected by the objective and imaged using an

EMCCD camera (Andor Technology). Series of fluorescence images were acquired at 10Hz for 40-180 seconds and analyzed using MATLAB. To measure dwell times for specific fluorescence states the program vbFRET was used to carry out Hidden Markov Modeling of fluorescence intensities prior to photobleaching of the dye (McKinney, et al. 2006). Dwell times for high and low fluorescence states were extracted using custom written MATLAB routines. ATPQ and ClpXTMR motors were made by B. Stinson (MIT) as described in (B. M. Stinson, et al. 2015).

### **Combined force-fluorescence measurements**

Flow cells used for the combined force-fluorescence assay were prepared as described in the fluorescence methods section above, except the final solution included a suspension of substrate coated beads. Substrate coated beads were prepared by crosslinking Anti-Digoxigenin antibody (Roche) with Protein-G coated beads (780nm in diameter, Spherotech, Inc.) using BS3 crosslinker (Thermo Scientific). Protein substrates with an *ssrA* tag, and a HaloTag domain (Promega), were incubated overnight with a 100bp dsDNA spacer labelled with a HaloTag Ligand (Promega) on one end, and a Digoxigenin tag on the opposite end. DNA-Substrate tethers were then incubated with Anti-Digoxigenin beads for at least 30 minutes prior to loading on the slide.

To assemble tethers, beads in solution were trapped and brought in the vicinity of the coverslip surface. A piezo-stage (Physik Instrumente) was used to scan the coverslip

surface underneath the trapped bead until a surface bound ClpXP motor engaged a DNA-substrate tether, as monitored by tracking the bead displacement from the trap center. Upon tether formation, fluorescence illumination was turned using a computer controlled shutter. Bead displacement and fluorescence data was acquired using a custom written LabView (National Instruments, Inc.) program at 90Hz. Upon tether breakage and fluorescence photobleaching, position and stiffness calibration of the optical trap was carried out as previously described (Lang, et al. 2002). The stiffness of the optical trap was kept  $\sim 0.10$  pN/nm.

## REFERENCES

Aubin-Tam, Marie-Eve, Adrian O. Olivares, Robert T. Sauer, Tania A. Baker, and Matthew J. Lang. "Single-Molecule Protein Unfolding and Translocation by an ATP-Fueled Proteolytic Machine." *Cell*, 2011: 257–267.

Baker, Tania A, and Robert T Sauer. "ClpXP, an ATP-powered unfolding and protein-degradation machine." *Biochimica et Biophysica Acta (BBA) - Molecular Cell Research*, 2012: 15-28.

Brau, Ricardo R., Peter B. Tarsa, Jorge M. Ferrer, Peter Lee, and Matthew J. Lang. "Interlaced Optical Force-Fluorescence Measurements for Single Molecule Biophysics." *Biophysical Journal*, 2006: 1069-1077.

Burton, Randall E., Tania A. Baker, and Robert T. Sauer. "Energy-dependent degradation: Linkage between ClpX-catalyzed nucleotide hydrolysis and protein-substrate processing." *Protein Science*, 2003: 893-902.

Cho, Carol, and Ronald D. Vale. "The mechanism of dynein motility: Insight from crystal structures of the motor domain." *Biochimica et Biophysica Acta (BBA) - Molecular Cell Research*, 2014: 182-191.

Comstock, Matthew J., et al. "Direct observation of structure-function relationship in a nucleic acid processing enzyme." *Science*, 2015: 352-354.

Cordova, Juan Carlos, Dibyendu Kumar Das, Harris W Manning, and Matthew J Lang. "Combining single-molecule manipulation and single-molecule detection." *Current Opinion in Structural Biology*, 2014: 142-148.

Cordova, Juan Carlos, et al. "Stochastic but highly coordinated protein unfolding and translocation by the ClpXP proteolytic machine." *Cell*, 2014: 647-658.

Crisalli, Pete, and Eric T. Kool. "Multi-Path Quenchers: Efficient Quenching of Common Fluorophores." *Bioconjugate Chemistry*, 2011: 2345-2354.

Dijk, Meindert A. van, Lukas C. Kapitein, Joost van Mameren, Christoph F. Schmidt, and Erwin JG Peterman. "Combining Optical Trapping and Single-Molecule Fluorescence Spectroscopy: Enhanced Photobleaching of Fluorophores." *Journal of Physical Chemistry B*, 2004: 6479-6484.

Ferrer, Jorge M., D. Fangyuan, Ricardo R. Brau, Peter B. Tarsa, and Matthew J. Lang. "IOFF Generally Extends Fluorophore Longevity in the Presence of an Optical Trap." *Current Pharmaceutical Biotechnology*, 2009: 502-507.

Funatsu, Takashi, et al. "Imaging and nano-manipulation of single biomolecules." *Biophysical Chemistry*, 1997: 63-72.

Glynn, Steven E, Andrew R Nager, Tania A Baker, and Robert T Sauer. "Dynamic and static components power unfolding in topologically closed rings of a AAA plus proteolytic machine." *Nature Structural & Molecular Biology*, 2012: 616-622.

Glynn, Steven E., Andreas Martin, Andrew R. Nager, Tania A. Baker, and Robert T. Sauer. "Crystal structures of asymmetric ClpX hexamers reveal nucleotide-dependent motions in a AAA+ protein-unfolding machine." *Cell*, 2010: 744-756.

Hanson, Phyllis I., and Sidney W. Whiteheart. "AAA+ proteins: have engine, will work." *Nature Reviews Molecular Cell Biology*, 2005: 519-529.

Hayer-Hartl, Manajit, Andreas Bracher, and F. Ulrich Hartl. "The GroEL–GroES Chaperonin Machine: A Nano-Cage for Protein Folding." *Trends in Biochemical Sciences*, 2016: 62-76.

Hohng, Sungchul, et al. "Fluorescence-Force Spectroscopy Maps Two-Dimensional Reaction Landscape of the Holliday Junction." *Science*, 2007: 279-283.

Hwang, Wonmuk, and Matthew J Lang. "Nucleotide-dependent control of internal strains in ring-shaped AAA+ motors." *Cellular and Molecular Bioengineering*, 2013: 65-73.

Iosefson, Ohad, Adrian O. Olivares, Tania A. Baker, and Robert T. Sauer. "Dissection of Axial-Pore Loop Function during Unfolding and Translocation by a AAA+ Proteolytic Machine." *Cell Reports*, 2015: 1032-1041.

Ishijima, Akihiko, et al. "Simultaneous observation of individual ATPase and mechanical events by a single myosin molecule during interaction with actin." *Cell*, 1998: 161-171.

Jang, Kyung-Jin, and Jwa-Min Nam. "Direct-Write Nanoparticle Microarrays for Cell Assays." *Small*, 2008: 1930-1935.

Kakihara, Yoshito, and Walid A. Houry. "The R2TP complex: Discovery and functions." *Biochimica et Biophysica Acta (BBA) - Molecular Cell Research*, 2012: 101-107.

Kenniston, Jon A., Tania A. Baker, and Robert T. Sauer. "Partitioning between unfolding and release of native domains during ClpXP degradation determines substrate selectivity and partial processing." *Proceedings of the National Academy of Sciences*, 2004: 1390-1395.

Kim, Young-Chan, Aaron Snoberger, Jane Schupp, and David M. Smith. "ATP binding to neighbouring subunits and intersubunit allosteric coupling underlie proteasomal ATPase function." *Nature Communications*, 2015: 1-13.

Lang, Matthew J, Polly M Fordyce, Anita M Engh, Keir C Neuman, and Steven M Block. "Simultaneous, coincident optical trapping and single-molecule fluorescence." *Nature Methods*, 2004: 133-139.

Lang, Matthew J., Charles L. Asbury, Joshua W. Shaevitz, and Steven M. Block. "An Automated Two-Dimensional Optical Force Clamp for Single Molecule Studies." *Biophysical Journal*, 2002: 491-501.

Maillard, Rodrigo A., et al. "ClpX(P) generates mechanical force to unfold and translocate its protein substrates." *Cell*, 2011: 459-469.

Martin, Andreas, Tania A. Baker, and Robert T. Sauer. "Rebuilt AAA + motors reveal operating principles for ATP-fuelled machines." *Nature*, 2005: 1115-1120.

McKinney, Sean A., Chirlmin Joo, and Taekjip Ha. "Analysis of Single-Molecule FRET Trajectories Using Hidden Markov Modeling." *Biophysical Journal*, 2006: 1941-1951.

Ogura, Teru, and Anthony J Wilkinson. "AAA+ superfamily ATPases: common structure—diverse function." *Genes to Cells*, 2001: 575-597.

Olivares, Adrian O, Andrew R Nager, Ohad Iosefson, Robert T Sauer, and Tania A Baker. "Mechanochemical basis of protein degradation by a double-ring AAA+ machine." *Nature Structural & Molecular Biology*, 2014: 871-875.

Olivares, Adrian O., Tania A. Baker, and Robert T. Sauer. "Mechanistic insights into bacterial AAA+ proteases and protein-remodelling machines." *Nature Reviews Microbiology*, 2016: 33-44.

Sen, Maya, et al. "The ClpXP Protease Unfolds Substrates Using a Constant Rate of Pulling but Different Gears." *Cell*, 2013: 636-646.

Shin, Yongdae, et al. "Single-molecule denaturation and degradation of proteins by the AAA+ ClpXP protease." *Proceedings of the National Academy of Sciences*, 2009: 19340-19345.

Stinson, Benjamin M, Vladimir Baytshtok, Karl R Schmitz, Tania A Baker, and Robert T Sauer. "Subunit asymmetry and roles of conformational switching in the hexameric AAA+ ring of ClpX." *Nature Structural & Molecular Biology*, 2015: 411-416.

Stinson, Benjamin M. "Nucleotide Binding and Conformational Switching in the Hexameric Ring of a AAA+ Machine." Thesis, Department of Biology, Massachusetts Institute of Technology, Boston, 2015.

Stinson, Benjamin M., Andrew R. Nager, Steven E. Glynn, Karl R. Schmitz, Tania A. Baker, and Robert T. Sauer. "Nucleotide binding and conformational switching in the hexameric ring of a AAA+ machine." *Cell*, 2013: 628-639.

Tarsa, Peter B., et al. "Detecting Force-Induced Molecular Transitions with Fluorescence Resonant Energy Transfer." *Angewandte Chemie International Edition* 46, no. 12 (2007): 1999-2001.

Zhou, Ruobo, Simone Kunzelmann, Martin R. Webb, and Taekjip Ha. "Detecting Intramolecular Conformational Dynamics of Single Molecules in Short Distance Range with Subnanometer Sensitivity." *Nano Letters*, 2011: 5482-5488.

## CHAPTER 4

### **Real-time visualization of subunit conformational switching during protein degradation by a AAA+ machine**

#### **ABSTRACT**

To degrade unneeded proteins, ATP-dependent proteases harness chemical and thermal energy to generate mechanical work. A model ATPase system is the ClpXP proteolytic enzyme. Subunits forming the ClpX hexameric ring catalyze ATP turnover to power conformational changes that lead to unfolding and translocation of substrates tagged for destruction. Here we use single molecule fluorescence to visualize conformational switching in single ClpX subunits during protein degradation. Large ring rearrangements are loosely coupled to nucleotide hydrolysis, supporting and support a model in which thermal energy drives conformational switching. To measure the effect of structural transitions on molecular function, we develop a novel combined optical force-fluorescence assay to directly visualize the structural conformation of the ClpX ring as it degrades a protein substrate in real time. Our results show large subunit conformational changes are not responsible for successful protein unfolding, but provide a way for stalled motors to regain functionality. Together, these findings corroborate a large set of structural and ensemble biochemical studies that suggested large conformational transitions occur dynamically in a functional AAA+ ring.



## INTRODUCTION

Across all kingdoms of life, members of the AAA+ superfamily of enzymes (ATPases associated with diverse cellular activities plus) harness the energy of ATP hydrolysis to generate mechanical work (Ogura, et al. 2001). These molecular motors power highly diverse, and vital, cellular tasks like transport of cellular cargo (Cho, et al. 2014), remodeling of protein aggregates (DeSantis, et al. 2012), and degradation of unneeded proteins (Olivares, et al. 2016). One of the best understood AAA+ systems is the ClpXP protease (Baker, et al. 2012). ClpXP consists of the ClpX unfoldase, a homohexameric ring, which partners with the ClpP peptidase, a barrel-shaped double ring that houses a high concentration of catalytic active sites. ClpXP powers protein degradation by binding proteins tagged for degradation, followed by ATP-dependent mechanical unfolding and translocation of the substrate into the lumen ClpP for fragmentation of the polypeptide (Figure 1A).

The majority of active AAA+ motors function as ring structures (Ogura, et al. 2001) usually hexameric, through which motion of a single subunit allosterically changes the structure of other subunits in order to maintain a closed ring topology. X-ray crystal structures have shown the ClpX ring is asymmetric (Glynn, et al. 2010). Although each ClpX subunit is identical in sequence, ring asymmetry stems from the fact that not all subunits bind ATP at the same time in a functional ring. Rather, two major structural classes of ClpX subunits are present. The first is a nucleotide loadable subunit (referred to as L), which binds ATP at the conserved AAA+ nucleotide binding pocket that links

together the large and small domains of ClpX subunits. The second type of subunit contains an inaccessible nucleotide binding pocket due to rotation of the small domain about the large domain, rendering the subunit unloadable (referred to as U). Ensemble measurements have provided strong evidence that individual ClpX subunits couple ATP hydrolysis to mechanical force generation by switching between the L and U conformations. For example, ClpX mutants containing a single covalently locked ClpX subunit, in either U or L conformations, is able to hydrolyze ATP robustly but generally unable to degrade substrate (Stinson, et al. 2015). Yet, these large conformational changes have never been directly visualized, and the kinetics of these transitions remain undetermined. Furthermore, it is not known whether U-L transitions in a single subunit lead to the successful unfolding of a protein domain, or to what extent these transitions are used during polypeptide translocation. Finally, these large ring rearrangements have been theorized to be a “fail-safe” mechanism that may provide a way for ClpXP to prevent stalling of motor activity by resetting the ring after a series of power strokes are unable to successfully degrade a bound substrate (Olivares, et al. 2016).

Here we carry out single-molecule measurements to investigate ClpX subunit conformation during degradation of protein substrates. Our results provide the first direct visualization of dynamic conformational changes in active ClpX rings using single-molecule fluorescence quenching. Furthermore, we develop the first combined force-fluorescence assay for a AAA+ enzyme to simultaneously visualize subunit

conformation and mechanical activity of single ClpXP motors in real time. Our experiments suggest ClpX subunits spend the majority of time in a loadable conformation, but dynamically switch to an unloadable conformation during protein degradation. Conformational switching of subunits is not dependent on nucleotide hydrolysis, as similar transition rates are observed for ATP and ATP $\gamma$ S, a slowly hydrolysable ATP analogue. These large conformational changes are not directly responsible for successful protein denaturation as they are not concomitant with unfolding events in combined force-fluorescence experiments. The techniques described here provide a platform for future single-molecule studies of molecular motors and AAA+ enzymes.

## **RESULTS**

### **Design of ClpX variants for single molecule fluorescence**

Crystal structures suggest the ClpX ring (PDB entry 4I81), at its widest, has a diameter  $\sim$ 13nm, with single subunits extending  $\sim$ 7nm when bound to nucleotide (L subunit). However, nucleotide unloadable subunits (U subunits) measure  $\sim$ 6.5nm end-to-end. Given the small differences in length between a subunit in the U and L conformation, we opted to think of the ClpX ring as an assembly of six rigid bodies, each made up of a large domain and a small domain from separate neighboring subunits, connected by hinges (i.e. nucleotide binding pocket). Rigid body units rotate around the hinge when undergoing L-U transitions (Glynn, et al. 2012). Estimates from the crystal structures suggest the distance between two neighboring large domains at positions Q167 and

K213 is ~0.8 nm when in the loadable conformation, and ~3.5 nm upon rigid body rotation to reach an unloadable conformation (Figure 1B). Although the separation distance between these two points is too small to track at high resolution using conventional single molecule FRET, it is well designed for a single molecule fluorescence quenching (smFQ) approach (Topraka, et al. 2009).

While *in vivo* ClpX subunits actively self assemble to form a hexameric ring, rebuilt single-chain ClpX hexamers (Martin, et al. 2005) lacking the N-terminal region, used for binding adaptor proteins, have been widely used to study ClpXP behavior at the single molecule level (Shin, et al. 2009) (Aubin-Tam, et al. 2011) (Maillard, et al. 2011) (Sen, et al. 2013) (Cordova, et al. 2014) (Iosefson, et al. 2015). Here we used a variation on this single-chain strategy and synthesized single-chain trimers that can then be covalently linked through a sortase-mediated reaction to form hexameric rings (Stinson, et al. 2013). This strategy allowed us to tag separate batches of trimers with either a fluorophore or a dark quencher molecule. Trimers containing a Q167C single point mutation were labeled with an ATTO550 dye, while trimers with the K213C mutation were labeled with DabcylPlus using maleimide conjugates of the molecules to generate ClpX<sup>FQ</sup> rings. With this construct design, when the labeled subunit adopts a loadable conformation the dye/quencher pair undergoes mostly contact quenching through which more than 95% of the fluorescence emission is expected to be quenched (Crisalli, et al. 2011). However, when the subunit is in an unloadable conformation, fluorescence

emission is expected to remain high given that quenching through a FRET mechanism is expected to be less than 50%.

Bulk degradation assays were carried out to test the degradation activity of labeled ClpX variants (Figure 1C). At saturating ATP concentrations (3 mM), ClpX<sup>FQ</sup>P motors degraded CFP-ssrA substrate at similar rates to those of wild type ClpXP as determined by disappearance of CFP fluorescence using a stopped-flow fluorimeter. Thus, ClpX variants containing two fluorophores remain catalytically active. Moreover, using 530nm excitation light bulk fluorescence measurements of ClpX<sup>FQ</sup> revealed emission spectra with high intensity distributed ~575 nm as expected for the ATTO550 dye (Figure 1D). When ClpX<sup>FQ</sup> hexamers were incubated with 3 mM ATP nucleotide, there was a pronounced decrease of the fluorescence intensity suggesting a large fraction of the labeled ClpX subunits assume an L conformation in presence of nucleotide, and that DabcylPlus reliably quenches ATTO550 fluorescence. In the presence of Elastase, which digests ClpX, the fluorescence intensity peak was ~18% higher than in the absence of nucleotide. This shows the quenching of fluorescence through a FRET based mechanism is markedly lower in magnitude compared to contact quenching.

### **ClpX subunits dynamically switch conformations**

To investigate whether subunits in individual ClpX rings dynamically switch conformations, and how often these transitions occur, we carried out single molecule fluorescence experiments using surface immobilized ClpXP motors (Figure 2A).

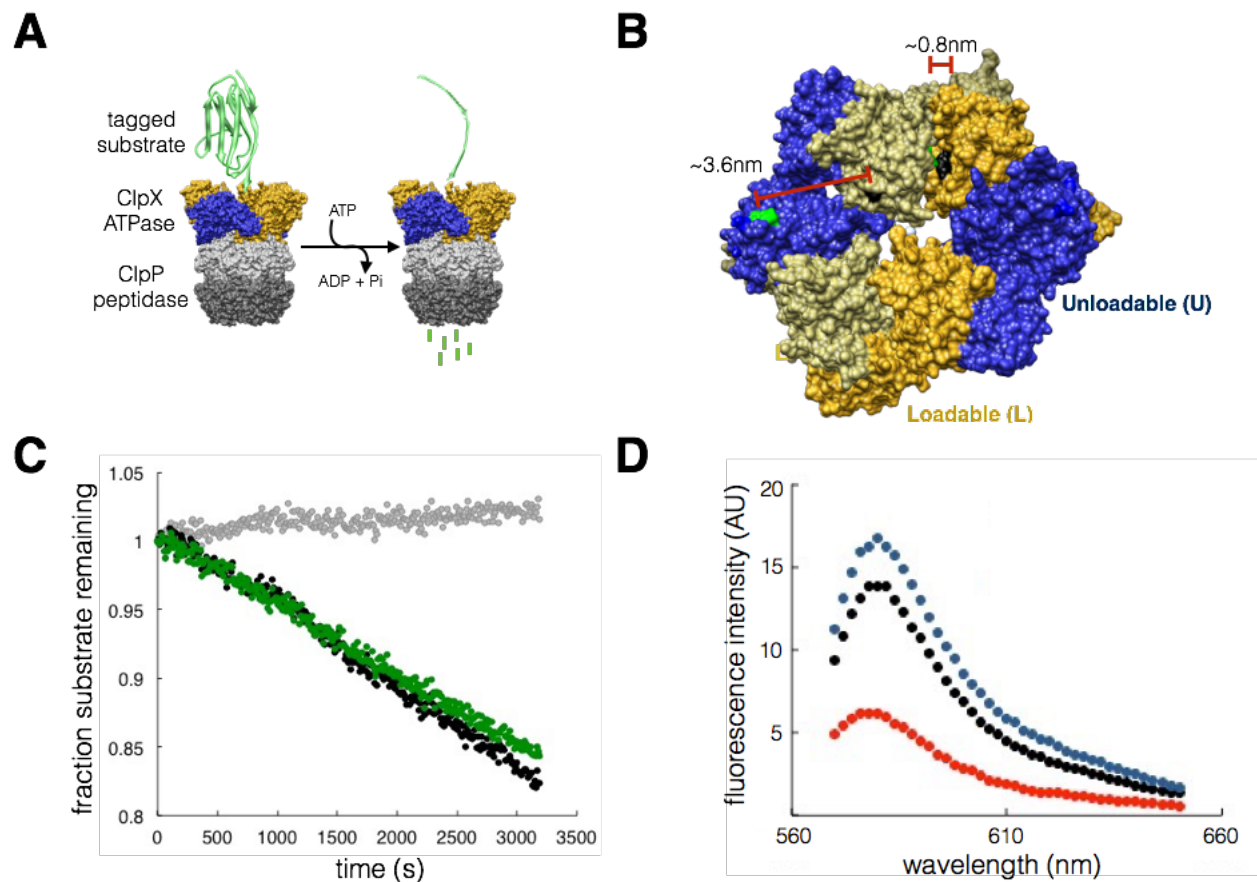


**Figure 1.** (A) The ClpX ATPase (PDB entry 3HWS) partners with the ClpP peptidase (PDB entry 1TYF) to power degradation of substrates tagged for destruction (substrate shown here is titin<sup>I27</sup>, PDB entry 1TIT). Cycles of ATP hydrolysis drive protein unfolding and translocation. The structures were stacked manually for visualization. (B) Crystal structure of the ClpX hexameric ring (PDB entry 3HWS), with nucleotide loadable subunits colored in yellow and unloadable subunits colored in blue. The Q167 and K213 residues in each subunit are labeled in green and black respectively. The distance between these two positions is ~0.8 nm when neighboring subunits are in an L conformation, and ~3.6 nm when neighboring subunits are in an U-L arrangement. (C) Ensemble degradation of the substrate ssrA-CFP in the presence of saturating ATP by parental ClpXP (black), the variant ClpX<sup>FQ</sup>P (green), or in the absence of ClpX (gray). (D) Fluorescence emission spectra (excitation at 530 nm) of ClpX<sup>FQ</sup> in the presence (red) or absence (black) of ATP, or in the presence of elastase which digests ClpX. Panels C-D courtesy of B. Stinson (MIT).

Glass coverslips were passivated using polyethylene glycol (PEG) to prevent nonspecific binding of proteins to the coverslip surface. A small fraction (1%) of

biotinylated PEG was used for targeted bottom-up assembly of ClpXP motors on the surface. First, streptavidin was used to bind the biotin-PEG, followed by incubation with ClpP molecules containing multiple biotin tags (Olivares, et al. 2014). Finally, ClpX<sup>FQ</sup> hexamers were added to the flow-cell and allowed to self-assemble with ClpP in the presence of ATP nucleotide.

Fluorescence intensity from individual surface tethered ClpXP motors was measured using a custom-built total internal reflection fluorescence (TIRF) microscope employing objective-side illumination. Analysis of individual trajectories shows a large fraction of molecules undergoing dynamic changes in intensity between high and low fluorescence states (Figure 2B). In the presence of saturating ATP, a histogram of normalized intensities for 151 separate ClpX<sup>FQ</sup>P molecules shows a bimodal distribution with populations centered around normalized intensity values of 0.02 and 0.69, as determined by a double Gaussian fit (Figure 2C). Based on the design of the ClpX construct, the low intensity population was assigned to subunits in the L conformation, and the high intensity population was assigned to those in the U conformation.

To measure the substrate dependence on conformational switching, experiments were carried out in the presence of 25  $\mu$ M titin<sup>I27</sup> domains, native or pre-unfolded, tagged with a C-terminal ssrA degron. Normalized intensity histograms for 247 ClpX<sup>FQ</sup>P molecules in the presence of a pre-unfolded titin<sup>I27</sup>, and 241 molecules in the presence of native titin<sup>I27</sup>, both show ClpX subunits have a higher probability of assuming an L

conformation, and a lower probability of assuming a U conformation, in the presence of substrate compared to the nucleotide only case. Notably, the histograms for subunits in the presence of folded or unfolded substrate show similar distributions (Figure 2D-E), suggesting ClpX subunits adopt similar arrangements when engaged to substrate regardless of the substrate's identity. Furthermore, the histograms show ~5:1 probability

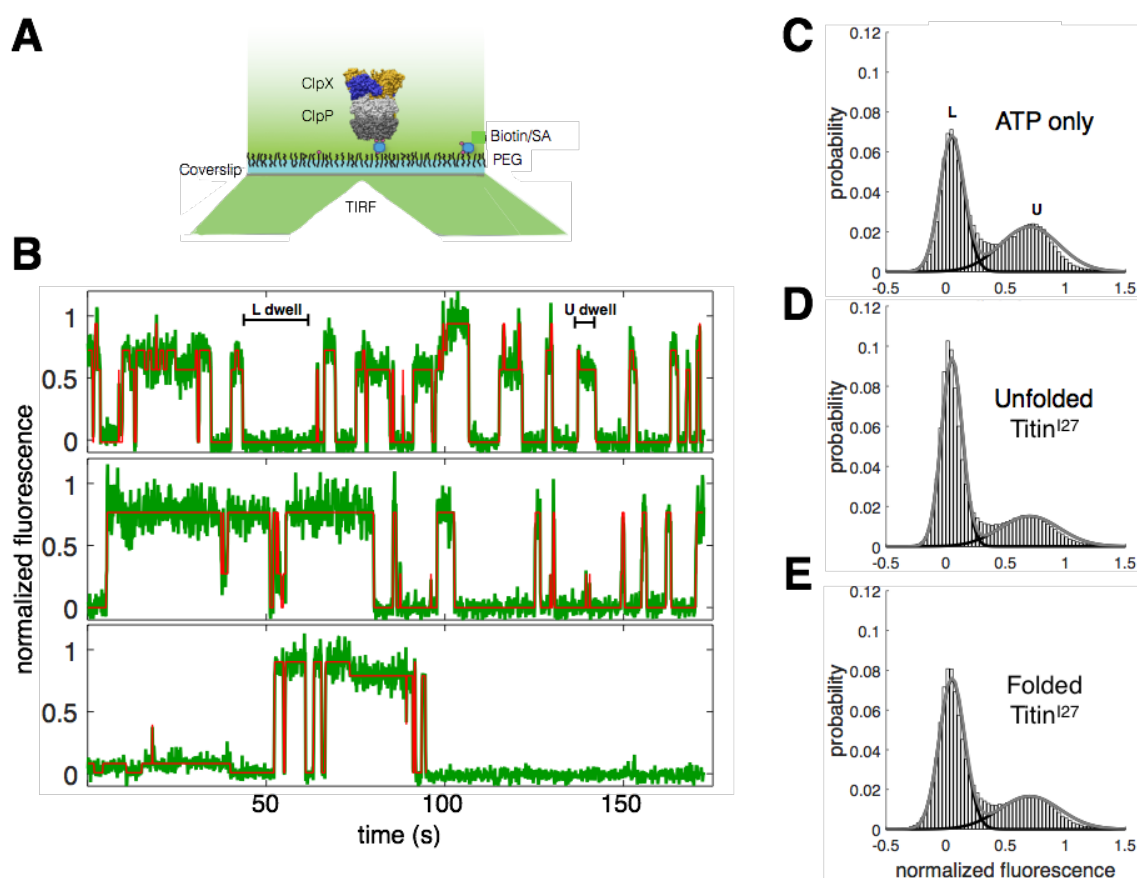


**Figure 2.** (A) For single molecule TIRF measurements, ClpXP motors were bound to a PEG-passivated coverslip surface using biotinylated ClpP and streptavidin. (B) Representative fluorescence trajectories for ClpX<sup>FQP</sup> motors in the presence of ATP only (top panel), and ATP plus pre-unfolded (middle panel) and native (bottom panel) ssaA-titin<sup>I27</sup> substrate. The red lines were fitted using HMM. (C-E) Fluorescence histograms of ClpX<sup>FQP</sup> in the presence of ATP or ATP plus different substrates. A double Gaussian distribution was fitted to each histogram.



of observing a subunit in an L conformation than a U conformation in the presence of substrate. This result is in agreement with ensemble studies proposing ClpX rings have a working conformation of 5-L and 1-U subunits (Stinson, et al. 2013).

To characterize the transition rates between L-U conformations, Hidden Markov Modeling (McKinney, Joo and Ha 2006) was used to fit traces with more than one L-U transition (red lines in Figure 2B) in the presence of ATP or ATP $\gamma$ S nucleotide at 3 mM, or ATP plus native and unfolded titin<sup>127</sup> substrate. Dwell times for each conformation were extracted for the HMM idealized traces, and used to generate the distributions shown in Figure 3. Cumulative frequency represents the fraction of total events that display a specific dwell time or lower. Across all conditions, the amount of time a ClpX subunits spends in the U conformation is shorter than in the L conformation. Dwell time distributions displayed double exponential behavior, suggesting there are two classes of U and L subunit conformations. Similar characteristic times for U and L subunits (Figure 3D) in the presence of ATP and ATP $\gamma$ S, an ATP analogue which ClpXP hydrolyzes ~30-fold slower (Burton, et al. 2003), suggests L-U switching is not tightly coupled to ATP hydrolysis. Notably, transition kinetics for U subunits remained constant for all the conditions tested, while subunits spend longer time in the L conformation when translocating substrate. The fact that U and L kinetics in the presence of native titin<sup>127</sup> highly resemble those for ATP only may suggest ClpX rings spend the majority of time unbound from substrate due to a higher propensity to release substrate to prevent motor stalling when encountering a mechanically stable protein (Kenniston, et al. 2004). This

is consistent with optical trapping assays where the overwhelming majority of native titin<sup>I27</sup> substrates are not successfully unfolded and are quickly released (Cordova, et al. 2014). To unambiguously visualize subunit conformation during active protein degradation we developed a combined optical trapping and fluorescence assay below.

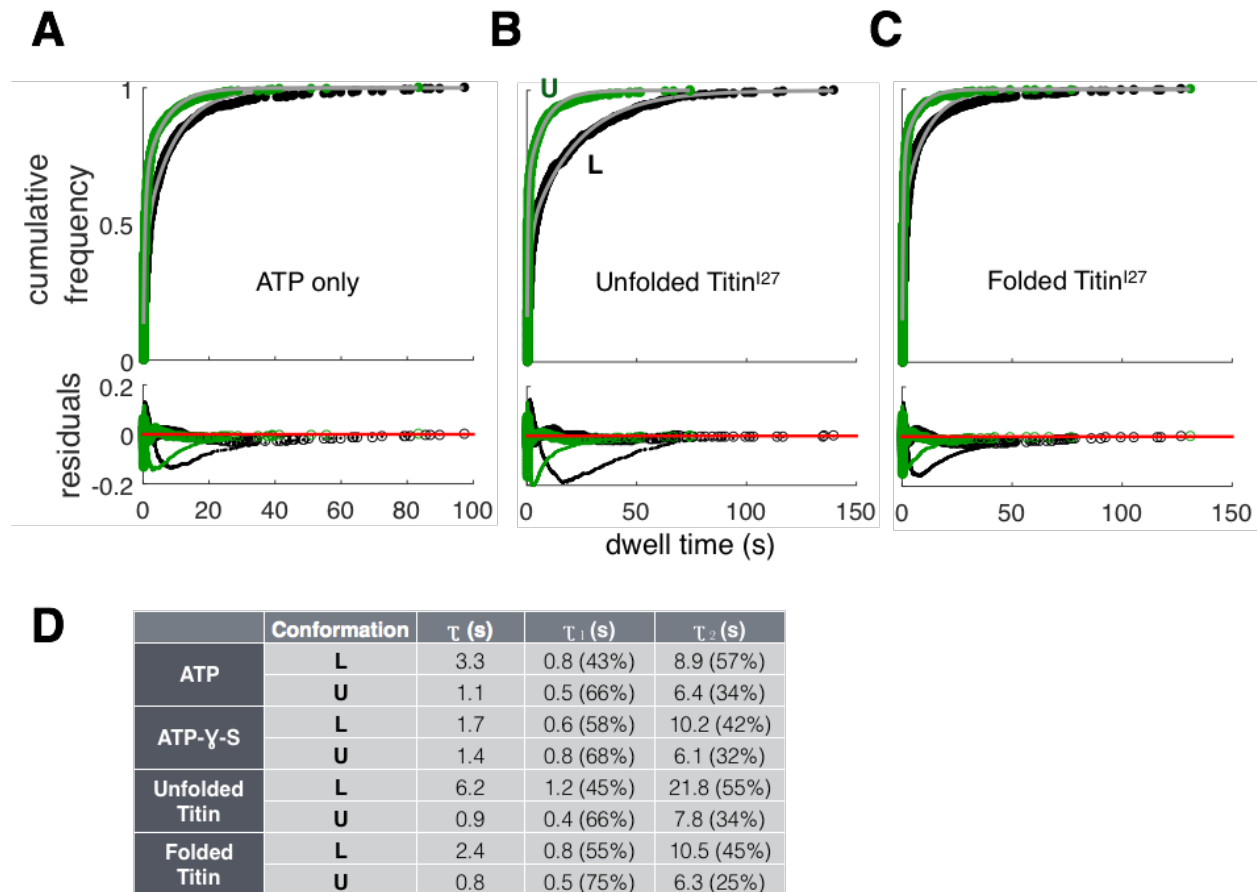


**Figure 3.** Dwell time distributions for L (black) and U (green) subunits for experiments in the presence of ATP only (A), and ATP plus unfolded (B) or folded (C) titin<sup>I27</sup> substrate. The distributions were fit to a double exponential function (gray line). The residuals for single (small green and black dots) and double (unfilled green and black circles) exponential fits are shown for each distribution. The predicted characteristic times from single ( $\tau$ ) and double ( $\tau_1$  and  $\tau_2$ ) exponential fits under different nucleotide and substrate conditions are summarized in (D). For double exponential fits, the percentage value corresponds to the contribution of that population to the overall fit.

## **Mechanical degradation by surface tethered ClpX<sup>FQ</sup>P molecules**

To simultaneously measure fluorescence intensity using TIRF microscopy while tracking ClpXP-driven mechanical motion using an optical trap, we engineered a single-trap mechanical assay with a surface tethered geometry (Figure 4A). Specifically, an anti-digoxigenin coated bead was functionalized with a multimeric substrate containing an ssrA degron to initiate ClpXP mediated substrate recognition and proteolysis. The substrate also included a terminal HaloTag domain, which was used to covalently bind the protein substrate to a short 100bp dsDNA tether labeled with a 3'-digoxigenin molecule. This short DNA tether was vital for successful assembly of ClpXP-substrate tethers.

While our group and others have previously developed an optical trapping assay to track mechanical force generation by ClpXP, those experimental geometries strictly relied on dual-trap setups uncoupled from the sample surface due to the concern of instrumental drift noise inherent to many surface-tethered optical trapping assays (Aubin-Tam, et al. 2011) (Maillard, et al. 2011) (Sen, et al. 2013) (Cordova, et al. 2014) (Olivares, et al. 2014). However, using a stable single trap instrument, we were able to reliably form ClpXP-substrate interactions and track mechanical degradation of multimeric substrates. Figure 4B shows single molecule degradation of model protein systems like titin<sup>V13P</sup> domains and green fluorescent protein (GFP), as well as substrates with multiple pre-unfolded titin<sup>I27</sup> domains (titin<sup>UF</sup>).

The mechanical degradation traces for folded substrates are characterized by large abrupt changes in distance representing successful domain unfolding. The size of the unfolding steps are dependent on the sequence length of the domain, and the optical force at unfolding. For example, Figure 4C shows a large unfolding distance for GFP (~238 amino acids in length) compared to the smaller Halo (~189 aa), and titin<sup>I27</sup> (89 aa) unfolding transitions. Unfolding events are directly followed by constant-rate decreases in relative distance corresponding to polypeptide translocation. The bottom trace of Figure 4B shows the long continuous translocation of a titin<sup>UF</sup> substrate with a terminal Halo unfolding and translocation. For substrates with multiple folded domains, upon completion of translocations, observed periods of constant trap position represent the time it takes ClpXP to unfold the abutting protein domain. The upper trace in Figure 4B shows the unfolding dwell time of the first GFP domain is ~7 sec, while the second domain requires ~70 sec before unfolding is achieved. While noise introduced by instrumental drift is sometimes observed (e.g. upper trace at time ~105 sec of Figure 3B), our surface tethered assay maintains high resolution as evident in the clear unfolding transitions (Figure 4C), and observation of clear discrete translocation steps (Figure 4D). Additionally, this custom built instrument was outfitted with a TRIF-based fluorescence excitation branch with confocal fluorescence detection of ATTO550 emission (See Methods section). We used this instrument below to directly visualize subunit conformation during protein unfolding and translocation.

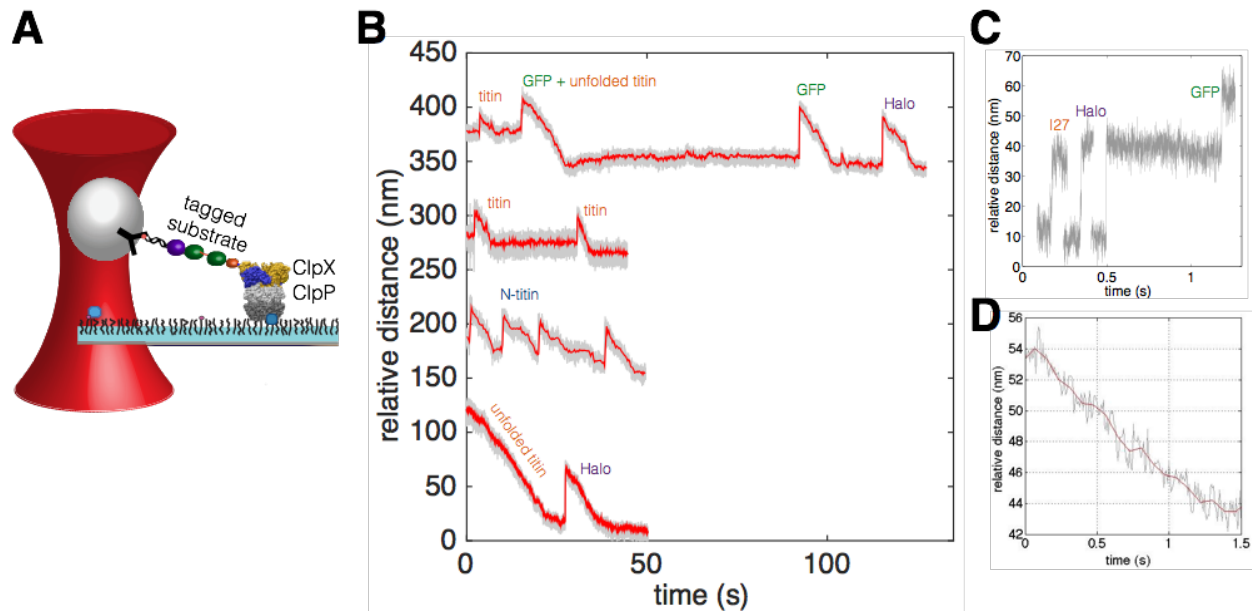


**Figure 4.** (A) Experimental geometry of the surface-tethered ClpXP optical trapping assay (not to scale). A laser trap was used to trap an anti-digoxigenin bead labeled with DNA-substrate tethers. The substrate was engaged by ClpXP motors bound to a PEG passivated coverslip. (B) Representative mechanical degradation traces by surface bound ClpXP motors. The upper trace shows the degradation of a titin<sup>V13P</sup>-GFP-titin<sup>UF</sup>-GFP-Halo substrate. The bottom three traces show the degradation of substrates with multiple titin<sup>V13P</sup> domains, titin<sup>I27</sup> domains with an N-terminal ssrA tag, or titin<sup>UF</sup> domains, respectively. (C) Comparison of the size of unfolding events for titin<sup>I27</sup>, Halo, and GFP. The GFP unfolding exhibits a well characterized intermediate (Maillard, et al. 2011). (D) Trace showing discrete steps during translocation of a Halo substrate at ~20 pN. For panels B-D raw data is shown in gray, and decimated data is shown in red.

### Combined force-fluorescence measurements

To actively assemble ClpXP-substrate complexes (Figure 5A) and simultaneously measure bead displacement and fluorescence intensities, we relied on a highly automated system which employs multiple computer controlled shutters to control the timing of fluorescence, trapping, and detection laser beam exposure. As displayed in Figure 4B, and quantified in previous studies (Cordova, et al. 2014) (Iosefson, et al. 2015), complete degradation of folded and unfolded substrates against an optical load normally takes ~20 sec to more than 100 sec depending on the mechanical stability of

the substrate. Yet, fluorophore photobleaching is enhanced in the presence of the high photon flux of the optical trap (Ferrer, et al. 2009) (Dijk, et al. 2004), leading to fluorescence lifetimes for single molecules of ~2 sec for the widely used Cy3 dye (Brau, et al. 2006). To help offset this effect, we employed an Interlaced Optical Force-Fluorescence (IOFF) strategy (Brau, et al. 2006). Using separate acousto-optic deflectors to rapidly modulate the intensity of the trapping and fluorescence lasers in an out-of-phase scheme (Figure 5A), we were able to observe sufficiently long fluorescence lifetimes while maintaining high resolution in the optical trap.

ClpXP-substrate complexes were actively assembled by stepping the coverslip surface, using a piezo nanopositioning stage, directly underneath a trapped bead coated with substrate. Upon successful substrate recognition, illustrated by bead displacement from the trap center ( $x_{\text{trap}}$ ), fluorescence excitation was turned on and both bead position and fluorescence counts were acquired until tether breakage and fluorescence photobleaching occurred. For the degradation of a titin<sup>UF</sup> substrate (Figure 5B), simultaneous trapping and fluorescence trajectories (Figure 5C-D) provide real time visualization of ClpX subunit conformation during translocation. While translocating substrate, our experiments show ClpX subunits preferably adopt an L conformation and dynamically convert to the U conformation (Figure 5). This is the first instance dynamic conformational switching in the ClpX AAA+ ring has been observed during substrate processing. Notably, these experiments suggest a ClpX subunit will on average switch conformations after translocating ~25 nm of substrate.

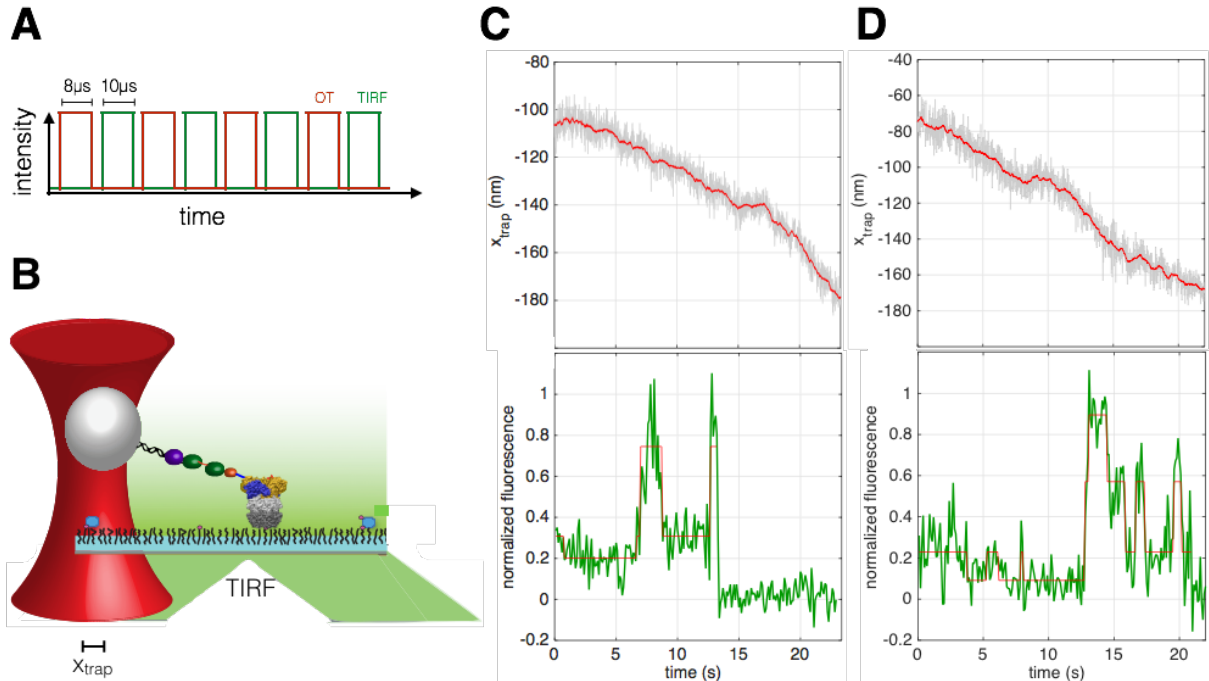


**Figure 5.** (A) For combined force-fluorescence experiments the intensities of the optical trap (OT) and the fluorescence (TIRF) lasers were interlaced in an out-of-phase scheme. The estimated durations of each laser pulse are shown. (B) Cartoon of the combined force-fluorescence assay geometry (not to scale). Bead displacement from the trap center ( $x_{\text{trap}}$ ) and fluorescence intensity are measured concurrently. (C-D) Simultaneous observation of translocation of a titin<sup>UF</sup> substrate and fluorescence intensity of the same ClpX<sup>FQ</sup> ring. Abrupt changes in intensity (fitted using HMM, red lines in fluorescence panels) correspond to L-U transitions.

To investigate importance of L-U switching during protein unfolding, we carried out combined force-fluorescence experiments using substrates containing multiple folded domains (Figure 6A). Similarly to the behavior observed during translocation, ClpX subunits spend a majority of time in an L conformation and briefly visit the U conformation. Given the importance of L-U switching to degradation activity of ClpX rings, we wondered if these transitions drive successful protein unfolding? Our experiments suggest this is not the case. When degrading a titin<sup>I27</sup> labeled with an N-terminal ssrA tag (titin<sup>N</sup>), L-U transitions are not concomitant with unfolding transitions

(Figure 6B). In more than 12 unfolding events, we did not observe a coincident unfolding event and an L-U transition. Since we are observing the conformation of only one of six ClpX subunits, one would expect to observe coincident unfolding and conformational switching in two of twelve events if L-U transitions are directly responsible for denaturation. We tested if this was also the case when unfolding more stable proteins, such as substrates containing multiple titin<sup>V13P</sup> domains (Figure 6C), which ClpXP normally degrades in ~7sec (Cordova, et al. 2014) compared to ~1sec for N-tagged titin<sup>I27</sup> (unpublished data). In more than six titin<sup>V13P</sup> unfoldings, L-U transitions did not directly lead to successful unfolding.

## **DISCUSSION**

The well studied ClpX AAA+ ring is composed of six separate subunits identical in sequence. Crystal structures of ClpX rings exhibit two main types of subunit orientations, nucleotide loadable and unloadable, which have been found to be vital for robust motor activity (Stinson, et al. 2015). Here we use fluorescence quenching between a donor fluorophore and a non-fluorescent acceptor to monitor these conformational changes in individual ClpX subunits. Single molecule fluorescence measurements using TIRF microscopy display two major populations corresponding to loadable (low fluorescence) and unloadable (high fluorescence) subunits (Figure 2B). During degradation of titin<sup>UF</sup> substrate, our experiments show a 5:1 probability of observing a subunit in an L versus U conformation (Figure 2D), consistent with



ensemble measurements suggesting the working conformation of the ClpX ring consists of 5L:1U subunits (Stinson, et al. 2013).

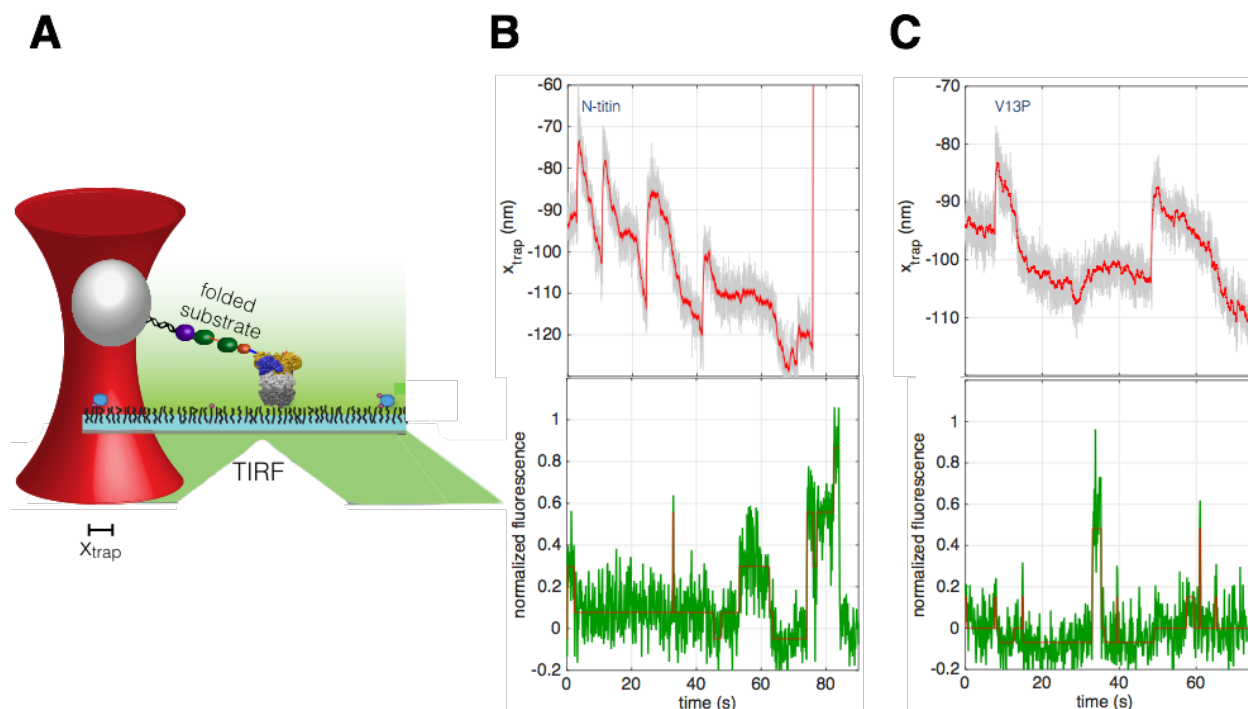


**Figure 6.** (A) Cartoon of the combined force-fluorescence assay geometry. The substrates used here contained multiple folded titin<sup>I27</sup> domains (not to scale). Mechanical protein unfolding and translocation with the corresponding fluorescence signal during degradation of titin<sup>N</sup> (B) or titin<sup>V13P</sup> domains (C). While both of these substrates are folded structures, their mechanical stability is very different. ClpXP unfolds titin<sup>N</sup> much faster than titin<sup>V13P</sup> as discussed in the text.

Fluorescence trajectories provide real-time visualization of dynamic L-U switching with high resolution between conformational states. Similar kinetics of L-U transitions (Figure 3) for ClpX motors in the presence of ATP and ATP $\gamma$ S suggest hydrolysis of ATP does not directly fuel L-U conformational switching. As characterized in Chapter 2 of this thesis, ClpXP takes advantage of stochastic thermal fluctuations to denature folded proteins, and degradation kinetics increase with temperature. Thus, we hypothesize L-U switching may also be largely driven by thermal energy in the environment.

Using a novel combined force-fluorescence assay we report on the conformational state of the ClpX ring as it degrades a substrate in real time, and probe the extent to which large subunit rearrangements are involved in protein unfolding and translocation. To our knowledge, these results provide the first combined measurement for an AAA+ motor, and elucidate the structure-function relationship of active ClpXP motors. An unresolved question has been whether L-U conformational switching is necessary for protein translocation? Our results provide direct evidence for L-U transitions during translocation of substrate, although these transitions do not result in specifically long steps sizes (Figure 5). Thus, ring rearrangements occur during translocation but may not be required. Are large conformational rearrangements in the ClpX ring used as a mechanism to prevent motor stalling? Our experiments provide some evidence that this may in fact be the case. As shown at the 45 sec mark in Figure 6B, during translocation of the fourth titin<sup>127</sup> domain a translocation pause is observed lasting ~20 s. Remarkably, an L-U transition is observed during this pause, yet it is only after the return U-L transition occurs that translocation is resumed, suggesting these large conformational changes may provide the ClpXP motor with a strategy to escape a futile conformation. Do large ring rearrangements compromise substrate gripping by ClpX? The majority of L-U transitions we observed do not coincide with substrate release represented by the return of the trapped bead to the center of the optical trap. However, there is one instance in which substrate release occurs shortly after an L-U transition (~75 sec in Figure 6B), suggesting the possibility that large ring rearrangements can compromise

substrate gripping and provide a mechanism for substrate release, a well characterized part of ClpXP function (Kenniston, et al. 2004). Are L-U transitions responsible for successful unfolding events? Optical trapping experiments have revealed long unfolding dwells are sometimes required to unfold mechanically stable proteins (Aubin-Tam, et al. 2011) (Cordova, et al. 2014) (Maillard, et al. 2011), yet it was undetermined whether successful unfolding was achieved due to large conformational changes in the ClpX ring or stochastic changes in protein stability due to thermal energy. Our measurements suggest L-U transitions are not directly responsible for successful unfolding, supporting a model where a power-stroke from a single subunit coinciding with thermal destabilization of the protein substrate drives protein unfolding (Martin, et al. 2005).

We anticipate future work employing the techniques presented here will allow for further dissection of the structure-function relationship during particular portions of the degradation cycle. For example, the conformational states observed when ClpX translocates two disulfide-linked substrates (Glynn, et al. 2010) where the ClpX pore must widen remain unknown, but could be probed with the approaches described here. More broadly, it remains to be determined whether other AAA+ motors share some of the mechanisms of force generation as the model ClpXP protease.

## **METHODS**

### **Fluorescence quenching measurements**

Surface tethered ClpX<sup>FQ</sup>P motors were assembled on a PEG coated slide to prevent non-specific adsorption onto the glass coverslip surface. PEGylation of coverslips was done using a slightly modified version of the method described by previously reported (Jang and Nam 2008). Single molecule fluorescence only measurements were carried out on a custom-built instrument using a 532nm illumination laser (Coherent, Inc). Excitation light at ~3mW was sent into the back aperture of a 100X 1.49NA objective (Olympus), mounted on a modified inverted microscope (Nikon), at a critical angle for TIR. Fluorescence emission was collected by the objective and imaged using an EMCCD camera (Andor Technology). Series of fluorescence images were acquired at 10Hz for 3 minutes and analyzed using MATLAB. To measure dwell times for specific fluorescence states, corresponding to subunit conformations, the program vbFRET was used to carry out Hidden Markov Modeling of fluorescence intensities prior to photobleaching of the dye (McKinney, et al. 2006). Dwell times for high and low fluorescence states were extracted using custom written MATLAB routines, and used to calculate cumulative frequency distributions.

### **Combined force-fluorescence measurements**

Flow cells used for the combined force-fluorescence assay were prepared as described in the fluorescence methods section above, except the final solution included a suspension of substrate coated beads. Substrate coated beads were prepared by

crosslinking Anti-Digoxigenin antibody (Roche) with Protein-G coated beads (780nm in diameter, Spherotech, Inc.) using BS3 crosslinker (Thermo Scientific). Protein substrates with an *ssrA* tag, and a HaloTag domain (Promega), were incubated overnight with a 100bp dsDNA spacer labelled with a HaloTag Ligand (Promega) on one end, and a Digoxigenin tag on the opposite end. DNA-Substrate tethers were then incubated with Anti-Digoxigenin beads for at least 30 minutes prior to loading on the slide.

To assemble tethers, beads in solution were trapped and brought in the vicinity of the coverslip surface. A piezo-stage (Physik Instrumente) was used to scan the coverslip surface underneath the trapped bead until a surface bound ClpXP motor engaged a DNA-substrate tether, as monitored by tracking the bead displacement from the trap center. Upon tether formation, fluorescence illumination was turned using a computer controlled shutter. Bead displacement and fluorescence data was acquired using a custom written LabView (National Instruments, Inc.) program at 90Hz. Upon tether breakage and fluorescence photobleaching, position and stiffness calibration of the optical trap was carried out as previously described (Lang, et al. 2002). The stiffness of the optical trap was kept  $\sim 0.10$  pN/nm.

The combined optical trapping and confocal TIRF instrument used is a modified version of the apparatus previously described (Brau, et al. 2006). Briefly, optical trapping (1064nm, Coherent, Inc.) and fluorescence (532nm, World Star Tech) lasers interlaced

out-of-phase at 50kHz using a two-function generator (Sony, Inc.) to control input signals into separate Acousto-Optic Deflectors (IntraAction). A low power detection laser (975nm, Corning Lasertron) was kept continuously on during the measurement to track displacement of the trapped bead. A set of computer automated shutters were used to control light exposure into a photon-counting silicon avalanche photodiode (PerkinElmer) to acquire photons filtered by a pinhole (Thorlabs). The pinhole was aligned at a conjugate plane to the coverslip surface, and centered directly at the position of the trapping and detection lasers.

## REFERENCES

Aubin-Tam, Marie-Eve, Adrian O. Olivares, Robert T. Sauer, Tania A. Baker, and Matthew J. Lang. "Single-Molecule Protein Unfolding and Translocation by an ATP-Fueled Proteolytic Machine." *Cell*, 2011: 257–267.

Baker, Tania A, and Robert T Sauer. "ClpXP, an ATP-powered unfolding and protein-degradation machine." *Biochimica et Biophysica Acta (BBA) - Molecular Cell Research*, 2012: 15-28.

Brau, Ricardo R., Peter B. Tarsa, Jorge M. Ferrer, Peter Lee, and Matthew J. Lang. "Interlaced Optical Force-Fluorescence Measurements for Single Molecule Biophysics." *Biophysical Journal*, 2006: 1069-1077.

Burton, Randall E., Tania A. Baker, and Robert T. Sauer. "Energy-dependent degradation: Linkage between ClpX-catalyzed nucleotide hydrolysis and protein-substrate processing." *Protein Science*, 2003: 893-902.

Cho, Carol, and Ronald D. Vale. "The mechanism of dynein motility: Insight from crystal structures of the motor domain." *Biochimica et Biophysica Acta (BBA) - Molecular Cell Research*, 2014: 182-191.

Cordova, Juan Carlos, et al. "Stochastic but highly coordinated protein unfolding and translocation by the ClpXP proteolytic machine." *Cell*, 2014: 647-658.

Crisalli, Pete, and Eric T. Kool. "Multi-Path Quenchers: Efficient Quenching of Common Fluorophores." *Bioconjugate Chemistry*, 2011: 2345-2354.

DeSantis, Morgan E., and James Shorter. "The elusive middle domain of Hsp104 and ClpB: Location and function." *Biochimica et Biophysica Acta (BBA) - Molecular Cell Research*, 2012: 29-39.

Dijk, Meindert A. van, Lukas C. Kapitein, Joost van Mameren, Christoph F. Schmidt, and Erwin JG Peterman. "Combining Optical Trapping and Single-Molecule Fluorescence Spectroscopy: Enhanced Photobleaching of Fluorophores." *Journal of Physical Chemistry B*, 2004: 6479-6484.

Ferrer, Jorge M., D. Fangyuan, Ricardo R. Brau, Peter B. Tarsa, and Matthew J. Lang. "IOFF Generally Extends Fluorophore Longevity in the Presence of an Optical Trap." *Current Pharmaceutical Biotechnology*, 2009: 502-507.

Glynn, Steven E, Andrew R Nager, Tania A Baker, and Robert T Sauer. "Dynamic and static components power unfolding in topologically closed rings of a AAA plus proteolytic machine." *Nature Structural & Molecular Biology*, 2012: 616-622.

Glynn, Steven E., Andreas Martin, Andrew R. Nager, Tania A. Baker, and Robert T. Sauer. "Crystal structures of asymmetric ClpX hexamers reveal nucleotide-dependent motions in a AAA+ protein-unfolding machine." *Cell*, 2010: 744-756.

Hanson, Phyllis I., and Sidney W. Whiteheart. "AAA+ proteins: have engine, will work." *Nature Reviews Molecular Cell Biology*, 2005: 519-529.

Iosefson, Ohad, Adrian O. Olivares, Tania A. Baker, and Robert T. Sauer. "Dissection of Axial-Pore Loop Function during Unfolding and Translocation by a AAA+ Proteolytic Machine." *Cell Reports*, 2015: 1032-1041.

Jang, Kyung-Jin, and Jwa-Min Nam. "Direct-Write Nanoparticle Microarrays for Cell Assays." *Small*, 2008: 1930-1935.

Kenniston, Jon A., Tania A. Baker, and Robert T. Sauer. "Partitioning between unfolding and release of native domains during ClpXP degradation determines substrate selectivity and partial processing." *Proceedings of the National Academy of Sciences*, 2004: 1390-1395.

Lang, Matthew J, Polly M Fordyce, Anita M Engh, Keir C Neuman, and Steven M Block. "Simultaneous, coincident optical trapping and single-molecule fluorescence." *Nature Methods*, 2004: 133-139.

Lang, Matthew J., Charles L. Asbury, Joshua W. Shaevitz, and Steven M. Block. "An Automated Two-Dimensional Optical Force Clamp for Single Molecule Studies." *Biophysical Journal*, 2002: 491-501.

Maillard, Rodrigo A., et al. "ClpX(P) generates mechanical force to unfold and translocate its protein substrates." *Cell*, 2011: 459-469.

Martin, Andreas, Tania A. Baker, and Robert T. Sauer. "Rebuilt AAA + motors reveal operating principles for ATP-fuelled machines." *Nature*, 2005: 1115-1120.

McKinney, Sean A., Chirlmin Joo, and Taekjip Ha. "Analysis of Single-Molecule FRET Trajectories Using Hidden Markov Modeling." *Biophysical Journal*, 2006: 1941-1951.

Ogura, Teru, and Anthony J Wilkinson. "AAA+ superfamily ATPases: common structure—diverse function." *Genes to Cells*, 2001: 575-597.

Olivares, Adrian O, Andrew R Nager, Ohad Iosefson, Robert T Sauer, and Tania A Baker. "Mechanochemical basis of protein degradation by a double-ring AAA+ machine." *Nature Structural & Molecular Biology*, 2014: 871-875.

Olivares, Adrian O., Tania A. Baker, and Robert T. Sauer. "Mechanistic insights into bacterial AAA+ proteases and protein-remodelling machines." *Nature Reviews Microbiology*, 2016: 33-44.



Sen, Maya, et al. "The ClpXP Protease Unfolds Substrates Using a Constant Rate of Pulling but Different Gears." *Cell*, 2013: 636-646.

Shin, Yongdae, et al. "Single-molecule denaturation and degradation of proteins by the AAA+ ClpXP protease." *Proceedings of the National Academy of Sciences*, 2009: 19340-19345.

Stinson, Benjamin M, Vladimir Baytshtok, Karl R Schmitz, Tania A Baker, and Robert T Sauer. "Subunit asymmetry and roles of conformational switching in the hexameric AAA+ ring of ClpX." *Nature Structural & Molecular Biology*, 2015: 411-416.

Stinson, Benjamin M., Andrew R. Nager, Steven E. Glynn, Karl R. Schmitz, Tania A. Baker, and Robert T. Sauer. "Nucleotide binding and conformational switching in the hexameric ring of a AAA+ machine." *Cell*, 2013: 628-639.

Tarsa, Peter B., et al. "Detecting Force-Induced Molecular Transitions with Fluorescence Resonant Energy Transfer." *Angewandte Chemie International Edition* 46, no. 12 (2007): 1999-2001.

Topraka, Erdal, Ahmet Yildizc, Melinda Tonks Hoffmanb, Steven S. Rosenfeldd, and Paul R. Selvin. "Why kinesin is so processive." *Proceedings of the National Academy of Sciences*, 2009: 12717-12722.

## CHAPTER 5

### **Bio-functionalization of core-shell particles with enhanced trapping stability**

#### **ABSTRACT**

Due to their high spatial resolution and precise application of force, optical traps are widely used to study the mechanics of biomolecules and biopolymers at the single-molecule level. Recently, newly developed trapping handles have shown a considerable improvement in trapping stability making them promising candidates for high-force experiments. However, a strategy for labeling these particles with biomolecules is yet to be developed. Here we provide a straightforward synthetic strategy to functionalize titania core-shell particles with proteins and nucleic acids by adding a silane-thiol functionalizer to the shell surface. These bio-functionalized particles display higher stability in an optical trap compared to the plastic beads commonly used as handles in optical trapping experiments. We anticipate the functionalized core-shells can be used to probe the mechanics of stable proteins structures, and employed in combined trapping and fluorescence experiments where lower trapping powers are advantageous.

## INTRODUCTION

Optical traps have been widely used as a tool to measure small displacements, exert finely controlled forces, and manipulate microscopic objects. By tethering a biomolecule of interest between a dielectric particle, like a plastic bead, and a glass coverslip surface the optical force can be finely controlled to measure the mechanical properties of proteins, biopolymers, and protein aggregates involved in disease (Fazal, et al. 2011). Micrometer sized beads, normally made of polystyrene, are widely employed in optical trapping experiments. These plastic beads can be functionalized at the surface with chemically reactive molecules like primary amines, carboxylates, and hydroxyls, which in turn can be conjugated to biomolecules of interest for single molecule experiments (Bugiel, et al. 2015).

An optical trap is formed by focusing a laser beam into a diffraction limited spot using a high numerical aperture objective lens. In the presence of the optical trap a dielectric particle will experience a gradient force toward the focus of the trap where the photon flux is highest, as well as a scattering force in the direction of propagation of light (Neuman, et al. 2004). A dielectric object, referred to as a trapping handle, is trappable when the magnitude of the gradient force is larger than that of the scattering force. Using a single gradient optical trap, objects with refractive indices larger than  $n=1.73$  become untrappable in an aqueous medium, such as biological buffers, due to large amounts of scattering (Hu, et al. 2008). Yet, fine tuning the difference in index of

refraction of the handle and the surrounding medium can lead to higher trapping stabilities (Horst, et al. 2008).

Recently, Schaffer and coworkers developed coated microspheres with decreased scattering and exceptionally high trapping stability (Jannasch, et al. 2012), without the need to use high laser powers that can lead to photodamage of biomolecules and sample heating (Peterman, et al. 2003). However, in order for these anatase-titania core-shell handles to become a useful tool in the field of single-molecule biophysics, a clear and straightforward method to synthesize these promising particles must be developed. Currently, the literature provides only vague descriptions of the synthesis of these microparticles, and a strategy to functionalize these handles with biomolecules relevant to biophysical assays has not been developed. Here we provide a synthetic strategy for making anatase-titania core-shell particles covalently linked to biomolecules like proteins (prion proteins, streptavidin) and nucleic acids (double stranded DNA). We anticipate the methods described here will allow for wider applicability of these improved trapping handles in optical trapping applications requiring the use of high forces (Dong, et al. 2010) (Castro, et al. 2011), as well as in combined coincident optical trapping and fluorescence assays (Lang, et al. 2004) (Tarsa, et al. 2007) (Brau, et al. 2006) where minimizing laser powers while maintaining trapping stability is vital (Dijk, et al. 2004).

## MATERIALS AND METHODS

### Core-Shell synthesis

Cores were synthesized by chelating a 0.46% (by weight) solution of titanium butoxide (TBT, Sigma Aldrich) with ethylene glycol (EG, Sigma Aldrich) overnight in a nitrogen environment under rotation. A 100 mL acetone solution with 2.03 mM Tween-20 (Sigma Aldrich) and 100  $\mu$ L of water was mixed with 18-20 mL of the TBT-EG solution depending on the size of cores needed (19 mL of TBT-EG solution produced  $\sim$ 500 nm cores, Figure 2B). The reaction mixture was agitated for 10 minutes and stored at room temperature for 24 hours. The particles were collected by centrifuging the solution for five minutes at 7,000 rpm and redispersed in cold ethanol a total of three times. After the final centrifugation step, the pellet was dried in a convection oven at 70°C for thirty minutes to evaporate any remaining solvent prior to calcination. The dried cores were then annealed for 1 hour at 500°C in a furnace to induce a transition of the titania into the anatase phase. The cores were sized using a light microscope with differential interference contrast microscopy (DIC).

For the addition of the amorphous titania shells, 0.5 mg of anatase cores were resuspended in 3.3 mL of ethanol with 800  $\mu$ M Lutensol (BASF) and disaggregated using a probe sonicator. This solution was then added to a 3.3 mL ethanol solution with 50-175  $\mu$ L of TBT. The amount of TBT added in this step dictates the diameter of core-shell particles after mixing, with 100  $\mu$ L TBT producing core-shell particles with diameter  $\sim$ 1,350 nm. The core-TBT mixture was reacted for a total of two hours in a temperature

controlled bath sonicator kept at  $\sim 30^{\circ}\text{C}$ . To incorporate surface exposed thiol groups, 80  $\mu\text{L}$  of a 1:100 dilution of (3-mercaptopropyl)trimethoxysilane (MPTS, Sigma Aldrich) in ethanol was added to the reaction mixture after 1 hour of sonication. The MPTS solution was prepared under a nitrogen environment. Upon completion of the reaction, the core-shell particles were cleaned by centrifuging for 5 minutes at 5,000 rcf resuspending in 3 mL of ethanol after each wash for a total of three times. After the final wash, the particles were sonicated for 2 minutes prior to heating.

To tune the index of refraction of the titania shell, a 100  $\mu\text{L}$  aliquot of the cleaned core-shells was centrifuged for 5 minutes at 1,500 rcf in a microcentrifuge tube, the supernatant was removed, and the pellet was heated at  $50^{\circ}\text{C}$  on a dry block heater for 5-15 minutes. The particles were then quenched by placing the microcentrifuge tube on ice for 1 min, followed by resuspension of the particles in 100  $\mu\text{L}$  of phosphate buffered saline buffer (137 mM NaCl, 2.7 mM KCl, 10 mM  $\text{Na}_2\text{HPO}_4$ , 2 mM  $\text{KH}_2\text{PO}_4$ , pH = 7.4), sonicated for 2 minutes, and stored at  $4^{\circ}\text{C}$  under rotation. The final diameter of the core-shell particles was determined similarly to the sizing process described for the anatase cores.

### **Covalent Crosslinking to Protein or DNA**

A two-step crosslinking reaction was used to covalently couple Amine-containing proteins or DNA strands to the surface exposed sulfhydryl groups of the particles. The procedure described here is for the Sup35 prion protein (Dong, et al. 2010) and a 3,500

base pair dsDNA tether harboring a terminal amine group opposite a terminal biotin tag, although the methodology is applicable to any biomolecule with a surface exposed primary amine moiety.

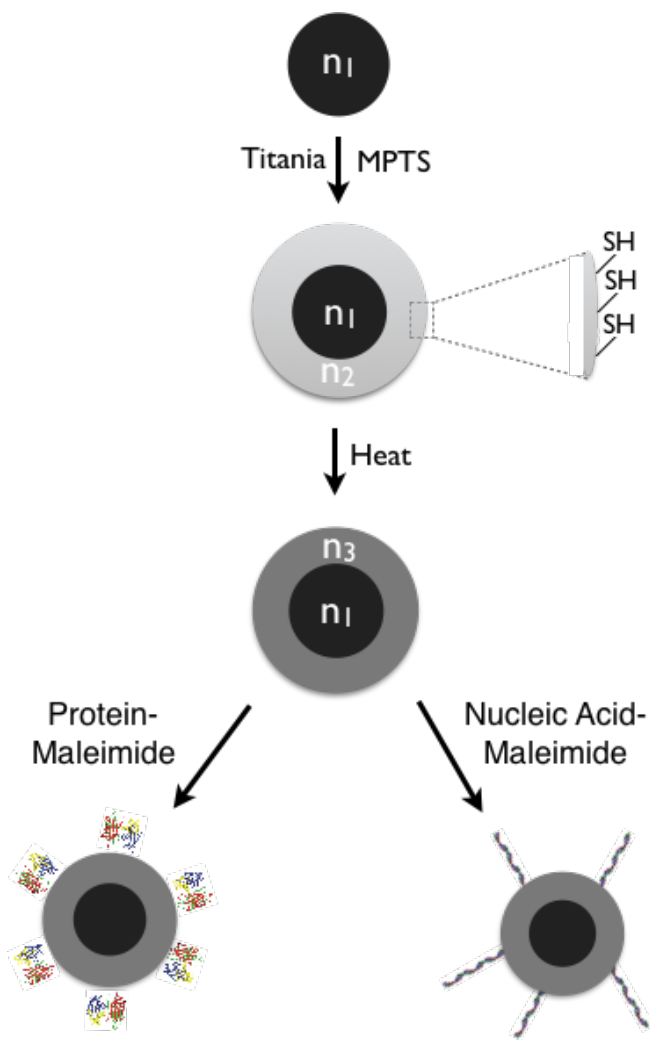


**Figure 1.** Synthetic strategy for the production of anatase-titania core-shell particles functionalized with proteins or nucleic acid structures. Anatase cores with a high index of refraction ( $n_1 \sim 2.3$ ) are coated with an amorphous titania shell (with index of refraction  $n_2 \sim 1.6$ ), and functionalized with surface exposed thiol groups using MPTS. The index of refraction of the shell can be tuned by heating to an estimated  $n_3 \sim 1.7-1.8$ , which leads to high trapping stability (see Discussion). The surface exposed thiol groups can be crosslinked to proteins and nucleic acids using thiol-maleimide chemistry.

A 30  $\mu\text{L}$  solution of 100  $\mu\text{M}$  protein in PBS was incubated with 3  $\mu\text{L}$  of 20 mM sulfosuccinimidyl 4-[N-maleimidomethyl]cyclohexane-1-carboxylate (sulfo-SMCC, Pierce Biotechnology) at room temperature for two hours. During the incubation period, 25  $\mu\text{L}$  of core-shell particles were cleaned in 500  $\mu\text{L}$  of PBST by centrifuging at 1,500 rcf for 2 minutes, resuspended in 100  $\mu\text{L}$  of PBS sonicated for 2 minutes. Excess sulfo-SMCC was removed from the protein solution using a disposable chromatography column (Micro Bio-Spin, Bio-Rad) in PBS buffer a total of three times. The maleimide activated protein was then immediately added to the core-shell suspension, and mixed overnight at 4°C. The bio-functionalized core-shells were then washed three times at 1,500 rcf for 2 minutes, and in 100  $\mu\text{L}$  of PBST buffer under rotation.

### **Optical trapping and TIRF**

To test the stability of the core-shell particles in an optical trap, we used a custom built optical trapping instrument. The optical trapping instrument relies on back focal plane detection of scattered photons. To quantify any improvement in trapping stability when using core-shells versus commercially available polystyrene particles, the trapping and detection lasers were first aligned and the trap stiffness was calculated using an equipartition based calibration. For each batch of core-shells the variance of at least five beads was measured.

For DNA stretching experiments, a glass coverslip (Fisher Scientific) was passivated with polyethylene glycol (PEG, Laysan Bio) as previously described (Jang and Nam



2008). The PEGylated coverslip was used to make a  $\sim 10$   $\mu\text{L}$  flow-cell by coupling the coverslip to a microscopy glass slide (Fisher Scientific) using double sided sticky tape. Then, a streptavidin solution (0.1 mg/mL in PBS) was flowed into to the flow-cell and incubated for 10 minutes at room temperature under high humidity. Excess streptavidin was removed by washing the flow-cell with 100  $\mu\text{L}$  of PBS. Particles coated with DNA-Biotin were introduced into the flow-cell (20  $\mu\text{L}$ ) and incubated for 30 minutes. Untethered particles were removed with a 100  $\mu\text{L}$  PBS wash, and the slide was loaded onto the optical trapping instrument. For DNA pulling experiments, a surface tethered bead was located on the coverslip surface, and centered in the detection laser. Then, the optical trap was turned on and a piezoelectric nanopositioning stage (Physik Instrumente) was moved at a constant rate (2  $\mu\text{m}/\text{sec}$  for 5  $\mu\text{m}$ ) displacing the bead from the trap center. Bead position was acquired at 3kHz using a custom-written LabVIEW routine.

To measure the presence of covalently linked proteins using fluorescence, we used a custom-built total internal reflection fluorescence (TIRF) microscope with a 532 nm excitation laser (World Star Technologies) used for excitation of the Sup35 proteins labeled with Alexa555. Fluorescence emission was imaged using an EM-CCD camera (Andor Technologies).

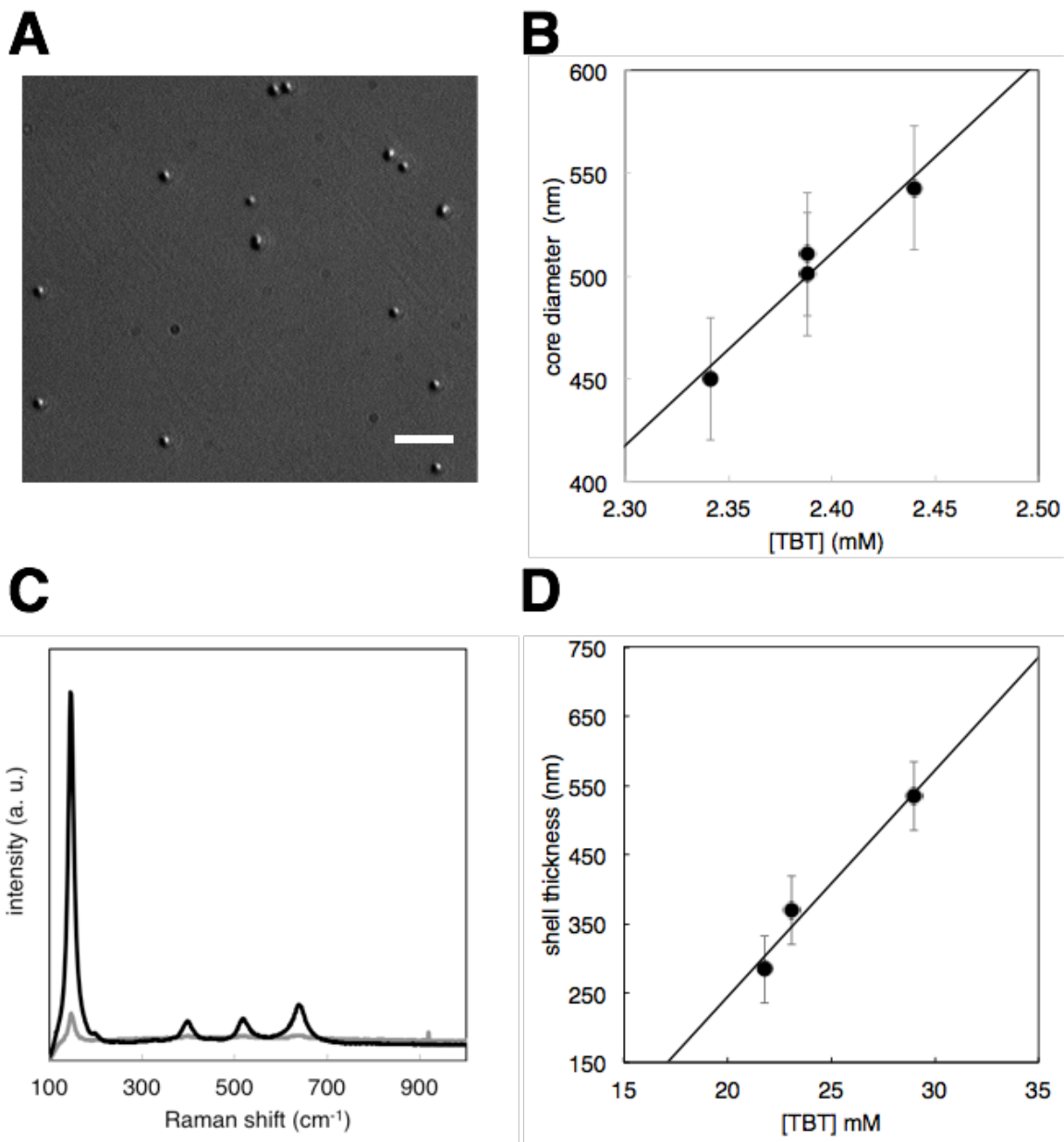


**Figure 2.** Synthesis and characterization of core-shell particles. (A) Image of anatase cores ( $\sim 400$  nm in diameter) obtained using a light microscope with DIC. The size bar is  $2 \mu\text{m}$ . Average anatase core size (B) and titania shell thickness (D) as a function of the concentration of TBT. (C) Raman spectra for cores before (gray) and after (black) calcination showing the transition of titania to the anatase phase. For (B) and (D) values are mean  $\pm$  SEM.

## RESULTS AND DISCUSSION

### Synthesis and characterization of core-shell particles

Using the synthetic strategy outlined in Figure 1, we provide a straightforward method for the synthesis of optical trapping handles with increased trapping stability. This strategy is based on a considerably modified version of work developed by several groups (Yu, et al. 2008) (Demirörs, et al. 2011) (Demirörs, et al. 2010). In the initial step, titania cores are synthesized by a nucleation reaction where the diameter of the cores is linearly dependent on the concentration of TBT used (Figure 2B). Using 1.5-3 mM TBT, we were able to synthesize cores with tightly controlled diameters between 200-800 nm. To determine the size of the particles, we found that particle diameters estimated using a scanning electron microscope (SEM) were close predicted (normally less than 10% error) using a custom-built light microscope equipped with a 100X objective (1.4 numerical aperture, Nikon) and DIC. A representative image of the cores is shown in Figure 2A. To calculate particle diameters, DIC images were used to measure the average number of pixels that make the diameter of a particular particle using the software ImageJ. With a predetermined pixel size of 50.4 nm/pixel for the CCD camera used (DAGE-MTI), we estimated the average diameter in nanometers for numerous beads per condition.

Since a mismatch in the index of refraction between the core ( $n = 2.3$ , (Demirörs, et al. 2011)) and shell ( $1.6 < n < 1.8$ , (Demirörs, et al. 2011)) materials is vital for enhanced trapping stability (Jannasch, et al. 2012), we used Raman spectroscopy to test whether

synthesized cores were in-fact in the anatase phase after calcination. Indeed, Raman spectra show the emergence of the characteristic peaks for anatase at wavenumbers 144, 399, 519, and 639  $\text{cm}^{-1}$  (Zhang, et al. 2000) (Ohsaka, et al. 1978) only upon heating the cores at 500°C (Figure 2C).

Coating of the anatase cores with amorphous titania shells was carried out at constant surfactant concentration, using varying concentrations of TBT precursor to dictate the shell thickness (Figure 2D). Previously, it had been suggested that a silica layer deposited on the surface of core-shells could provide a conjugation strategy to couple molecules of interest to the particles, but was mainly used as a way to generate fluorophore-free luminescent beads upon calcination (Demirörs, et al. 2011) (Demirörs, et al. 2009). However, silica coating of particles can be a tedious reaction and often leads to particle clumping (Bharti, et al. 2014). Instead, here we employed a silane functionalizer, MPTS, to insert thiol groups on the titania shell surface. Although thiol chemistry provides a convenient strategy for coupling to primary amines in biomolecules, other silane analogues can easily be used to insert different surface chemistries including amines, and hydroxyls.

### **Particle size and trapping stability are temperature dependent**

The amorphous titania shell has an index of refraction of  $\sim 1.55$  which is lower than the suggested  $n=1.75$  for optimal trapping stability of the core-shells, as predicted by theory (Jannasch, et al. 2012). However, the titania index of refraction can be tuned by heating.

Upon heating at 50°C, the particle diameter decreased ~15% within 15 minutes (Figure 3A). Thus, to synthesize core-shells with a final diameter of 1.0-1.1 μm we started with core-shells ~1.25 μm in diameter prior to heating.

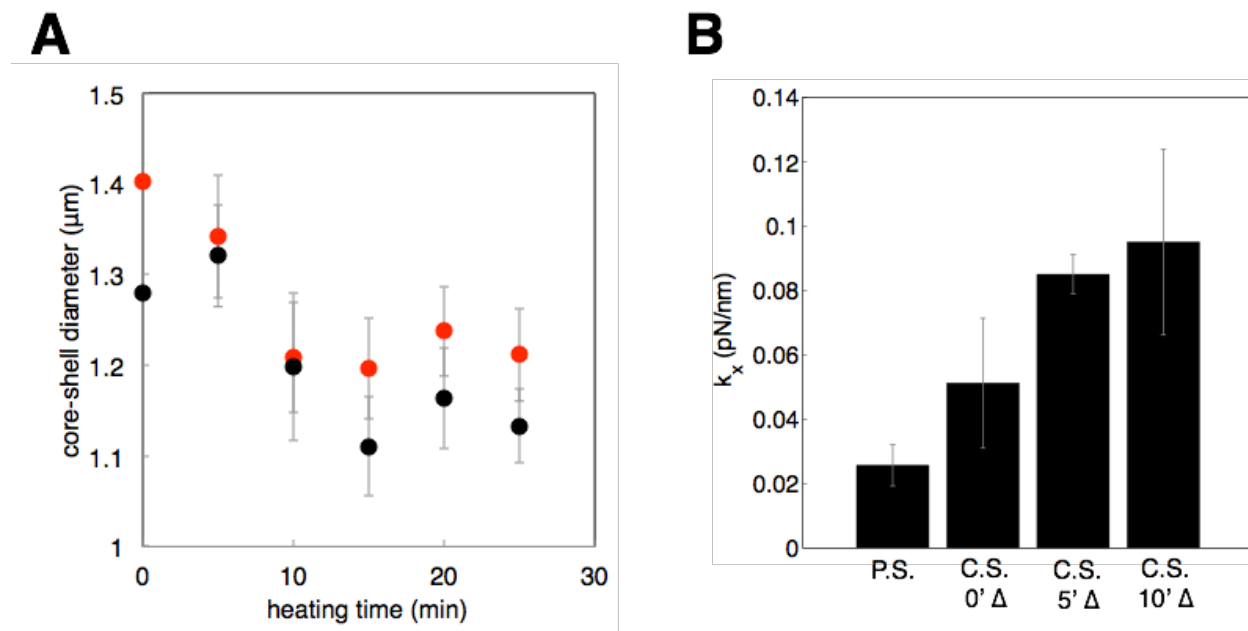


**Figure 3.** (A) Average diameter of anatase-titania core-shell particles as a function of heating time at 50°C. Two separate batches of core-shells are plotted, with initial diameters of 1.28 μm (black) and 1.4 μm (red). (B) Average trapping stiffness for conventional polystyrene beads (P.S., diameter ~ 1 μm), and core-shells (C.S.) heated for 0, 5, or 10 minutes. Values are mean ± SEM.

Using a single beam optical trapping instrument, we characterized the trapping stability of the particles by comparing the trap stiffness, at a constant laser power (~80mW at the back aperture of the objective), between the core-shells and polystyrene beads of a similar size (1.025 μm,  $n=1.57$ , Spherotech). Polystyrene beads are widely used in the field of single-molecule biophysics for optical trapping experiments, including at high forces (Dong, et al. 2010). Even in the absence of heating, the core-shell particles

displayed higher trapping stability than the polystyrene beads (Figure 3B). Upon heating, the change in density of the titania shell leads to an increase in index of diffraction (Demirörs, et al. 2011), and we observe increased trap stiffness for the core shells (Figure 3B). When heated for longer than 10 minutes, the core-shells were no longer trappable with a single beam trap likely due to an increase in the scattering force (Jannasch, et al. 2012). These results show functionalized anatase-titania core-shell particles display a 5-fold improvement in trapping stability compared to standard polystyrene beads.

### **Biophysical experiments using core-shell particles**

To demonstrate the use of the core-shell particles in biophysical experiments, we coated the particles with either proteins or strands of DNA. The DNA was produced by PCR amplification on an M13mp18 bacteriophage plasmid to make 3,500 base pairs long strands harboring opposite 5'-Biotin or primary amine moieties. The heterobifunctional amine-thiol crosslinker sulfo-SMCC was used to couple the NH<sub>2</sub>-DNA-Biotin to the functionalized core-shells. To test the efficiency of this reaction, DNA coated core-shells were tethered to a PEGylated coverslip through a biotin/streptavidin interaction (Figure 4A). Successfully tethered beads were stretched by turning on an optical trap and moving the coverslip surface at a constant rate using a piezoelectric microscope stage. The pulling trace shown in Figure 4B shows DNA stretching up to ~100pN before tether breakage. Although an overstretching transition is not observed in this trace due to the presence of two tethers, as suggested by the dual transition break

~3.3 sec, this and other traces obtained suggest DNA coupling to the core-shell surface was achieved.

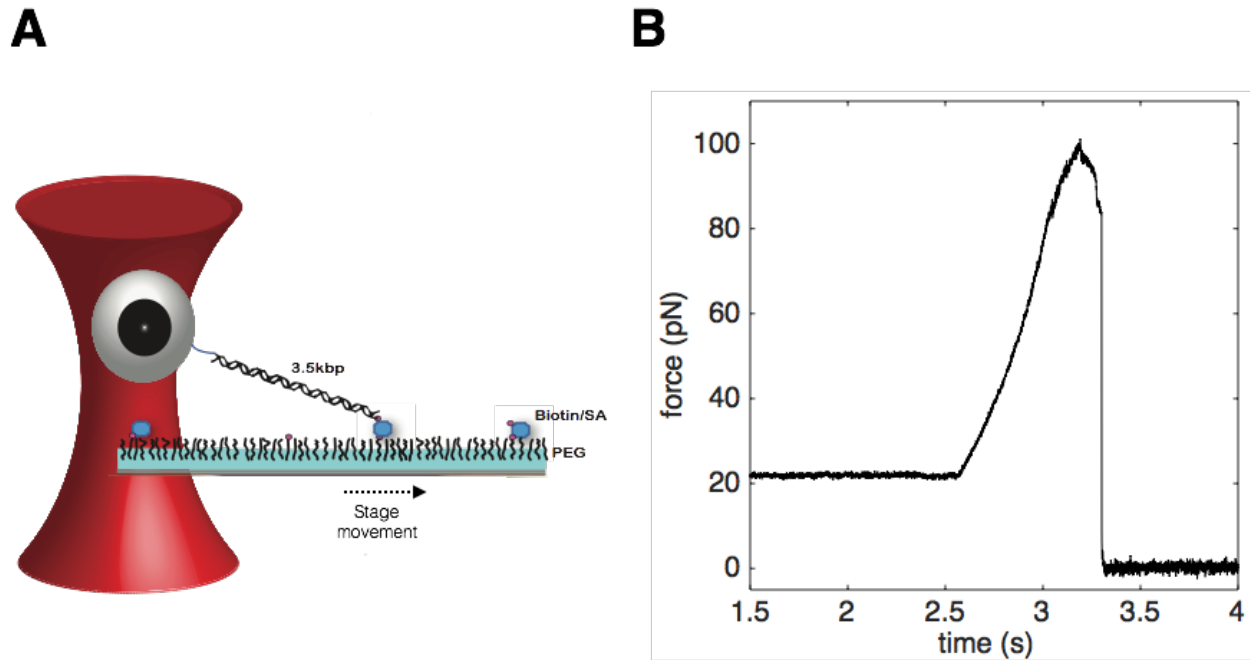


**Figure 4.** (A) Cartoon of the optical trapping assay used to stretch DNA tethers (not to scale). A core-shell particle covalently labeled with 3,500bp dsDNA is tethered to the PEG-passivated coverslip surface through a biotin-streptavidin connection. When the optical trap is on, controlled stage movement displaces the particle from the center of the trap and applies tension across the DNA. (B) Representative pulling trace showing an increase in force across the tether as the stage is moved at 2  $\mu\text{m}/\text{sec}$ . A two step rupture occurs at ~3.3 sec as the core-shell returns to the trap center.

Furthermore, as an extension of this approach, we coupled core-shell particles to the prion protein Sup35 labeled with an Alexa555 fluorescent tag. We chose to use the Sup35 protein, produced in *Saccharomyces cerevisiae*, due to its involvement in amyloid fibril formation (Dong, et al. 2010). To study the mechanics of these protein aggregates using optical trapping, Lang and coworkers tethered amyloid fibrils between a coverslip surface and a polystyrene bead (Castro, et al. 2011). To do so, a Sup35 protein seed was coupled to the polystyrene bead through a biotin-streptavidin

connection. Here we used sulfo-SMCC to covalently bind the amine-terminus of Sup35 to surface exposed thiol groups on the core-shells. Sup35 coated core-shells were imaged using DIC, and TIRF microscopy (Figure 5 A and B).

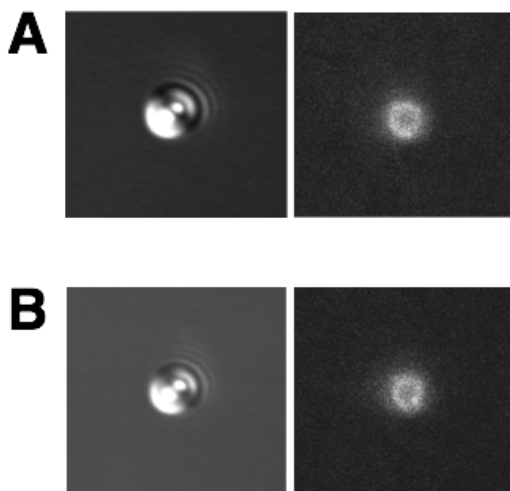


**Figure 5.** DIC image of anatase-titania core-shell particles coated with Sup35 proteins (left panels (A) and (B)). TIRF microscopy images (right panels (A) and (B)) show fluorescence emission of the Alexa555 dye on the surface-bound Sup35 protein. The fluorescence intensity from the beads decreased with time due to photobleaching of the dye.

Fluorescence intensity of the core-shells decreased with time due to photobleaching of the Alexa555 dye, suggesting the Sup35 protein successfully bound the core-shell surface. These Sup35 coated core-shells can be used to probe amyloid fibril mechanics (work in progress). The same process was successfully carried out to covalently bind the protein streptavidin to the core-shell surface. Given the ubiquitous use of biotinylated proteins, nucleic acids, and molecular motors in single-molecule experiments, streptavidin coated core-shells can be easily introduced into well developed assays to probe biomolecule mechanics and activity (e.g. ClpXP mechanical



protein degradation (Aubin-Tam, et al. 2011), protein folding-unfolding (Ritchie, et al. 2015)).

## **CONCLUSIONS**

Here we provide a synthetic strategy for making optical trapping handles that display increased trapping stability. These handles are composed of a high-refractive-index anatase cores coated with an anti-reflection titania shell. By introducing a silane functionalizer to the particle surface, we provide a straightforward method for covalently coupling nucleic acid and protein structures. We anticipate this approach will allow the single-molecule biophysics community to employ these next-generation trapping handles in experiments probing mechanically stable biological interactions/structures such as studying the mechanics of amyloid fibrils. Furthermore, these particles are promising candidates for use in combined optical trapping and fluorescence approaches where decreasing trapping laser intensity can provide longer fluorophore lifetimes (Peterman, et al. 2003).

## REFERENCES

Aubin-Tam, Marie-Eve, Adrian O. Olivares, Robert T. Sauer, Tania A. Baker, and Matthew J. Lang. "Single-Molecule Protein Unfolding and Translocation by an ATP-Fueled Proteolytic Machine." *Cell*, 2011: 257–267.

Bharti, Bhuvnesh, Jens Meissner, Sabine H. L. Klappb, and Gerhard H. Findenegg. "Bridging interactions of proteins with silica nanoparticles: The influence of pH, ionic strength and protein concentration." *Soft Matter*, 2014: 718-728.

Brau, Ricardo R., Peter B. Tarsa, Jorge M. Ferrer, Peter Lee, and Matthew J. Lang. "Interlaced Optical Force-Fluorescence Measurements for Single Molecule Biophysics." *Biophysical Journal*, 2006: 1069-1077.

Bugiel, Michael, et al. "Versatile microsphere attachment of GFP-labeled motors and other tagged proteins with preserved functionality ." *Journal of Biological Methods* 2, no. 4 (2015): 1-8.

Castro, Carlos E., Jijun Dong, Mary C. Boyce, Susan Lindquist, and Matthew J. Lang. "Physical Properties of Polymorphic Yeast Prion Amyloid Fibers." *Biophysical Journal* 101, no. 2 (2011): 439–448.

Demirörs, Ahmet Faik, Alfons van Blaaderen, and Arnout Imhof. "A General Method to Coat Colloidal Particles with Titania." *Langmuir*, 2010: 9297-9303.

Demirörs, Ahmet Faik, Alfons van Blaaderen, and Arnout Imhof. "Synthesis of Eccentric Titania–Silica Core–Shell and Composite Particles." *Chemistry of Materials*, 2009: 979-984.

Demirörs, Ahmet Faik, Anita Jannasch, Peter D. J. van Oostrum, Erik Schäffer, Arnout Imhof, and Alfons van Blaaderen. "Seeded Growth of Titania Colloids with Refractive Index Tunability and Fluorophore-Free Luminescence." *Langmuir*, 2011: 1626-1634.

Dijk, Meindert A. van, Lukas C. Kapitein, Joost van Mameren, Christoph F. Schmidt, and Erwin JG Peterman. "Combining Optical Trapping and Single-Molecule Fluorescence Spectroscopy: Enhanced Photobleaching of Fluorophores." *Journal of Physical Chemistry B*, 2004: 6479-6484.

Dong, Jijun, Carlos E Castro, Mary C Boyce, Matthew J Lang, and Susan Lindquist. "Optical trapping with high forces reveals unexpected behaviors of prion fibrils." *Nature Structural & Molecular Biology*, 2010: 1422-1430.

Fazal, Furqan M, and Steven M Block. "Optical tweezers study life under tension." *Nature Photonics* 5 (2011): 318-321.

Horst, Astrid van der, Peter D.J. van Oostrum, Alexander Moroz, Alfons van Blaaderen, and Marileen Dogterom. "High trapping forces for high-refractive index particles trapped in dynamic arrays of counterpropagating optical tweezers." *Applied Optics*, 2008: 3196-3202.

Hu, Ying, Timo A. Nieminen, Norman R. Heckenberg, and Halina Rubinsztein-Dunlop. "Antireflection coating for improved optical trapping." *Journal of Applied Physics* 103, no. 9 (2008): 093119-093119-6.

Jang, Kyung-Jin, and Jwa-Min Nam. "Direct-Write Nanoparticle Microarrays for Cell Assays." *Small*, 2008: 1930-1935.

Jannasch, Anita, Ahmet F. Demirörs, Peter D. J. van Oostrum, Alfons van Blaaderen, and Erik Schäffer. "Nanonewton optical force trap employing anti-reflection coated, high-refractive-index titania microspheres." *Nature Photonics*, 2012: 469-173.

Lang, Matthew J, Polly M Fordyce, Anita M Engh, Keir C Neuman, and Steven M Block. "Simultaneous, coincident optical trapping and single-molecule fluorescence." *Nature Methods*, 2004: 133-139.

Neuman, Keir C, and Steven M Block. "Optical Trapping." *Review of Scientific Instruments*, 2004: 2787-2809.

Ohsaka, Toshiaki, Fujio Izumi, and Yoshinori Fujiki. "Raman Spectrum of Anatase, TiO<sub>2</sub>." *Journal of Raman Spectroscopy*, 1978: 321-324.

Peterman, Erwin JG, Frederick Gittes, and Christoph F Schmidt. "Laser-Induced Heating in Optical Traps." *Biophysical Journal*, 2003: 1308-1316.

Ritchie, Dustin B, and Michael T Woodside. "Probing the structural dynamics of proteins and nucleic acids with optical tweezers." *Current Opinion in Structural Biology*, 2015: 43-51.

Tarsa, Peter B., et al. "Detecting Force-Induced Molecular Transitions with Fluorescence Resonant Energy Transfer." *Angewandte Chemie International Edition* 46, no. 12 (2007): 1999-2001.

Yu, Hyung Kyun, et al. "Surfactant-Assisted Synthesis of Uniform Titania Microspheres and Their Clusters." *Chemistry of Materials*, 2008: 2704-2710.

Zhang, WF, YL He, MS Zhang, Z Yin, and Q Chen. "Raman scattering study on anatase TiO<sub>2</sub> nanocrystals ." *Journal of Physics D: Applied Physics*, 2000: 912-916.

## CHAPTER 6

### Conclusions and Future Directions

Molecular motors from the AAA+ superfamily of enzymes are ubiquitously employed across all forms of life to carry out highly diverse and vital cellular tasks. AAA+ molecular machines largely assume a hexameric ring-shaped structure that is used to generate mechanical work. Although structural and biochemical studies on AAA+ systems have been used to decipher some of the operating principles of these versatile machines, a molecular mechanism of how these ring-shaped motors convert chemical energy to mechanical work remains largely undetermined. Using the ClpXP protease as a model AAA+ system, the work presented in this thesis provides detailed insights into fuel consumption, force generation, and conformational switching by a ring-shaped motor at the single molecule level.

Using an optical trapping assay to track mechanical degradation of homopolymer titin substrates, we develop a mechanochemical cycle for the ClpXP protease that accounts for structural, ensemble, and single-molecule experimental data. The impact of this work is evident in the fact that the same single-molecule approach has since been used in several studies to investigate the molecular mechanisms of protein degradation by the double-ring system ClpAP (Olivares, et al. 2014), as well as characterize the impact of individual ClpX pore-loops on substrate gripping (Iosefson, et al. 2015). Future work

studying the mechanics of protein degradation using an optical trapping assay could focus on probing the molecular communication between ClpX and ClpP. Specifically, stacked assembly of the ClpX ring atop the ClpP barrel occurs through a set of peripheral and axial interaction loops (Joshi, et al. 2004). Peripheral loops, referred to as IGF loops, on one interface of the ClpX ring bind to hydrophobic clefts in six of the seven ClpP subunits leading to an asymmetric ClpX ring structure (Glynn, et al. 2010). Binding of these ClpX loops to ClpP results in widening of the entrance pore into the ClpP barrel. Mutagenesis of multiple IGF loops in a single ClpX ring largely abolishes proteolytic activity but does not hobble chaperone activity (Kim, et al. 2001). Interestingly, recent work by our collaborators using a ClpX variant containing a single IGF loop mutation displays ~50% degradation activity compared to wild-type ClpXP in ensemble biochemical studies (unpublished results). Thus, this construct provides an interesting avenue to probe the communication between ClpX and ClpP during substrate processing. Are the lower degradation kinetics observed at the bulk level for ClpX-IGF mutants due to slower unfolding dwell times, translocation velocities, or changes in translocation step sizes? If ClpX constructs with a mutated IGF loop display similar translocation velocities to that of wild-type ClpXP, this would support a model in which the ClpP central pore remains closed and therefore translocation of the polypeptide must occur through the space between the ClpX and ClpP interface. Contrastingly, if translocation velocities are significantly slower for ClpX-IGF mutants, then a model in which the ClpP pore opens only transiently could account for the slower kinetics.

Furthermore, the dual-trap assay presented in this thesis can be slightly altered to study protein degradation under an assisting load. In the experimental geometry shown in Figure 1 of Chapter 2 in this thesis, an optical load is applied in a direction opposite that of ClpXP mechanical pulling. Thus, ClpXP must not only mechanically pull on a protein to catalyze unfolding and translocation, but it must also work against the force from the optical trap. However, *in vivo* ClpX, and other AAA+ chaperones, unfold unstrained substrates by applying force only to the portion of the protein proximal to the ClpX pore. To investigate single-molecule protein degradation under an assisting load, preliminary work used a dual-trap assay strategy (Figure 1A) in which substrate harboring a C-terminal Histidine-6 tag, directly following the *ssrA* tag, was pre-engaged to ClpX hexamers on a streptavidin bead. A separate bead coated with a DNA-Antibody conjugate was used to specifically bind the His-tag of the partially translocated substrate thereby applying an optical load in the same direction as ClpX pulling. Single molecule trajectories using this strategy (Figure 1B-C) display segments with constant interbead-distance presumed to be unfolding dwell times, followed by quick increases in distance interpreted as translocation. Here, unfolding events don't result in abrupt changes in distance since the substrate is unstrained, and thus the dumbbell length is only expected to change during translocation. Future work using this strategy will allow for the calculation of unfolding dwell time and translocation velocity distributions to determine what effect tilting the reaction coordinate has on the kinetics of protein degradation by ClpX.

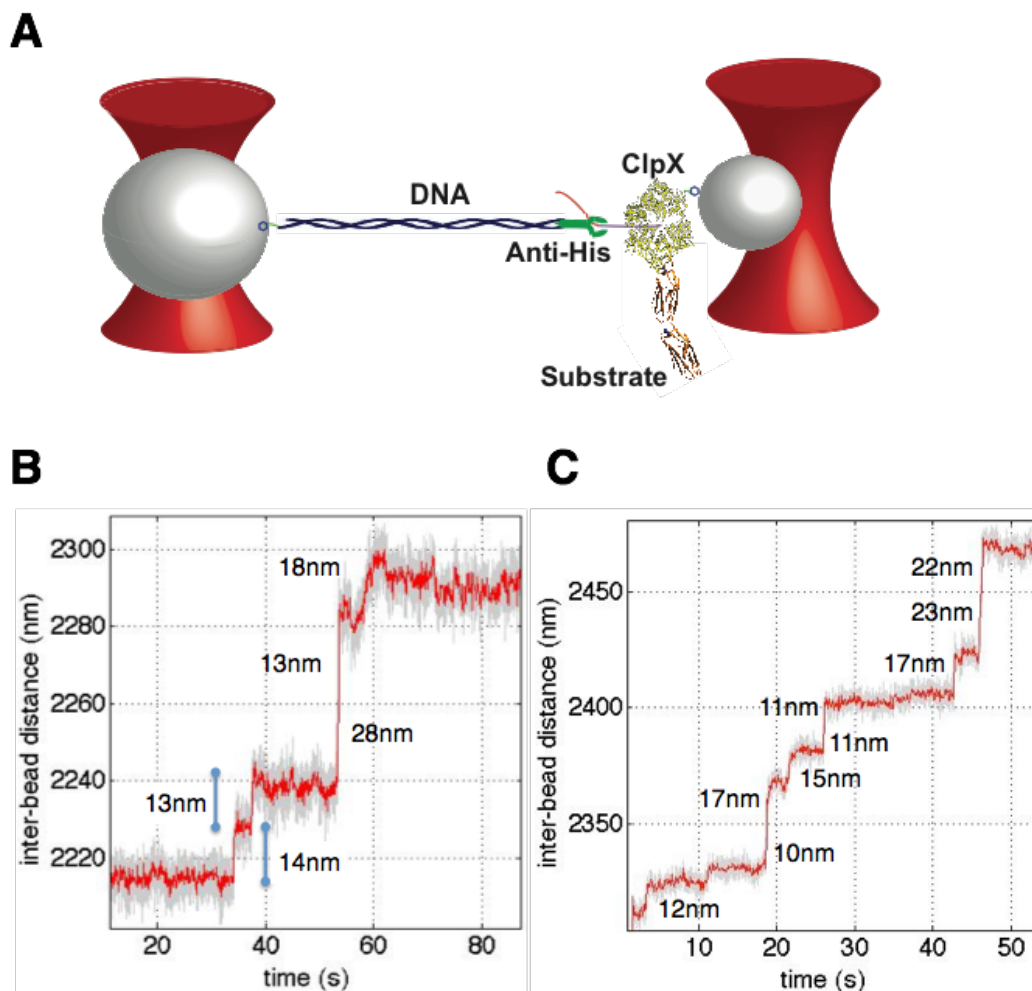


**Figure 1.** (A) Experimental setup for single molecule assays of ClpX unfolding and translocation under an assisting optical load. A laser trapped streptavidin bead is coated with biotinylated ClpX motors pre-engaged with a multimeric substrate. A second trapped bead coated with DNA-Antibody conjugates is used to bind a Histidine-6 tag near the C-terminus of the substrate after it has been translocated by ClpX. This dual-trap assembly imparts an optical load in the same direction as ClpX pulling. (B and C) Sample optical trapping trajectories for the unfolding and translocation of an *ssrA*-His6-FilaminA(1-8)-HaloTag substrate. The force during the experiments is clamped at 12pN (B) and 9pN (C).

The first observation of ClpXP-mediated proteolysis at the single molecule level was achieved by monitoring the kinetics of degradation of fluorescently tagged substrates (Shin, et al. 2009). In this thesis we expand on this work by using a fluorescence

quenching strategy to characterize nucleotide binding (Chapter 3) and ClpX subunit conformational changes (Chapter 4) in real time. The fluorescence-quenching approach used here has several advantages over other widely used fluorescence approaches like smFRET and fluorescence colocalization. First, given that dark quencher molecules do not fluoresce, high concentrations (micromolar) of quencher-labeled ATP molecules can be used. Previous demonstrations of nucleotide binding to individual molecular motors required the use of picomolar concentrations of fluorescently labeled ATP analogs (Ishijima, et al. 1998). Additionally, in molecular ruler applications, fluorescence quenching provides higher resolution at small displacements (1-3 nm) compared to smFRET due to the fact that energy transfer between a fluorophore and a dark quencher occurs only when both molecules are in physical contact, rather than through a resonance energy transfer mechanism. Thus, the fluorescence-quenching strategy described here provides a reliable approach to study conformational transitions in other AAA+ ring-shaped motors. Lastly, the fluorescence quenching approach used here employs only a single rhodamine fluorophore, which is less susceptible than other organic dyes to enhanced photobleaching from reactive oxygen species in the buffer medium or by the proximity of an optical trap (Ferrer, et al. 2009).

The combined force-fluorescence assays developed in Chapters 3 and 4 provide unprecedented insight into the structure-function relationship of ring-shaped motors during substrate processing. By simultaneously watching and manipulating single ClpXP



motors we can characterize the structure of ClpX subunits while performing highly specific tasks (*e.g.* protein unfolding, nucleotide binding) in real time. Future work using this approach can focus on characterizing whether the ClpX ring assumes significantly different conformations during chaperone activity compared to proteolysis. Similarly, the ClpX ring is known to be highly flexible and adaptable, as evidenced by the fact that ClpXP can degrade substrates with highly diverse polypeptide identities (Barkow, et al. 2009) as well as multiple substrates covalently linked through disulfide bonds (Glynn, et al. 2010). Future work employing combined force-fluorescence assays can be used to decipher the specific contortions in the ClpX ring as it translocates multiple covalently stapled substrates.

## REFERENCES

Barkow, Sarah R., Igor Levchenko, Tania A. Baker, and Robert T. Sauer. "Polypeptide Translocation by the AAA+ ClpXP Protease Machine." *Chemistry & Biology*, 2009: 605-612.

Ferrer, Jorge M., D. Fangyuan, Ricardo R. Brau, Peter B. Tarsa, and Matthew J. Lang. "IOFF Generally Extends Fluorophore Longevity in the Presence of an Optical Trap." *Current Pharmaceutical Biotechnology*, 2009: 502-507.

Glynn, Steven E., Andreas Martin, Andrew R. Nager, Tania A. Baker, and Robert T. Sauer. "Crystal structures of asymmetric ClpX hexamers reveal nucleotide-dependent motions in a AAA+ protein-unfolding machine." *Cell*, 2010: 744-756.

Iosefson, Ohad, Adrian O. Olivares, Tania A. Baker, and Robert T. Sauer. "Dissection of Axial-Pore Loop Function during Unfolding and Translocation by a AAA+ Proteolytic Machine." *Cell Reports*, 2015: 1032-1041.

Ishijima, Akihiko, et al. "Simultaneous observation of individual ATPase and mechanical events by a single myosin molecule during interaction with actin." *Cell*, 1998: 161-171.

Joshi, Shilpa A, Greg L Hersch, Tania A Baker, and Robert T Sauer. "Communication between ClpX and ClpP during substrate processing and degradation." *Nature Structural & Molecular Biology*, 2004: 404 - 411.

Kim, Yong-In, Igor Levchenko, Karolina Fraczkowska, Rachel V. Woodruff, Robert T. Sauer, and Tania A. Baker. "Molecular determinants of complex formation between Clp/Hsp100 ATPases and the ClpP peptidase." *Nature Structural Biology*, 2001: 230-233.

Olivares, Adrian O, Andrew R Nager, Ohad Iosefson, Robert T Sauer, and Tania A Baker. "Mechanochemical basis of protein degradation by a double-ring AAA+ machine." *Nature Structural & Molecular Biology*, 2014: 871-875.

Shin, Yongdae, et al. "Single-molecule denaturation and degradation of proteins by the AAA+ ClpXP protease." *Proceedings of the National Academy of Sciences*, 2009: 19340-19345.

## **APPENDIX A**

### **Protocols**

## **PCR amplification of dsDNA for ClpXP assays**

To amplify dsDNA of different predetermined lengths from the same M13mp18 plasmid we use the same reverse primer and change the forward primer to yield the desired length of the dsDNA.

The Primers used here are:

### Reverse Primer:

5'- Amino - TTG AAA TAC CGA CCG TGT GA - 3'

5'- Dithiol - TTG AAA TAC CGA CCG TGT GA - 3'

### Forward Primers:

For 100bp DNA: 5' - Dig - TGT ATA ACG CAT ATG ATA CT - 3'

For 1010bp DNA: 5' - Dig - TAT TGC GTT TCC TCG GTT TC - 3'

For 3500bp DNA: 5'- Biotin - AAT CCG CTT TGC TTC TGA CT- 3'

### Materials

Flat cap PCR tubes (Thermo Sci. cat#AB-0620)

Forward Primer(IDT, custom oligo)

Reverse Primer(IDT, custom oligo)

dNTP solution (New England Biolabs cat#N04475)

m13mp18 plasmid (Bayou Biolabs cat#P-105)

Phusion DNA Polymerase (New England Biolabs cat#M0530S)

TE buffer (Ambion cat#AM9849)

UltraPure water (Invitrogen cat#10977-015)

QIAquick PCR purification kit (Qiagen cat# 28106)

UV-Vis spectrophotometer (Thermo Sci. NanoDrop 2000)

1. Remove all materials from the freezer and allow any frozen solutions to thaw at room temperature. Upon thawing, immediately transfer and maintain in ice.

2. To prepare 1mL of PCR reaction mixture, mix the following in a 1.7mL microtube:

- 715uL U.P. water
- 25uL of 20uM biotin primer in TE buffer
- 25uL of 20uM amino primer in TE buffer
- 20uL of 10mM dNTPs mixture
- 5uL of 50ng/uL m13mp18 plasmid in TE buffer
- 200uL of 5X GC buffer
- 10 uL Phusion polymerase

3. Mix thoroughly by gently pipetting the solution up and down.

4. Add 100uL of PCR reaction mixture to 10 flat-cap PCR tubes

5. Immediately transfer tubes to PCR machine and run the “PHUSION” program/routine (outlined below)

PHUSION PCR program:

- 1) 98<sup>0</sup>C during 30sec
- 2) 98<sup>0</sup>C during 10sec
- 3) 49<sup>0</sup>C during 30sec
- 4) 72<sup>0</sup>C during 90sec
- 5) repeat steps 2-3-4 for a total of 35X
- 6) 72<sup>0</sup>C during 10 min
- 7) keep at 4<sup>0</sup>C

6. Upon completion of PCR program, purify with the DNA using the Qiaquick purification kit (protocol for purification is included in the kit). Last step in purification resuspend using 30uL of PBS instead of elution buffer included in kit.

7. Measure nucleic acid concentration of the purified DNA using the NanoDrop. Normal yields for us are reproducibly ~200ng/uL (~100nM for 3500bp dsDNA)

## DNA-Amine to Thiol-HaloTag Ligand Conjugation

### Materials

NH<sub>2</sub>-DNA @~200ng/uL in PBS (see protocol on PCR amplification)

Ultrapure distilled water (Invitrogen cat#10977-015)

Sulfo-SMCC (Pierce cat#22622 in 2 mg sealed tubes)

PBS buffer at pH 7.4

HaloTag Thiol Ligand (Promega cat#P6761)

Bio-Rad Micro Bio-Spin 30 columns (BioRad cat#732-6223)

Bio-Rad Micro Bio-Spin 6 columns (BioRad cat#732-6221)

UV-Vis spectrophotometer (Thermo Scientific NanoDrop 2000)

1. Remove a 2mg Sulfo-SMCC tube from the freezer and allow it to equilibrate to room temperature for 30min.
2. Dissolve 2mg of Sulfo-SMCC in 200  $\mu$ L Ultrapure water by perforating the tube with a pipette tip only. This may take ~15minutes of mixing.
3. Immediately combine 60 $\mu$ L of Sulfo-SMCC solution with 60  $\mu$ L NH<sub>2</sub>-DNA-Biotin @~200ng/uL
4. Incubate for 2 hours at room temperature on a rotator
5. Remove unreacted Sulfo-SMCC with gel chromatography columns:
  - a. Prepare six MBS6 columns by exchanging the buffer to PBS as described below (\*)
  - b. Place 60uL of DNA-SMCC solution into two columns
  - c. Spin column at 1000g for 4 mins, collect flow through
  - d. Clean a total of 3X
6. Combine cleaned DNA-Maleimide with 2uL of 100mM Thiol-Halotag Ligand, wrap in aluminum foil, and rotate overnight at 4°C
7. Remove unreacted HaloTag Ligand using gel chromatography columns:
  - a. Prepare 10 MBS6 columns by exchanging the buffer to PBS as described below (\*)
  - b. Place a maximum of 70  $\mu$ L DNA-HaloTag Ligand on each column
  - c. Spin at 1000 g for 4 mins and retain flow through
  - d. Clean a total of 3X(\*\*)
8. Measure nucleic acid concentration of the biotin-DNA-HaloTag Ligand using the NanoDrop. Normal yields for us are reproducibly ~100ng/uL

Note: During the SMCC conjugation, there must not be any other primary amines present.

This means any samples in a Tris buffer (TE) must undergo a buffer exchange. Best results have been obtained when samples originated in a non-NH<sub>2</sub> buffer.

(\*) Exchange buffer in MBS columns:

- (a) Invert/mix the MBS column, snap tip, and drain for 2 mins into a 2 mL tube
- (b) Empty flow through, spin at 1000 g for 2 mins and discard flow through
- (c) Load 500  $\mu$ L PBS, spin 1000 g for 1 min and discard flow through
- (d) Repeat PBS load and spin a total of 3 times

(\*\*)Alternatively you can desalt 2X in MBS6 columns and then once in MBS30 columns

## **Making ATP regeneration solution (20X) for ClpXP experiments**

Adapted by the Sauer Lab (MIT)

### Materials

Creatine Phosphokinase (CalBioChem 238395)

Creatine Phosphate (CalBioChem 2380)

Adenosine Triphosphate (Sigma A7699)

PD buffer

1. Prepare the following stock solutions in PD buffer, and keep on ice:
  - 300mM ATP (pH to 7.6 with KOH)
  - 3mg/mL Creatine Phosphokinase
  - 1M Creatine Phosphate
2. In a 1.7mL microtube on ice, mix the following:
  - 633.4uL PD
  - 200uL Creatine Phosphokinase stock
  - 100uL Creatine Phosphate stock
  - 66.6uL ATP stock
3. Vortex, and aliquot (40uL per aliquot)
4. Flash freeze with liquid nitrogen and store @-80°C
  - Use aliquots within 3 months.



## ClpXP dumbbell assay

Developed with M.E. Aubin-Tam, and A. Olivares

### Materials

3 $\mu$ L of ~5-6 $\mu$ M ClpX (biotinylated)  
11 $\mu$ L of 20 $\mu$ M ClpP (with his tag)  
20X ATP with regeneration system  
3 $\mu$ L of 20 $\mu$ M HaloTag terminated Substrate with ssrA tag  
15 $\mu$ L of ~150ng/ $\mu$ L HaloTag-3500bpDNA-biotin in PBS  
50 $\mu$ L of 0.5ng/ $\mu$ L A08-3500bpDNA-biotin  
1  $\mu$ m streptavidin coated polystyrene beads (Polysciences Inc 24162-1)  
1.26  $\mu$ m streptavidin coated polystyrene beads (Spherotech SVP-10-5)  
100X catalase (3 mg/mL in PD, Sigma C40)  
100X glucose oxidase (25 mg/mL in PD, CalBioChem 345386)  
100X glucose (500 mg/ml  $\beta$ -D-glucose in PD, CalBioChem 34635)  
Dithiothreitol (100mM, Thermo 20290)  
Casein (Sigma C7078)  
Bovine Serum Albumin (CalBioChem 2905-OP)  
PD buffer  
PBS  
0.2 $\mu$ m Syringe filters (Fisher SLMP025SS)  
Microcentrifuge tubes (1.5mL and 0.7mL, Fisher 02-682-556 and 05-408-120)  
Vacuum grease

9. Prepare surface blocking buffer: Make a 1mg/mL casein solution in PBS, filter with 0.2 $\mu$ m syringe filter and keep in a microtube on ice.
  - a. This solution must be made fresh everyday and used within 6 hours
10. Prepare anti-clumping buffer: Make a 5mg/mL BSA solution in PD, filter with 0.2 $\mu$ m syringe filter, transfer 1.5mL of buffer to a microtube and add 15 $\mu$ L of DTT @100mM and keep on ice.
  - a. This solution must be made fresh everyday and used within 6 hours. BSA must always be stored at 4<sup>0</sup>C
11. Make a narrow flow chamber with an etched coverslip (See Protocols 1 and 2)
12. Flow 0.5ng/ $\mu$ L A08-3500bpDNA-biotin into flow chamber and incubate 30min in a humidity chamber\*.
  - a. When adding solution to the flow cell for the first time, add solution to one side of the channel and allow capillary action to fill the flow cell.
  - b. Normally 3-5 tethers per field of view are desired, so this A08 concentration can be tuned.
13. Remove unbound A08-DNA-Biotin and coat coverslip surface by flowing 100 $\mu$ L of casein solution through the flow cell. Incubate 20min.

- a. To establish fluid flow through the cell we use a vacuum line connected to a pipette tip with a plastic piece of tubing. Flowing 100uL through the channel should take ~3minutes to ensure that flow is slow enough to prevent unbinding and shearing of flow cell contents.
14. During the casein incubation, prepare bead solutions:
    - a. In two separate tubes, mix 180μL PD with 3μL of 1μm and 1.26μm streptavidin bead stock solution, respectively.
    - b. Wash beads by spinning down at 10,000rpm for 3 min, remove supernatant, and resuspend thoroughly in 180μL PD.
      - i. After centrifugation, a white pellet of beads is clearly visible near the bottom of the microtube. Use a pipette to remove the supernatant without disturbing the pellet.
    - c. Repeat for a total of three washes. The final resuspension is in 60uL of BSA solution.
    - d. To breakup any bead clumps that may have formed during bead storage, and cleaning, sonicate both bead solutions for 2 minutes at 40% in a cup sonicator. (Fill the cup sonicator with cold water, but no ice)
    - e. Keep beads on ice
  15. Flow 20 μL of cleaned 1μm streptavidin beads into flow chamber, incubate 10 minutes.
  16. During this incubation period, functionalize 1.26um beads with ClpXP (see procedure below)
  17. Wash flow cell with 100μL of BSA solution to remove unbound beads.
  18. Mix 6μL of substrate-DNA-biotin with 12μL of BSA solution, flow in channel, and incubate 20min.
  19. Wash channel with 100μL BSA solution to remove unbound substrate-DNA-biotin
  20. In a 0.7mL microtube, mix the following immediately before flowing into flow cell:
    - 15μL of 1.26μm beads functionalized with ClpXP
    - + 8.1μL of BSA solution
    - + 6μL of 20X ATP with regeneration system
    - + 0.3μL of 100X catalase
    - + 0.3μL of 100X glucose oxidase
    - + 0.3μL of 100X glucose
  21. Flow into channel, and seal chamber with vacuum grease. Start a timer for 1 hour (after which ATP regeneration system is no longer effective) and load slide on optical trap.

*ClpXP functionalization of beads*

- Mix the following in a microtube:
  - 14μL of 1.26μm streptavidin beads solution
  - + 5μL of ~5-6μM ClpX

- + 2.3 $\mu$ L of 44.4 $\mu$ M ClpP
- + 6 $\mu$ L 10X ATP with regeneration system
- +  $\mu$ L BSA solution
- Allow protein to bind beads by incubating 30 minutes at room temperature
- To remove unbound ClpXP, spin down at 7500rpm for 1 min
- Remove supernatant (the pellet is very small/almost invisible, look carefully to make sure pellet is not removed along with supernatant) and resuspend gently in:
  - 51 $\mu$ L BSA solution
  - 6 $\mu$ L of 20X ATP Regeneration system
  - 3 $\mu$ L of 44.4 $\mu$ M ClpP
- Keep on ice

\* For humidity chambers we fill with water the bottom of an empty pipette tip box, then we store flow-cells on the pipette tip tray and close the lid of the box during incubations to maintain a high humidity environment during incubation periods. This is vital in preventing evaporation of the flow cell contents during incubation periods in this assay. All incubations are at room temperature.

## Anti-Digoxigenin coated beads

### Materials

Protein G beads (Spherotech PGP-08-5)

Anti-Digoxigenin (Roche 11333089001)

PBS buffer

PBST buffer

BS3 Crosslinker (Lifetechnologies )

Ethanolamine (Sigma )

1. Wash 25uL of Protein G bead stock solution with 500uL PBST by spinning down for 3 minutes at 8000rpm (repeat a total of three times)
2. Remove the supernatant and resuspend in 500uL PBST (repeat a total of three times). Final resuspension is in 100uL of PBS.
3. Sonicate for 3min at 30% (fill cup sonicator with cold water, but no ice)
4. Add 80uL of 200ug/mL Antibody to the cleaned bead solution (make sure Anti-Dig bottle is not past the use-by date)
5. Mix for 1hr @ R.T. on a rotator
6. Spin down for 2min at 8000rpm
7. Remove supernatant, and gently resuspend beads with 500uL PBST (repeat wash a total of 3 times).
8. Resuspend after last wash in 475uL of PBST
9. Prepare 100mM BS3 crosslinker by adding 35uL PBS\* to a pre-weighed 2mg tube of BS3
10. Add 25uL of 100mM BS3 to the bead solution in step 8 (final concentration of 5mM BS3 in the tube)
11. Sonicate the tube for 2min @ 20% (fill cup sonicator with cold water, but no ice)
12. React for 1hr @ R.T. on a rotator.
13. Quench reaction by adding 250uL of 50mM ethanolamine to the bead solution (to make 50mM ethanol amine mix 2uL of ethanolamine with 658uL PBS)
14. Incubate for 30min @ R.T. on rotator
15. Spin down for 2min at 8000rpm
16. Remove supernatant, and gently resuspend beads with 500uL PBST (repeat wash a total of 3 times). Final resuspension is in 250uL PBST
17. Store @4<sup>0</sup>C on rotator
  - Use beads within 2 months

## TiO<sub>2</sub> Core/Shell Microsphere synthesis

NOTE: Ethanol used in these experiments is refrigerated.

Procedure:

### I) Preparation of Anatase Core Particles

- 1) Chelate 0.46% (by weight) Titanium butoxide solution (97%) by mixing Ethylene glycol in a glovebox for 10 hours (or overnight). Alternatively, create the mixture inside the glovebox and paraflim the reaction vessel vigorously to mix overnight in open air. Take 30mL EG and mix with 154 $\mu$ L TBT. These amounts should produce somewhere from 15-35 milligrams of cores.
- 2) Dissolve 226.7 $\mu$ L Tween 20 [2.03 mM] in 100mL acetone (reagent grade) with rigorous stirring for 10 minutes. Add 100 $\mu$ L of water (or 100 $\mu$ L H<sub>2</sub>O/100mL acetone). The amount of water is crucial for the spherical shape of these titania cores.
- 3) Mix 19mL TBT with the 100mL acetone solution. (To use the full 30 we can scale up step 2 to 158mL of acetone solution with 158 $\mu$ L H<sub>2</sub>O and 358.2 $\mu$ L Tween 20). The amount of TBT solution added to the acetone solution affects the size of the cores. (19mL will produce ~500nm cores).
- 4) Agitate reaction mixture for 10 minutes, then remove the stir bar and leave for 24 hours. The relatively transparent solution will turn milky white and form precipitate on the bottom.
- 5) Clean this white precipitate by centrifugation at 7000rpm for 5 minutes and then redisperse in refrigerated ethanol. Wash the mixture TWICE. (During these washes reduce the resuspension volume to make the next step easier. I.E. resuspend the 100mL acetone mixture in 10-15mL ethanol and transfer to 1.7mL microtubes.)
- 6) Dry precipitate in convection oven at 70°C. Having the precipitate in a microtube during the drying makes transfer to our heating vessel significantly easier during this step.
- 7) Transfer dried precipitate to foil and anneal particles for 1 hour at 500°C in a furnace. The furnace takes about 1 hour to heat to 500°C.
- 8) After annealing weigh product and suspend with concentration of about 1mg cores/1mL EtOH. Keeping track of this concentration makes step II easier to keep track of.
- 9) Before storage on a rotator in a refrigerator, make sure to sonicate at 80% for 2:30 as this keeps clumping at a minimum. Make sure to do this routine sonication before every use of these particles.

NOTE: Changing the TBT concentration will affect core size. Refer to Diameter of Core Particles vs. TBT Concentration to adjust the diameter of the cores. (19mL → 500nm; 19.5mL → 550nm)

### II) Addition of Amorphous Titania Shells

- 1) Prepare 1mL of 0.1M Lutensol ON60 solution by adding 41.8 $\mu$ L Lutensol to 1mL DI H<sub>2</sub>O.

2) Sonicate cores at 80% for 2:30. Take 0.5mg cores and disperse in 1 mL EtOH and sonicate again. Now add this 1mL core dispersion to 2.3mL EtOH to make a 3.3mL total dispersion.

3) Add 26.6 $\mu$ L 0.1M Lutensol solution to your 3.3mL core dispersion and mix this solution.

4) In the glove box in a different vial, take 3.3mL EtOH and add (50 - 175) $\mu$ L TBT. The amount of TBT is vital in the sizing of core-shell particles post-mixing. Refer to the Core-Shell Size vs. Sonication Time graph with various concentrations experimented with. 100 $\mu$ L TBT produces ~1350nm core-shell particles. The reaction is quite sensitive to small changes in TBT amounts so be sure to measure this accurately. Close the vial prior to taking the mixture outside the glove box.

5) Outside of the glove box add the core dispersion to the EtOH/TBT solution and close immediately. Parafilm the vial vigorously and quickly vortex this mixture before the next step.

6) Add the vial to a sonication bath and sonicate for 2 hours.

NOTE: The specimen jar should be tightly parafilm and the level of water in the sonication bath should not be higher than the lip of the jar. This reaction is quite sensitive to water. Also, be sure to monitor the temperature of the sonication bath. Exchange the water in the bath if the temperature exceeds about 45°C (this will likely happen 30 minutes or so). A high temperature and an ice-bath sonication both had negative effects on titania addition to the core seeds.

OPTIONAL: Add 80 $\mu$ L of a 1:100 dilution of MPTES in EtOH to the reaction mixture at the 1 hour sonication mark. (This addition will functionalize the core-shells). The MPTES in EtOH should be prepared in the glove box as MPTES is hyper-sensitive to moisture.

7) Collect the titania core-shell particles by centrifuging for 5 minutes at 1500 rcf. Redisperse in the balance EtOH. Wash THREE times. After the final wash, resuspend the particles in half of the EtOH used previous. (6.6mL reaction will produce 3mL+ core-shells). This halving is important as the heating step data was collected with these concentrations. Make sure to sonicate these core-shell particles at 40% for 2 minutes prior to storage and prior to any use.

### III) Heat Tuning of Core-Shell Particles

1) Distribute desired amount of core-shell particles as 100 $\mu$ L aliquots in tubes.

2) Spin down particles at 1500rcf for 5 minutes. Then resuspend in about 10 $\mu$ L EtOH. Sonicate this small suspension at 40% for 2 minutes. Then spin down this suspension using the mini-centrifuge for only a couple seconds and remove the supernatant.

3) Heat these particles on the heating block at 50°C for 5-30 minutes. After 30 minutes, most particles become untrappable. As a general model, particle size shrinks 20-25%

with 30 minutes of heating. Resuspend these particles in 100mL EtOH. Sonicate before storage.

NOTE: During steps 2 and 3 particles tend to clump so sonicating them before every use is necessary. In order to get mainly single particles it is advised to spin down the particles at 100rcf for 5 minutes. The supernatant will contain mostly single particles and smaller junk that made its way through the reaction. This supernatant is still decently populated and must be diluted if expecting to run force and/or binding experiments with the particles.